

-博士論文-

**Propagation of Surface Leader Discharge in
Atmospheric Air**

(大気圧空気中における沿面リーダ放電の進展)

2010年6月15日提出

指導教官： 日高 邦彦
熊田 亜紀子

東京大学大学院工学部電気工学専攻

077074 邓 军波

ACKNOWLEDGEMENT

First of all I would like to express my sincerest and deepest gratitude and respect to my supervisors, Professor Kunihiko Hidaka and Associate Professor Akiko Kumada. They gave me many opportunities to participate in the research conferences and meeting. It is their kind and continues guidance, invaluable support and encouragement that lead me to pass through the long and dark tunnel. It is a great honor and pleasure for me to conduct this research under their supervision.

I also would like to express my appreciation to Prof. T. Oda, Prof. Y. Ono, and Prof. M. Ishi, for their precious comments and fruitful discussions.

The frequent help and advice from the staff members, Prof. H. Ikeda, Assistant Prof. S. Matsuoka and secretary K. Takebayashi, K. Naito, Y. Matsuzaki, S. Ikeya, they give a lot of good suggestions and selfless help to me. The help also comes from the staff, Mr. Shibuya and Mr. Uchida of machine shop. With their endless help, I made my experimental setups.

Thanks also extend to the students and staffs, who have worked with me together. They are I. Isao, Y. Suzuki, L. Oliver, Z. Li and W. Qin. What they have done for me is highly appreciated. L. Oliver, a student for Germen, helped me to assemble the charge scanning system and the work is crucial to my research.

The discussion and advices are also received from all the members of the laboratory students, especially from H. Matsumoto, T. Takeda, D. Tanaka, R. Fatima, Y. Inada, Y. Sugimoto and H. Iwabuchi. The Laboratory is a warm family, and it is a good experience for me to study here, and my gratitude should be expressed to all the members, they are T. Nishimura, J. Hayashi, Myo Min, H. Yamaguchi, H. Yonezawa, H. Uo, Y. Oida, Y. Okazaki, T. Donen, T. Itou, M. Sakuda, M. Suzuki, T. Yagi, S. Yokoyama, A. Watanabe, M. Ueda, S. Ueno, T. Takewa, T. morimot.

The help, encouragement and advice from Prof. T. Takada of Tokyo City University, Associate Prof. M. Kawada of University of Tokushima and Dr. E. Zaima of Tokyo

Electric Power Company are highly appreciated.

The author is grateful to Ministry of Education, Culture, Sports, Science and Technology (MEXT) of Japan for providing me the scholarship and giving me the great chance to study at the University of Tokyo.

Sincere gratitude is expressed to the Global Centers of Excellence (G-COE) and the Center for Advanced Power & Environmental Technology (APET). They organized a lot of academic activities which are valuable experience for me.

Finally, the most important thing is to thank my parents, my wife, my son and my daughter, my brothers and sisters for their endless support.

Propagation of Surface Leader Discharge in Atmospheric Air

(大気圧空気中における沿面リーダ放電の進展)

邓 军波

Surface discharge is a kind of discharge which propagating on the surface of insulators, such as an interface between gas/solid, an interface between liquid/solid, and an interface between gas/liquid. The flashover electric field of the surface discharge is relatively weak. The surface discharge occurs from triple junction, firstly as a streamer and then transforms into a leader. Compared with the streamer, the leader can develop over a longer distance with a lower potential gradient, and leads to flashover on the insulator. For designing highly reliable electric power apparatus, it is of great importance to clarify the process of discharge propagation, especially the transformation process from a streamer to a leader.

In this thesis, the investigations are performed with a cylindrical insulator configuration in atmospheric air. There are two ring electrodes and one rod back-electrode. The distance between two ring electrodes is aligned from 100 mm to 300 mm. One of pair ring electrodes is grounded and 1.2/50 μ s standard lightning impulse voltage or 50Hz-ac voltage is applied to the other ring electrode so that a surface discharge occurs and propagates on the insulator surface. Two cameras are used to observe the discharge. One is a high speed video camera (10⁶ frames/s), and the other is an ultra high speed framing and streak camera (10⁸ frames/s, streak duration: 1 μ s).

From a series of measurement, the propagation characteristics of AC surface discharge are summarized as follows: With increasing the voltage, leader discharges are recognized, whose occurrences concentrate in negative half-cycles of AC voltage applications. When the application voltage is enough high, some positive leader discharges are also observed. The maximum length of surface discharge L_{MAX} under AC voltage can be denoted by $L_{MAX} \propto V_p^n$, where V_p is the amplitude of the AC voltage and n is 1.5 to 3.3, whereas the propagation length of the surface discharge under impulse voltage is denoted by $L \propto V^n$, where V is the peak value of the impulse voltage and n is 3 to 5.

The residual charge distributions of impulse surface discharges are also measured with an electrostatic probe (measuring range: ± 20 kV), which utilizes a voltage feedback to the probe housing to null the electric field between the charged surface and the probe. With keeping 1mm air gap, the electrostatic probe moves in axial direction to the pipe and measures the surface voltage at every 0.25 mm. After measuring one line the pipe is rotated by 2 degree and the probe is moved back rescanning the surface.

When the applied voltage is too high, the potential caused by the residual charge of a surface

discharge will be very high and unexpected discharge will occur between the probe and the insulator surface. To reduce the surface potential, a two-layer structure is also designed. It can successfully reduce the surface potential during the measuring process with the electrostatic probe. With the two-layer structure pipe, the leader discharge propagation is studied on a clear insulator surface. The charge, electrical field, and potential distributions on the pipe are calculated from the distribution of the probe outputs.

The information on the residual charge distributions of impulse surface discharges reveals the structure of the discharge, which consists of leader part and streamer part: in streamer part, the potential gradient is from 0.5 kV/mm to 1.0kV/mm; in leader part, it is from 0.12 kV/mm to 0.15 kV/mm. The dividing point of the leader and streamer parts is 6-8 kV corresponding to 350-600 pC/mm². From the calculated electrical field distribution, it is found that the electrical field is very low and the conductivity is very high in a thin leader channel. The electrical field is 0.1-0.3 kV/mm around the thin leader channel. In the streamer zone, the electrical field is 0.5-1.0 kV/mm and it is estimated to reach 3 kV/mm in its tip region.

The residual charge of surface discharge changes the electrical field distribution on the insulator and strongly influences the propagation characteristics of the subsequent surface discharge. In this research, the propagation of surface discharges on a PET film under impulse voltage applications are observed by high speed cameras and their residual charge distributions are measured with an electrostatic probe.

Due to the residual charge of a previous opposite polarity discharge on an insulator, the propagation velocity increases three to eight times as large as that of the surface discharge on a clear insulator without residual charge. The peak current of surface discharge with residual charge also becomes much higher than that without residual charge.

When 25-times consecutive impulse voltages are applied with changing its polarity, the propagation length of the surface discharge increases gradually from 79 mm to 164 mm and hardly converges. On the other hand, the propagation length of ac 50-Hz discharge under the same peak voltage is 40 mm at most. Under the application of consecutive impulse voltages, the potential gradient in the leader part decreases with the consecutive number of impulses, while that in the streamer part keeps constant and the value is 0.5-0.6 kV/mm. This phenomenon indicates that the surface discharge propagates unexpected length under polarity-reversed repetitive pulse voltages when the wave front time of pulses matches the required time for the formation and development of surface discharge.

Contents

Acknowledgements	i
Abstract	ii
1. Introduction	1
1.1 Background of Research	1
1.2 Study methods for surface discharge investigation	2
1.3 Objective of research	4
1.4 Structure of this Paper	5
References	6
2. Design of Experimental Setup	8
2.1 Introduction	8
2.2 Experimental Setup for Discharge	8
2.3 Impulse Generators	13
2.4 Potential Distribution Measuring Apparatus	16
2.5 Principle of Electrostatic Probe	21
2.6 Structure of Potential Distribution Measuring Apparatus	24
2.7 Two-Layer Structure Pipe	31
2.8 Summary	34
References	34
3. Calculation Method of Surface Charge Density Distribution and Electrical Field Distribution	36
3.1 Introduction	36
3.2 Multipoint measurement technique	36
3.3 Surface charge distribution calculation and spatial resolution	37
3.4 Electrical field distribution calculation	41
3.5 Summary	44
References	44

4. Propagation Characteristics of AC Surface Discharge	45
4.1 Introduction	45
4.2 Typical Discharge Images under AC and Impulse Application Voltage on PMMA Pipe Surface	45
4.3 The Influence of Grounding Conditions to Surface Discharge Propagation	49
4.4 Propagation Length and Occurrence Phase of AC Surface Discharge	54
4.5 Summary	76
References	76
5. Charge Density Distribution and Potential Distribution under Impulse Surface Discharge	77
5.1 Introduction	77
5.2 Propagation Length of Surface Discharge	77
5.3 Potential and Charge Density Distribution of Positive Surface Discharge	82
5.4 Potential and Charge Density Distribution of Positive Surface Discharge	97
5.5 Summary	110
References	110
6. The influence of residual charge on surface discharge propagation	111
6.1 Introduction	111
6.2 Experimental Setup	111
6.3 Experimental Results and discussion	113
6.4 Summary	135
References	135
7. Conclusions	138
List of Publications	141

Chapter 1

Introduction

1.1 Background of Research

Surface discharge is a kind of discharge which propagates on the surface of insulators, including the interface of gas/solid phase, liquid/solid phase and gas/liquid phase. The breakdown field of the surface discharge is relatively weak, for example, for the solid insulation, the breakdown field is about 1 MV/cm; for SF₆ at 5 atm., it is several 100 kV/cm; but for the spacer in SF₆ at 5 atm., it is only several 10 kV/cm [1]. For high voltage apparatus with a solid-gas insulation system, insulator surface is the weakest part. At triple junction, where a gas, a solid dielectric, and a conductor coincide in one point, the electrical field stress is very high, and the surface discharge occurs from there, first as streamer, and then into leader, finally flashover occurs, accompanying with ionization of gas molecule and light emission as shown in Fig.1.1. After discharge, charge accumulates on the surface of insulator.

Compared with streamer, leader can develop over a longer distance with a lower potential gradient, and easy to lead to flashover of insulation [2]. For designing highly reliable electric power apparatus, it is of great importance to clarify the discharge propagation process, especially the transformation process from streamer to leader, and the influence of the residual charge accumulated on the surface of the insulating material to the discharge propagation.

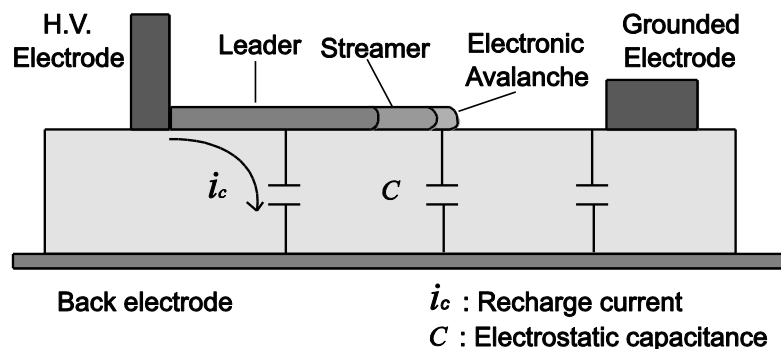


Fig.1.1. Scheme of surface discharge

1.2 Study Methods for Surface Discharge Investigation

Many researchers have investigated the characteristics of the surface discharge propagation with different methods, including dust figure method, optical method and electrostatic probe method.

Dust figure method

Dust figure method has a very long history and is still widely used. In 1778, Lichtenberg [3], [4] found a peculiar pattern created by sprinkling the charged sulfur powders on the surface of insulating materials where the surface discharge occurred. This technique was initially called “a Lichtenberg figure method,” and later called “a dust figure method [5].” In 1788, Villarsy [6] found that when fine dust consisting of both red-colored lead oxide and yellow-white-colored sulfur particles are sprinkled on the surface of insulators where the surface discharge occurred, the discharge pattern can be colorfully recorded in color. Here, the lead oxide is positively charged, while the sulfur is negatively charged. In 1884, Ducretet found a new technique using a photosensitive plate to record the surface discharge patterns [7]. This is called “a photographic figure method.”

Using dust figure method, M. Chiba *et al.* [8], [9] studied many factors that influence the developing length of surface discharge, such as inception voltage and pressure. Murooka *et al.* [7] used dust figure method to determine the statistical time lag of corona streamer inception and the developing velocity of corona streamer. The typical dust figures of surface streamer are shown in Fig. 1. Dust figure can only display the charge accumulation pattern after discharge not quantitatively but qualitatively.

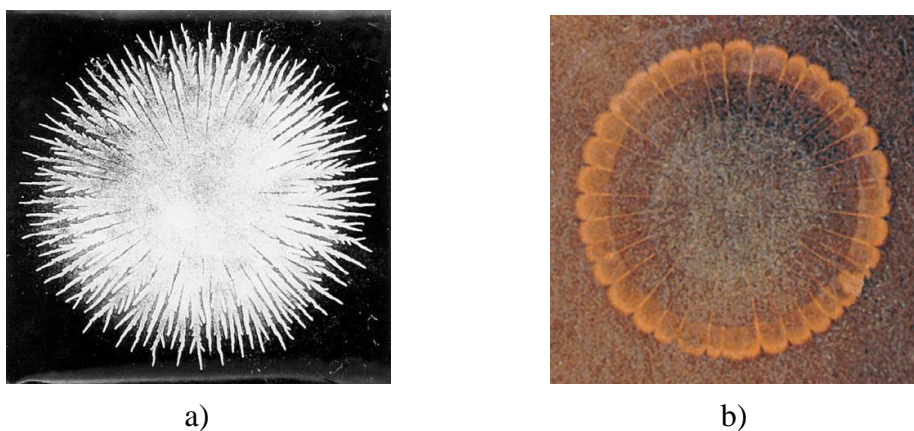


Fig.1.2 typical dust figure of surface streamer: a) positive streamer, b) negative streamer.

Optical method

Y. Yamano [10] and N.L. Allen [11] used photomultiplier to detect the luminescence due to discharge. This method can only detect several points at the time of discharge, and from the intensity of the luminescence, the value of discharge cannot be directly obtained.

Discharge are often completed in several μs , super high speed streak camera and frame camera have also been used to record the image of propagating discharge. From these images, the instantaneous developing length and speed of discharge can be obtained [12], [13].

Using Pockels effect, that is a linear electro-optic effect, several kinds of experimental setups have been reported, which can measure the surface charge and potential with a high time resolution [14, 15, 16].

Electrostatic probe method

Electrostatic probe is one of the most popular devices for measuring charge and potential on an insulator [17, 18, 19, 20]

Although the electrostatic probe is inferior to the above mentioned optical method in a viewpoint of time resolution, it has an advantage of easy handling and relatively low noise. Sakai *et al.* measured the residual charge distribution along a positive surface streamer using the electrostatic probe with 10 mm spatial resolution [17, 18].

In the case of charge distribution measurement on an insulating material using an electrostatic probe, the inverse calculation from the probe signal-output to the charge distribution is inevitable, because the probe signal-output is influenced by the surface charges on the measured object which are deposited not only in the front of the probe but also on the entire area of the object [21, 22, 23]. In recent years, the advance of numerical computation techniques using computers enables to treat more complicated objects with thousands of measuring points [19, 24, 25]. Kumada *et al.* have introduced a digital image processing technique using the two-dimensional Fourier transformation in spatial domain and the regularized inverse calculation for measuring detail of charge distribution on an insulating plate, and have evaluated the spatial resolution of the measuring system [14, 15, 16].

1.3 Objectives of Research

Although surface discharge has been studied by many researchers for more than 100 years with all kinds of methods, but till now, its development process has not been clarified.

The objectives of this research are to clarify the propagation process of surface discharge. In this paper, the following items are focused on:

- 1) Relation between the discharge length and application voltage.
- 2) Potential and charge density distributions of streamer and leader.
- 3) The criteria of leader transformation from streamer.
- 4) The influence of the residual charge on the surface discharge propagation.

1.4 Structure of Dissertation

In the first chapter, background and objectives of this research are introduced.

In the second chapter, designing principles of the experiment setup are described.

The charge measuring system was developed with a feedback type electrostatic probe. Since leader usually occurs under high voltage, the potential caused by the accumulated charge often exceeds the measuring range of electrostatic probe, which is +/-20kV, two-layer structure pipe is designed to reduce the potential of the measured object during the measurement process.

In the third chapter, analysis method of charge distribution is described.

Multi-point measuring technique is used to measure the potential distribution caused by the residual charge on the surface of pipe. From the potential distribution, the charge distribution can be calculated. To reduce the excessive amplification of noise in the inverse calculation from the measured potential to the charge distribution, The spatial resolution including the inverse calculation process reaches 1.8 mm.

In the fourth chapter, propagation characteristics of AC surface discharge are studied.

Under AC voltage, relation between length of discharge and applied voltage are studied.

In the fifth chapter, Charge density distribution and potential distribution after positive impulse surface discharge is studied.

Changing the insulator thickness, the distance between two ring electrodes, and the intensity of the application voltage, the residual charge distribution of the impulse surface discharge is measured. From the measured data, the structure of the leader and streamer is discussed.

In the sixth chapter, the influence of residual charge to the surface discharge is studied.

The impulse voltage is applied to the sample for two times, and the propagation of the surface discharge is measured with a high speed video camera. In addition, the propagation speed and the residual charge distribution of the discharge are also measured.

It is found that with the residual charge of the former discharge accumulated on the insulator pipe surface, the propagation of the subsequent discharge is greatly influenced, including the propagation pattern, velocity and distance.

In the seventh chapter, conclusions are given.

References

- [1] IEEJ, “Handbook of discharge”, Tokyo, Japan, 1998 (in Japanese).
- [2] L. Niemyer and F. Pinnekamp, “Leader discharge in SF₆”, *J. Phys. D: Appl. Phys.*, Vol.16, 1983, pp. 1031-1045.
- [3] G.C. Lichtenberg, “Nova Methodo Naturam AC Motum Fluidi Electrici Investigandi,” *Comment. Soc. Göttingen*, vol. 8, Feb., pp. 168-179, 1778.
- [4] G.C. Lichtenberg, “Nova Methodo Motum AC Naturam Fluidi Electrici Investigandi,” *Comment. Soc. Göttingen*, vol. 8, Dec., pp. 65-79, 1778.
- [5] Y. Toriyama, “Dust Figure of Surface Discharge and its Applications,” Tokyo: Kinokuniya Press, Ltd, 1961.
- [6] D. Villarsy, *Journal General de France*, No. 9, p. 34, 1788.
- [7] Y. Murooka, T. Takada and K. Hidaka, “Nanosecond Surface Discharge and Charge Density Evaluation Part 1: Review and Experiments”, *IEEE Electrical Insulation Magazine*, Vol.17, Mar. 2001, pp.6–16.
- [8] M. Chiba, “Study about the Developing Mechanism of Surface Discharge on the Solid Dielectrics” Ph.D. dissertation, Dept. Elect. Eng., Tokyo Univ., Tokyo, Japan, 2002.
- [9] IEEJ Technical Report for Surface Discharge, *IEEJ Technical Report 892*, Japan, 2002.
- [10] Y. Yamano, “Leader-like Discharge in a Crack Running Parallel to a Plane of an underlying Grounded Conductor”, *IEEE Trans. on DEI*, Vol.12, Feb. 2005, pp.127-132.
- [11] N.L. Allen, P.N. Mikropoulos, “Dynamics of Streamer Propagation in Air”, *J. Phys. D: Appl. Phys.*, Vol.32, 1999, pp. 913-919.
- [12] T. Shimazaki and I. Tsuneyasu, “Flashover Processes on the Surface of Solid Insulators under Positive Impulse Voltage in the Atmosphere”, *IEEE Trans. on Electrical Insulation*, Vol.25, Dec. 1990, pp.1161-1169.
- [13] Q Zhang, Y Khan, Y Qiu and M Hara, “Streamer Corona Propagation of an Inhomogeneous field gap in SF₆ Gas Stressed by Steep-fronted Impulse”, *J. Phys. D: Appl. Phys.*, Vol.35, 2002, pp. 2605-2607.

- [14] A. Kumada, Y. Shimizu, M. Chiba, K. Hidaka, "Pockels Surface Potential Probe and Surface Charge Density Measurement", *J. of Electrostatics*, Vol.58, 2003, pp.45-58.
- [15] A. Kumada, S. Okabe, K. Hidaka, "Resolution and Signal Processing Technique of Surface Charge Density measurement with Electrostatic Probe", *IEEE Trans. on DEI*, Vol.11, Feb. 2004, pp. 122-129.
- [16] A. Kumada, "Study about the Measurement of Charge Density on Insulator Surface and the Characteristic of Accumulated Charge on the Surface of Spacer Model", Report of Tokyo Electrical Power, 2003.
- [17] A. Kumada, S. Okabe, K. Hidaka, "Residual Charge Distribution of Positive Surface Streamer", *J. Phys. D: Appl. Phys*, Vol.42, 2009, pp.1-8.
- [18] T. Sakai, M. Matsuyama and T. Takada 1978 IEE Conference Publication (Liverpool) No. 165m p77.
- [19] Y. Shirasaka, M. Yumoto and T. Sakai, "Charge density distribution of a positive streamer on a dielectric surface", 1983 Trans. of IEE Jpn. 103-A 17 (in Japanese).
- [20] Kumada A, Shimizu Y, Chiba M and Hidaka K 2003 *J. of Electrostatics* 58 45
- [21] Faircloth D C and Allen N L 2003 *IEEE Trans. Dielect. Elect. Ins.* 10 285
- [22] Pedersen A 1987 On the electrostatics of probe measurements of surface charge densities *Gaseous Dielectrics V* eds Christophorou L G and Bouldin D W (New York: Pergamon Press) p 235
- [23] Takuma T, Yashima M and Kawamoto T 1998 *IEEE Trans. Dielect. Elect. Ins.* 5 497
- [24] Tatematsu A, Hamada S, Takuma T and H. Morii 2002 *IEEE Trans. Dielect. Elect. Ins.* 9 406
- [25] Faircloth D C and Allen N L 2003 *IEEE Trans. Dielect. Elect. Ins.* 10 285

Chapter 2

Design of Experimental Setup and Potential Distribution Measuring System

2.1 Introduction

To study the surface discharge, proper experimental setup and potential distribution measuring system is indispensable. At the beginning of this dissertation, in this chapter, the experimental setup and the measuring system are introduced.

2.2 Experimental Setup for Discharge

The investigations are performed in a cylindrical insulator configuration in atmospheric air. The Schematic of experimental setups are shown in Figs. 2.1: Fig. 2.1(a) is the schematic of experimental setup for impulse discharge and Fig. 2.2(b) is for AC discharge.

Insulator sample

Cylindrical insulators of 600 mm in length and of 30mm in their outer diameter are used in this research. Two kinds of insulators are adopted. One is a PMMA (polymethylmethacrylate, 3.2 in relative permittivity at 1 MHz [1]) pipe, and the other is a PET (Polyethyleneterephthalate, 3.2 in relative permittivity at 1 MHz [1])-film wrapped aluminum rod. The detail of these insulator samples will be described later in subsection 2.7.

Electrodes

There is a pair of electrodes as shown in Fig. 2.2, one of which is grounded and 1.2/50 μ s standard lightning impulse voltage or 50Hz AC voltage is applied to the other ring electrode so that a surface discharge occurs and propagates on the insulator surface. The distance between two ring electrodes is set to 100 mm, 200 mm and 300 mm.

In some cases, a rod electrode is put inside of the pipe as the back electrode. By changing the grounding condition of the back electrode, the applied electric field forms a parallel/perpendicular to the propagation direction of surface discharge.

Measurement of current and voltage

Discharge current is measured through a Rogowski coil or through a 50 Ω resistance, as shown in Fig. 2.3, and the application voltage is measured by a high voltage divider (PR-100GL, Pulse Electronic Inc., divider ratio: 2000:1). The waveforms are recorded by an oscilloscope.

Oscilloscope

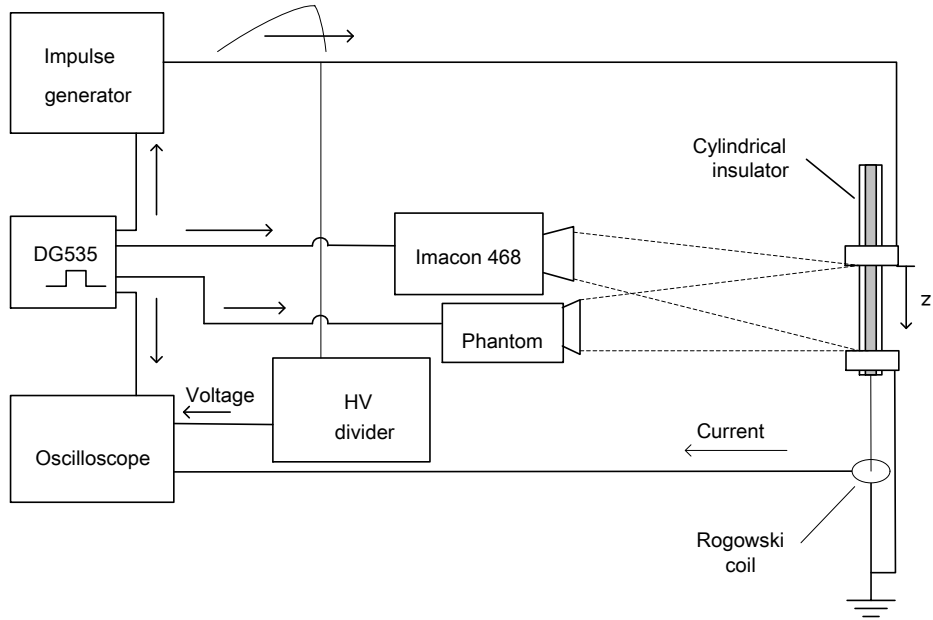
The oscilloscope is Tektronix 3053, with a maximum sampling rate of 2.5 GS/s, and a bandwidth of 500 MHz.

Cameras

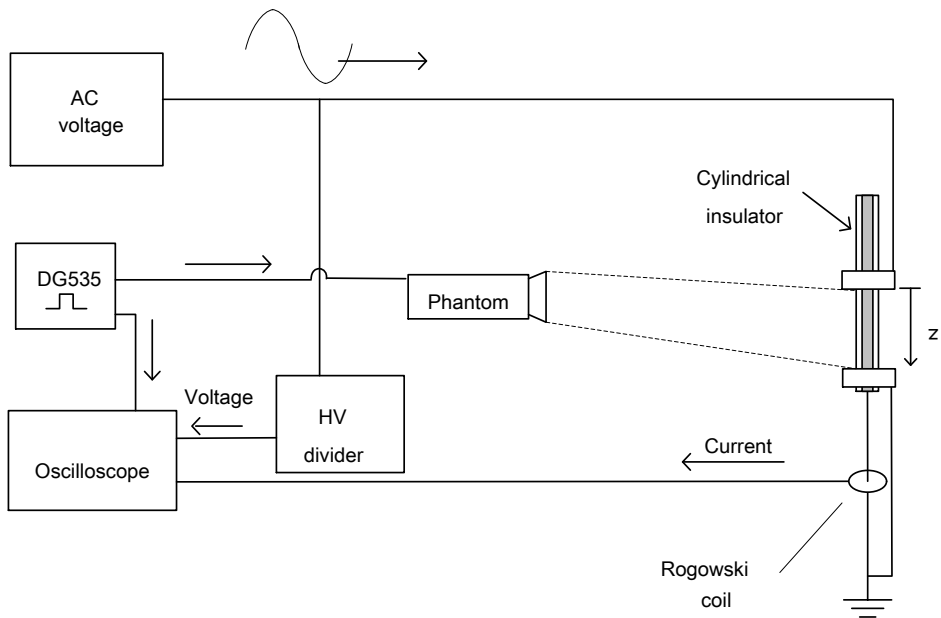
When high voltage is applied, discharges start from the high voltage electrode and subsequently develop along the surface of the pipe. The luminescence of the discharge is recorded by two cameras. One is a high speed video camera (Phantom, Vision Research Inc. the maximum speed is 100,000 frame/s), and the other is an ultra high speed camera (Imacon 468, Hadland Photonics), which can be operated in framing and streaking mode at the same time, the shortest time for each frame is 5 ns and the shortest streak duration is 10 ns.

Synchronization operation of measuring apparatus system

All of the electrical and optical instruments are operated simultaneously by control pulse from DG535 digital delay/pulse generator (Stanford Research Systems, Inc., with a 5 ps delay resolution and <100 ps rms jitter. The timing chart of impulse discharge and AC discharge are shown in Fig. 2.4 and Fig. 2.5.



(a)



(b)

Fig. 2.1 Experimental setup; (a) for impulse discharge, (b) for AC discharge.

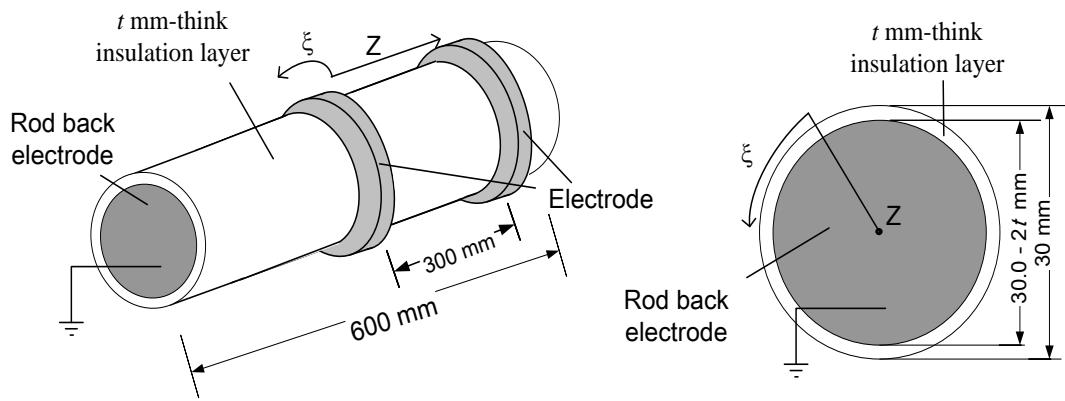


Fig. 2.2 Experimental setup, (a) Schematic of experimental setup and (b) Structure of cylindrical insulator.

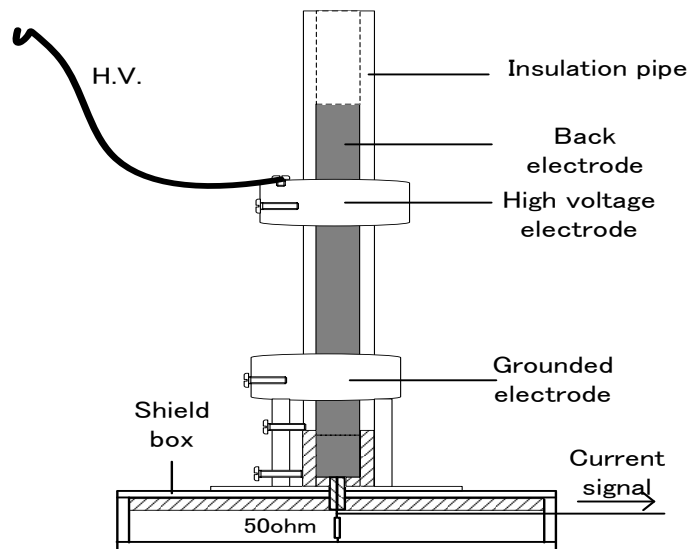


Fig. 2.3 Schematic diagram of the experimental sample.

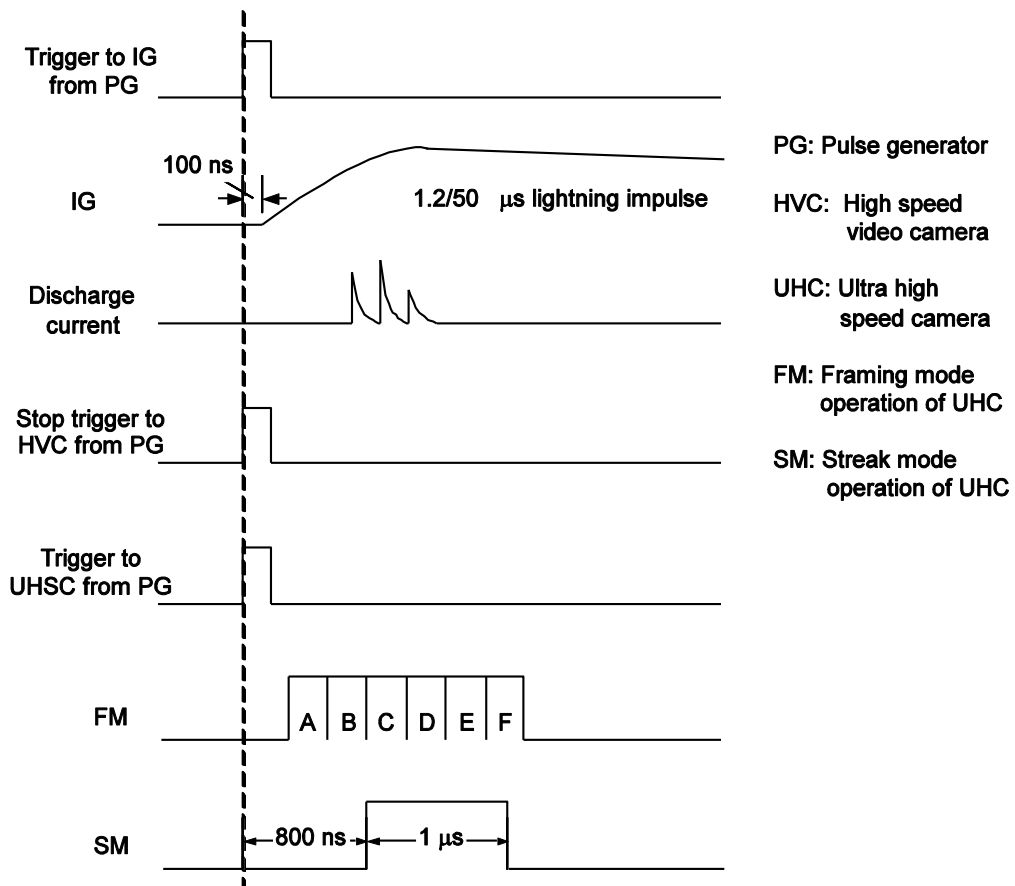


Fig. 2.4 Timing chart for impulse discharge

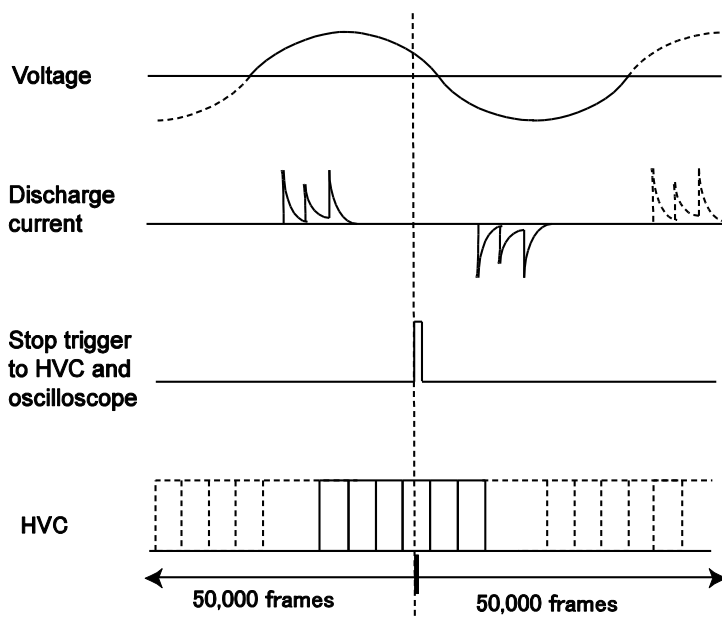


Fig. 2.5 Timing chart for AC discharge

2.3 Impulse Generators

At the beginning of the research, the traditional multistage impulse generator with a Marx circuit was used, the circuit including 6 gaps and 12 capacitors as shown in Fig. 2.6. The maximum output impulse amplitude is 420 kV. At the ignition of IG, serious electromagnetic noise is produced which interferes with the current waveform. Figure 2.7 shows an example of the discharge current waveform together with the application voltage to PMMA pipe from impulse generator.

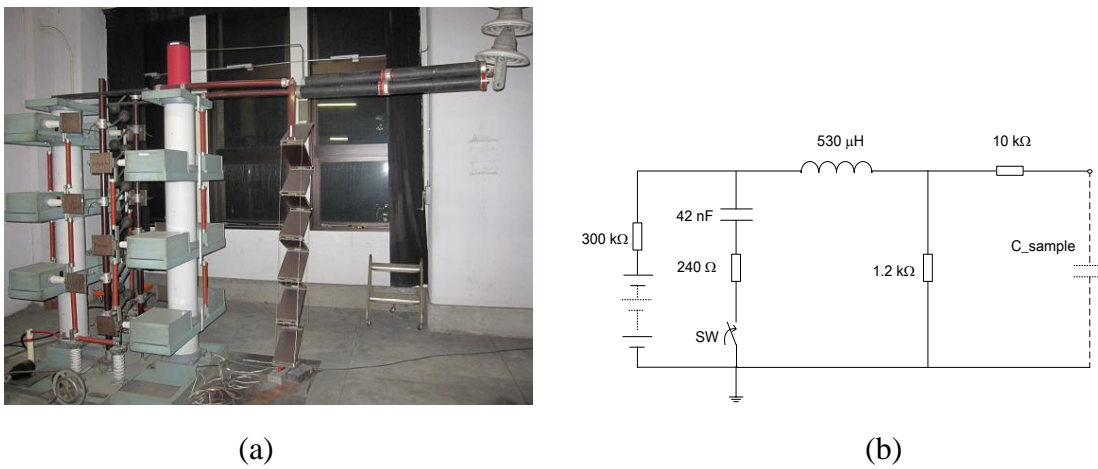


Fig. 2.6 Multistage impulse generator with a Marx circuit; (a) overview, (b) equivalent circuit.

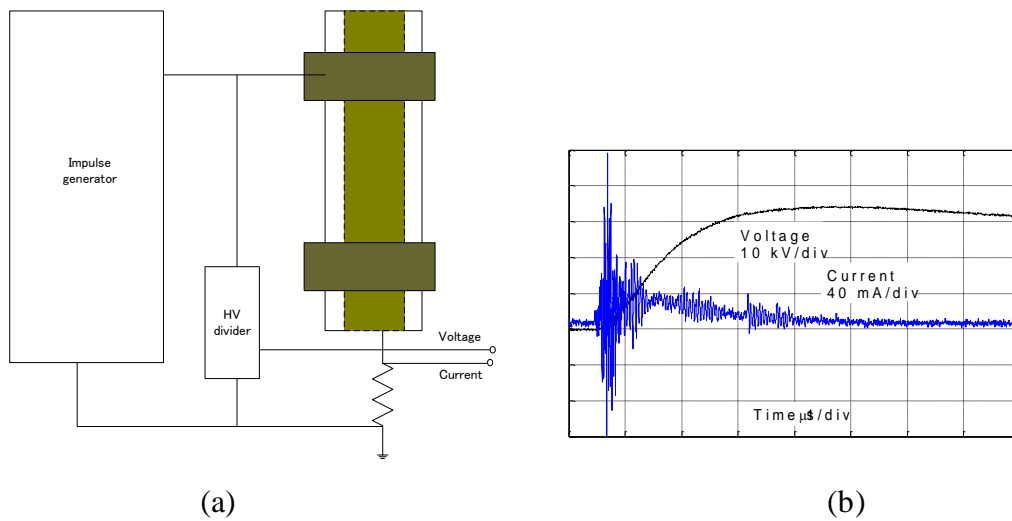


Fig. 2.7 Noise from IG; (a) experimental setup, (b) example of voltage and current waveform.

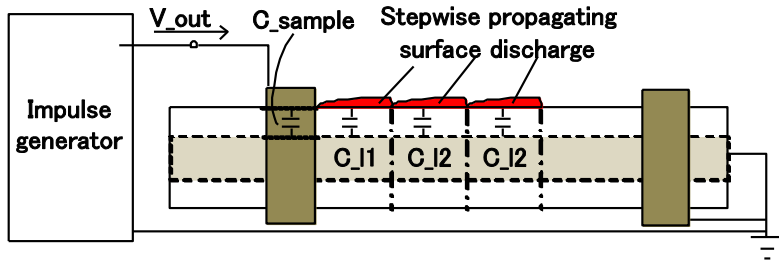
When a PET-wrapped aluminum rod, which has large intrinsic capacitance, is used as the insulator sample, the voltage drop at the inception and the propagation of surface discharge becomes too big to be ignored due to the high charging current.

To settle these problems, a new impulse generator with a thyristor-switch (HTS 300-100-SCR, Belkhe Electronic Inc.) is designed. The main technical data of the thyristor-switch are listed in Table 2.1.

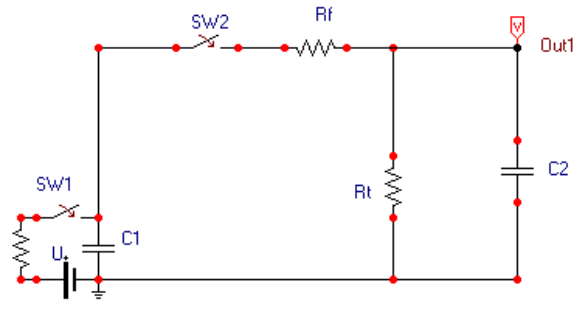
To design the new impulse generator, three EMTP cases are used to verify the circuit, as shown in Fig. 2.8. Fig. 2.8(a) shows the simulation object, (b), (c) and (d) show the three cases be simulated. The symbols R_f and R_t are the front resistor and the tail resistor, respectively. The values of elements in the impulse generator are listed in Table 2.2. There are two switches, at $t=0$, switch SW1 is switched on, the capacitor C1 is charged by DC supply to 10 kV, and at $t=20 \mu\text{s}$, switch SW2 is switched on, an impulse is produced. Fig. 2.8(b) shows the IG circuit without insulator sample. The width of the electrode is 30 mm. In Fig. 2.8(c), the capacitance C_{sample} , which is the capacitance below the ring electrode, is considered to simulate the case of impulse voltage applied on the insulator sample without surface discharge propagation. In Fig. 2.8(d), the surface discharge propagate stepwise along the insulator surface is simulated. For every step, the propagation distance is 20 mm.

The simulation results are shown in Fig. 2.9: V_{out1} , V_{out2} and V_{out3} are respectively the simulated output voltage at point Out1, Out2 and Out3, and I_d is the discharge current in case 3. V_{out1} is a standard lightning waveform of 1.2/50 μs , and the peak voltage is 8.4 kV, V_{out2} is a lightning waveform of 1.3/50 μs , and the peak voltage is 8.3 kV, V_{out3} is a lightning waveform of 1.3/50 μs , and the peak voltage is 8.0 kV. There is no obvious voltage drop in the process of discharge, which means that the sample has a negligible small influence to the output of the new Impulse Generator.

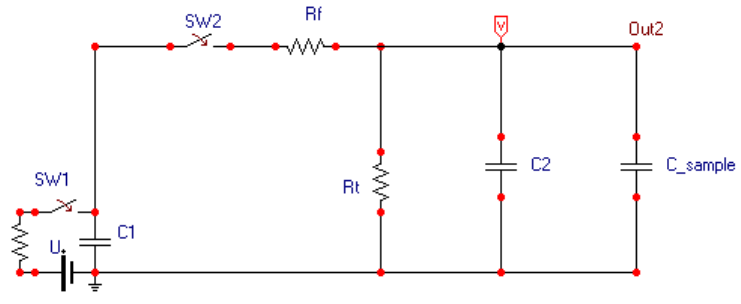
Based on the simulated result, the impulse generator is constructed. The main capacitor C_1 is charged by a DC power supply of 50 kV in its maximum output (Pulse electronic engineering Co.). Figure 2.10 shows the (a) overview and (b) equivalent circuit of the new impulse generator, which is very compact.



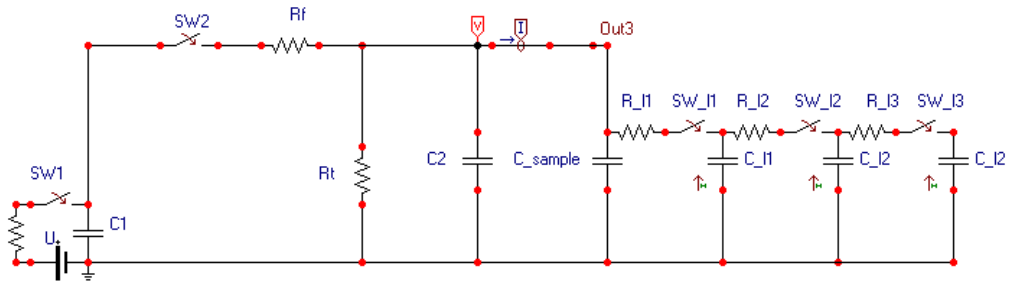
(a)



(b)



(c)



(d)

Fig. 2.8 EMTP circuit of lightning impulse generator; (a) simulation object, (b) discharge without sample, (c) discharge on the sample without surface discharge propagation, (d) discharge on the sample with surface discharge propagation.

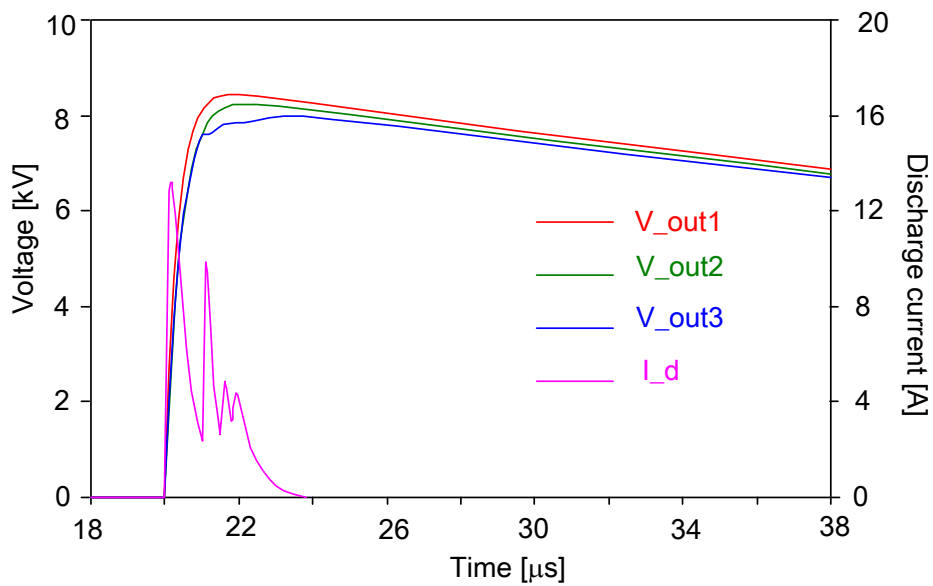


Fig. 2.9 Output impulse of impulse generator.

Table 2.1 Main technical data of fast high voltage thyristor switch

Type:	HTS 300-100-SCR
Maximum operating voltage:	30 kV DC
Maximum peak current:	1 kA
Critical Rate-of-Rise or Off-State Voltage:	80kV/ μ s

Table 2.2 Values of elements in impulse generator

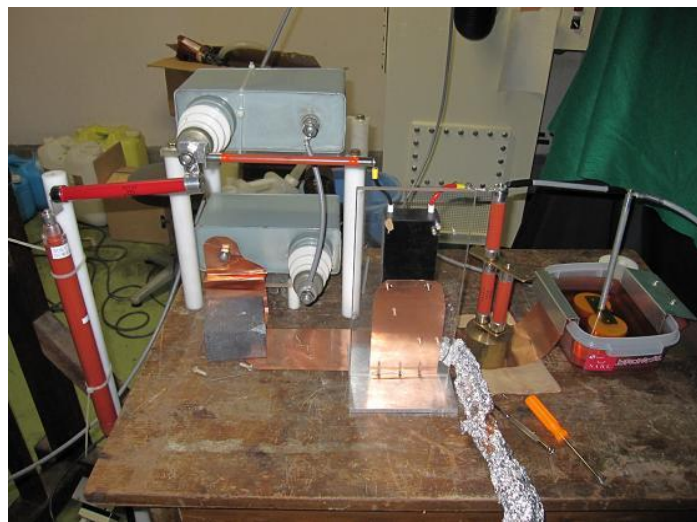
R_f	100 ohm
R_t	1670 ohm
C_1	40 nF
C_2	4 nF

2.4 Potential Distribution Measuring Apparatus

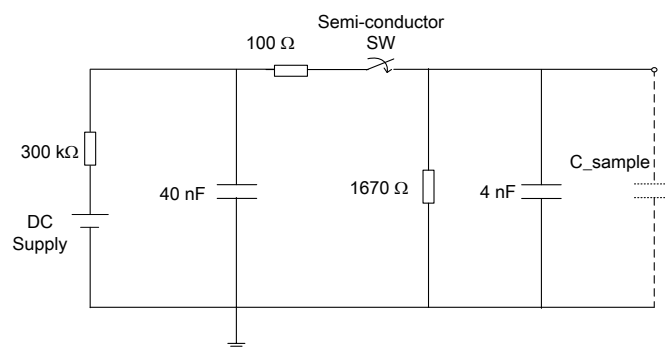
2.4.1 Configuration of the potential distribution measuring apparatus

After discharge, the pipe is put on the scanning apparatus as shown in Fig.2.11 to measure the potential distribution caused by the charge accumulated on the surface of

the pipe by using an electrostatic probe. The probe is Trek 341B, which utilizes a voltage feedback to the probe housing to null the electric field between the charged surface and the probe. The measuring range is ± 20 kV. It is positioned by the adjustable scanning platform using 4 stepper motors. A computer controls the whole scanning system with a program specially programmed in Labview, which is also called Potential Measurement Program. A distance laser sensor is used to fix the distance between the probe and the surfaces of the pipe to 1 mm. With keeping 1mm air gap, the electrostatic probe moves in axial direction to the pipe and measures the surface voltage at every 0.25 mm. After measuring one line the pipe is rotated by 2° and the probe is moved back rescanning the surface.



(a)



(b)

Fig. 2.10 New impulse generator with semiconductor switch; (a) overview, (b) equivalent circuit.

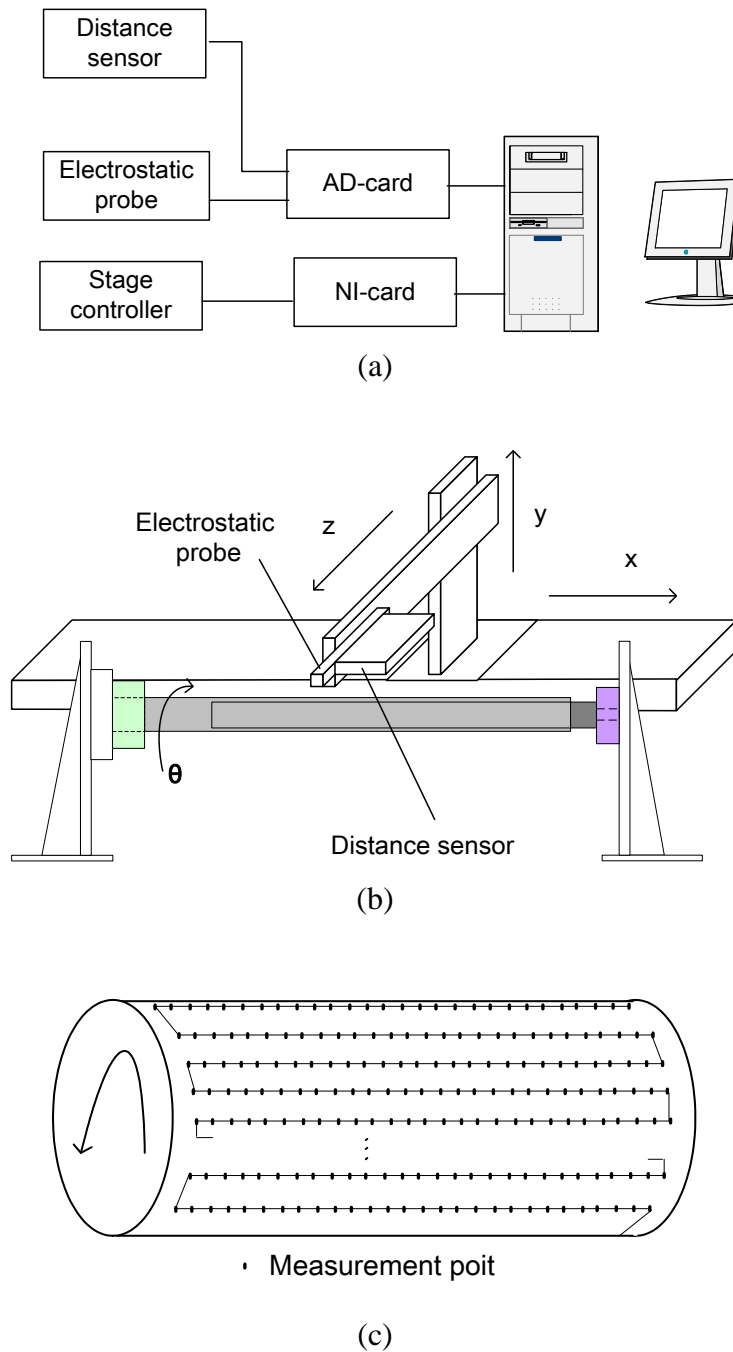


Fig. 2.11 Scanning apparatus for measuring the potential distribution: (a) configuration, (b) stages with 4 stepper motors, (c) scanning method.

The measuring system including the following parts is shown in Table 2.3 and the main technical data of stepper motors are shown in Table 2.4.

Table 2.3 Components of potential distribution measuring apparatus.

Table 2.4 Main technical data of stepper motors

Name of Motor	Connector	Movable pitch	Positioning Accuracy
SGSP 46 - 400	Stage 1	20 μm	25 μm
SGSP 26 - 50	Stage 2	4 μm	5 μm
SGSP 20 - 35	Stage 3	2 μm	5 μm
SGSP – 80YAW	Stage 4	5×10^{-3} deg	2×10^{-2} deg

2.4.2 Settings of Potential Measurement Program

The settings of potential measurement program are made in the Settings menu, as shown in Fig. 2.12. The scanning speed, the radial pitch, the axial pitch, the start position, measuring length and so on can be set in this menu.

Speed

With the upper knobs the speed for every axis can be set. The values are given in Pulses per second. The standard values are 1000 pps for every axis.

Sometimes it happens that the resisting torque is too big. Then the motors will not move and make strange noises. In such case, the motors should be stopped immediately with the alarm stop button at the stage driver (the red one) and the speed of the motor should be set to a slower speed.

Resolution

With the lower knobs, the sampling pitch for each axis can be set.

Start position

The starting position of the measurement can be set by filling the mechanical position into the “start position box.”

Sample length

The measuring length in z-direction can be set by filling the “sample length box.”

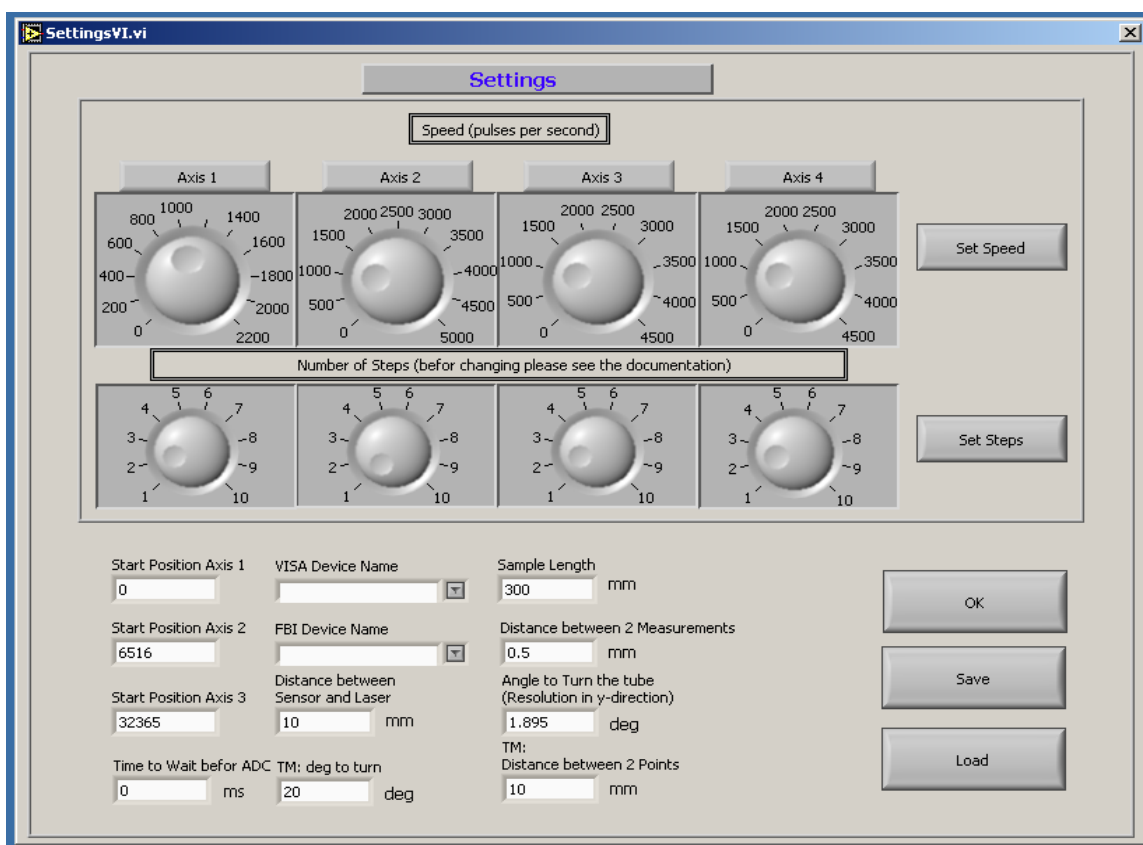


Fig. 2.12. Setting menu of potential measuring program.

2.4.3 Measurement

Before the operation of potential measurement, the distance between the probe and the insulator pipe is adjusted manually to 1 mm at first, and then the distance is measured by the laser displacement sensor at each measuring point. In the process of potential measurement, the distance between the probe head and the insulator surface is adjusted to 1mm automatically.

2.5 Principle of Electrostatic Probe

In this research, electrostatic probe Trek 341B is used to measure the potential distribution on the insulator pipe caused by the residual charge of surface discharge.

Trek 341B is a DC stable, high-voltage precision electrostatic probe for making non-contacting surface voltage measurements in the range of 0 to ± 20 kV DC or peak AC. It employs a field-nulling technique for non-contacting voltage measurement, as shown in Fig. 2.13 [2, 3].

The sensing electrode of the probe vibrates mechanically. The displacement current from this sensing electrode is detected by the “synchronous detection unit” and it drives the high voltage feed back circuit which supplies bias voltage to the guard electrode. The bias voltage of the guard electrode increases up to the surface potential of the measured object, where the electric field in front of the sensing electrode becomes zero. The comparison between the output of traditional electrostatic probe, where the induced charge of the sensing electrode surrounded by grounded guard electrode is detected by a voltmeter as shown in Fig. 2.14, and that of Trek 341B is shown in Fig. 2.15 as a function of the distance to the measured object [5]. It is possible to say that this field-nulling technique achieves DC stability and high accuracy even if the experimental error of the distance between the probe head and the measured insulator surface is not so small.

The specification of the electrostatic probe Trek 341B is listed in Table 2.5.

Table 2.5 Specification of Trek 341B

<ul style="list-style-type: none">• Measuring Range 0 to ± 20 kV• Measuring Frequency DC to 5 kHz, peak value is measured for AC.• Accuracy Better than $\pm 0.1\%$• Speed of Response Less than 200 μs for a 1 kV step change. Less than 5 ms for a 20 kV step change.• Full Signal Bandwidth DC to better than 25 Hz.• Stability Drift with Time: Less than 100 ppm/hour, noncumulative. Drift with Temperature: Less than 200 ppm/$^{\circ}\text{C}$.

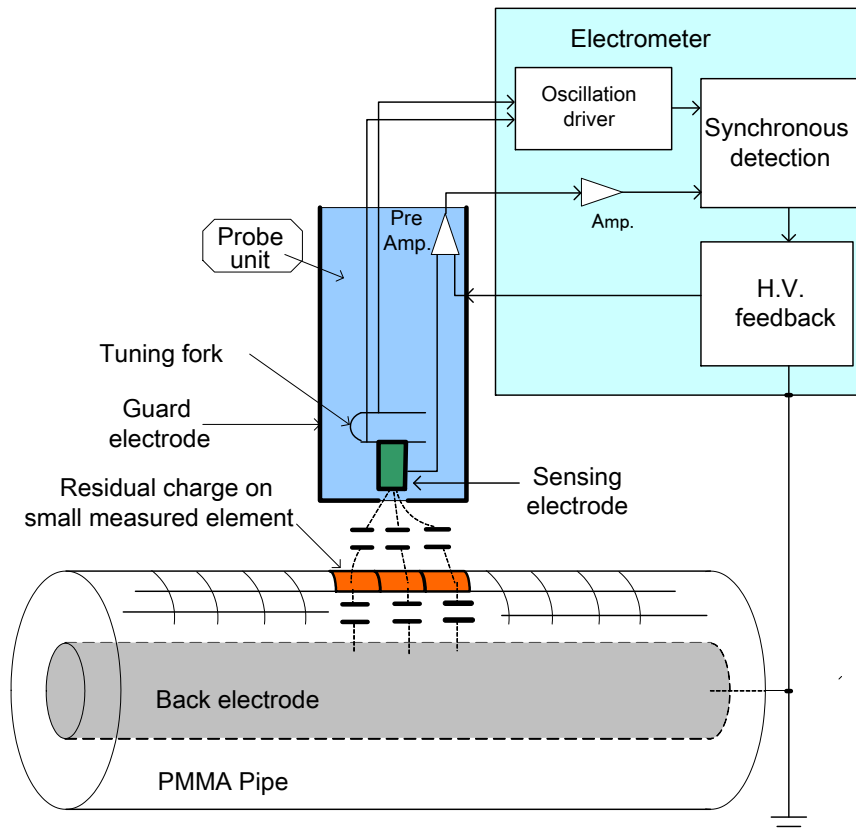


Fig. 2.13 Principle of feedback type electrostatic probe

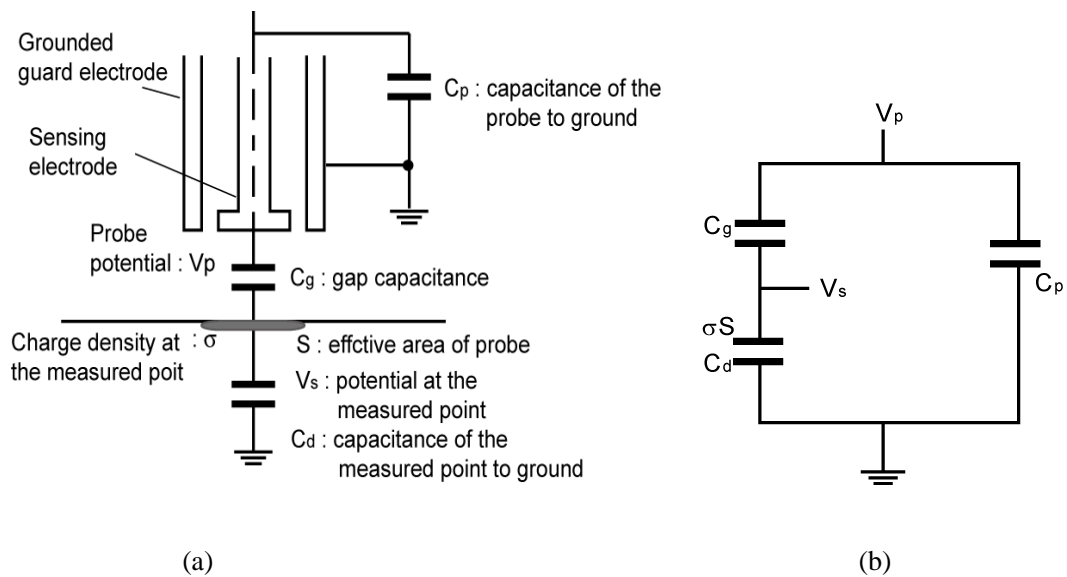


Fig. 2.14 Principle of traditional electrostatic probe; (a) Schematic of measurement, (b) equivalent circuit [4].

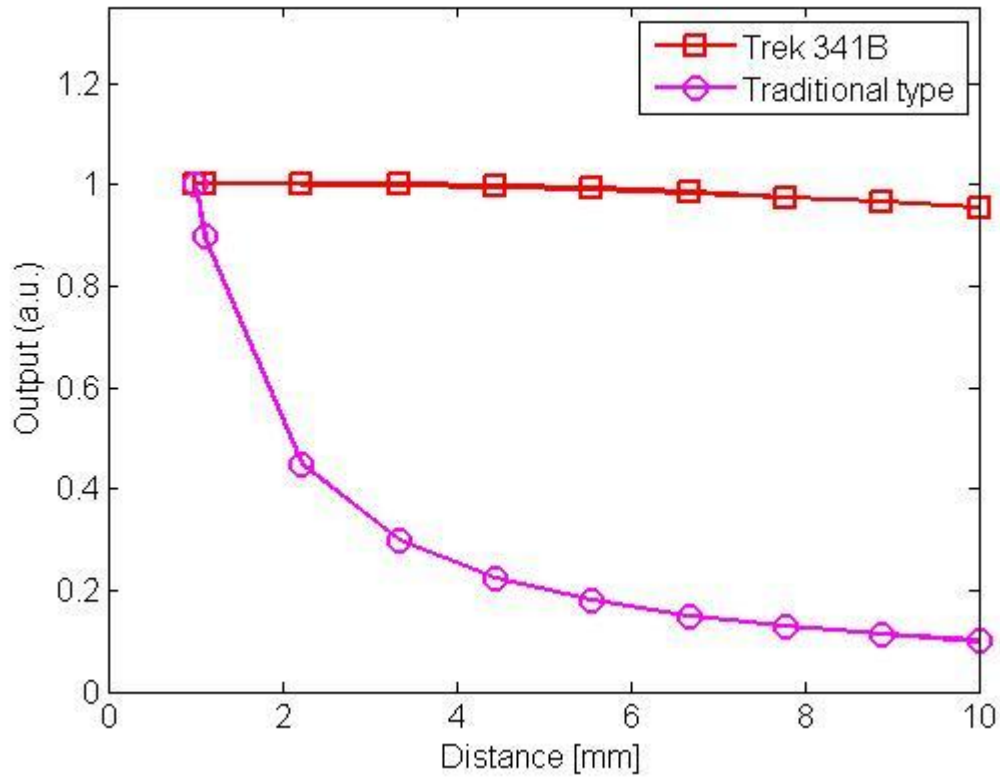


Fig. 2.15 Relation between the output and the distance of traditional electrostatic probe and Trek 341B.

As the spatial resolution of the measuring system will later be discussed quantitatively in subsection 3.3, the resolution is related with the distance between the probe and the insulator surface [6]. When the distance between probe and the measured insulator surface is big, or the measured insulator is thick, the electric field in front of the sensing electrode of the probe is determined by not only the charge in the vicinity but also the charge on the large surface of the measured object as shown in Fig. 2. 16.

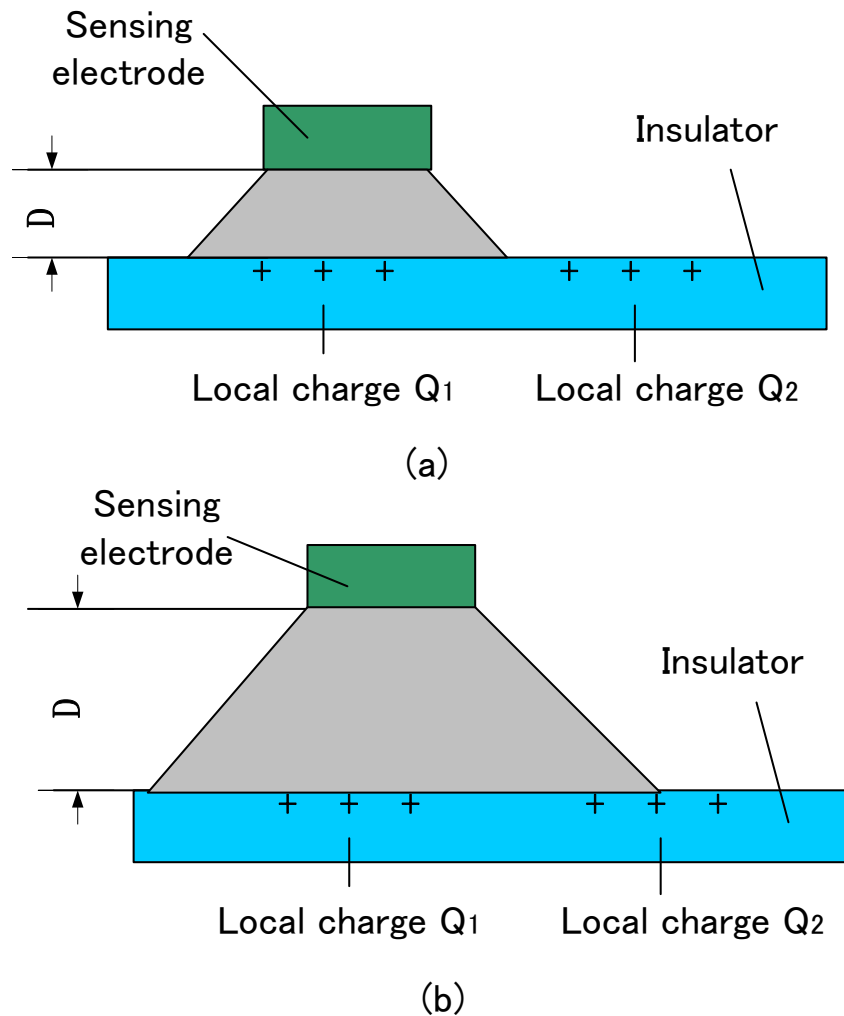


Fig.2.16 Resolution and spacing of the probe: (a) Short distance from the probe to the Surface, (b) Long distance from the probe to the surface

2.6 Two-Layer Structure Pipe

In case of measuring highly charged insulator, there is possibility that potential on the insulator exceeds measurable range. It has been reported that the maximum residual surface potential of negative surface streamer decreases almost to the half value of its inception voltage due to the back discharge [7, 8]. It is, therefore, tried to measure residual charge distributions of surface discharges on the 5 mm-thick PMMA pipe under the application of positive impulse voltages of 35 kV and 55 kV in their peak values, which are lower than twice value of the measurable range of the electrostatic

probe Trek 341B. The conditions of the experiments are shown in Table 2.6 and Table 2.7.

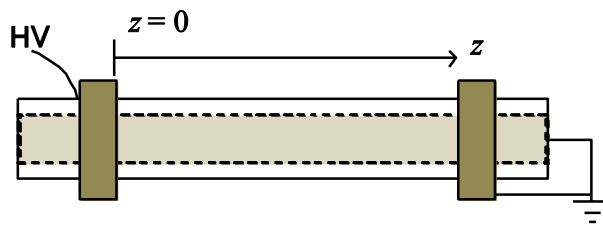
Figure 2.17 shows the potential distribution and Lichtenberg figure of surface discharge under the application of 35 kV-impulse voltage together with the detail of the experimental condition. Several surface streamers have propagated in parallel. As back discharge has occurred, the potential within 20 mm from the high voltage electrode is less than 8 kV. The potential takes the maximum value of 16 kV at $z = 25$ mm, and then decreases almost linearly with the distance from the electrode. This distribution coincides well with the potential distribution of propagating streamer, which is measured by Pockels device [9].

Figure 2.18 shows the potential distribution, Lichtenberg figure of the potential distribution and Lichtenberg figure of surface discharge under the application of 55 kV-impulse voltage, together with the detail of the experimental condition. Many spots are recognized in the Lichtenberg figure, and the maximum value of the potential is limited to around 16 kV. This is because the potential on the surface is very high, which might be around 30 kV, and a lot of discharge occur between the probe and the pipe during the potential measurement by the electrostatic probe.

From these results, the range of the potential measuring system is roughly estimated to 16 kV at most.

Table. 2.6 Experiment conditions

Insulator	5 mm-thick PMMA
Back electrode	Grounded
Distance between ring electrodes	$d = 100\text{mm}$
Application Voltage	Impulse, 35 kV



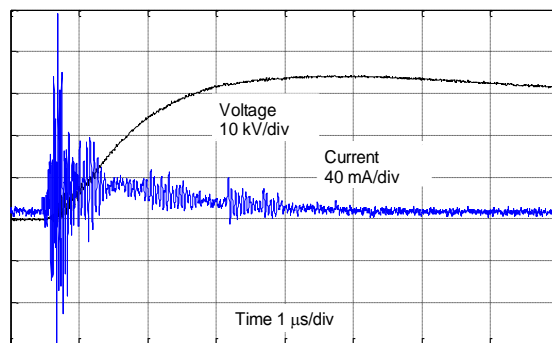
(a)



(b)



(c)

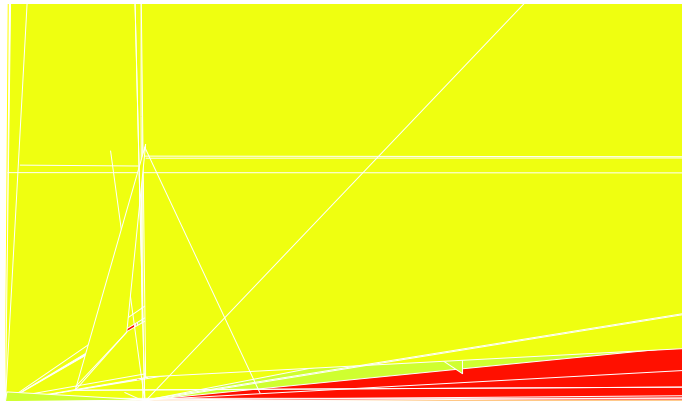


(d)

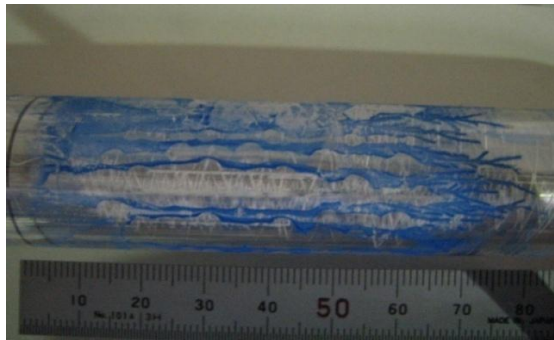
Fig.2.17 Experimental results of surface discharge under the application of impulse voltage of 35kV in its peak value, (a) experimental condition, (b) potential distribution, (c) Lichtenberg figure and (d) voltage and current waveform.

Table. 2.7 Experiment conditions

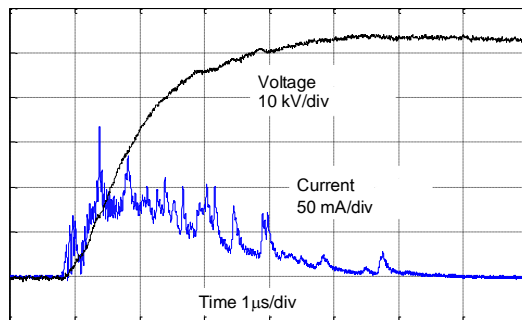
Insulator	5 mm-thick PMMA
Back electrode	Grounded
Distance between ring electrodes	$d = 100\text{mm}$
Application Voltage	Impulse, 55 kV



(a)



(b)



(c)

Fig. 2.18 (a) Potential distribution, (b) dust figure and the (c) applied impulse voltage and discharge current of a 55kV discharge

To reduce the potential of the accumulated charge, two-layer structure pipe as shown in Fig. 2.19 is designed. The outer layer is a 100 μm -thick PET film. The central axis is a metal rod of 20 mm in the diameter and there is a rubber layer with a low resistivity between the PET film and the metal rod. The characteristics of the material are listed in Table 2.7.

The equivalent circuit of this pipe can be expressed as Fig. 2.19(b) and Fig. 2.20.

During the impulse voltage application and the propagation of the surface discharge, the electric field distribution is determined by the capacitance of the material. Assuming that charge Q is accumulated on the PET surface at $t=0$, the potential on the PET surface U , which is the sum of the potential differences for PET, U_p , and rubber, U_r , can be denoted by

$$U(0) = U_p(0) + U_r(0) = \frac{Q}{C_p} + \frac{Q}{C_r} \quad (2.3)$$

where C_p and C_r are capacitances of PET layer and rubber layer, respectively.

Since the charge on the rubber layer will leak due to the resistivity of the rubber with the time constant of $8.2\mu\text{s}$, the potential difference of the rubber layer U_r will reduce to zero in $20\mu\text{s}$. On the other hand, the time constant of PET is $2.8 \times 10^7\text{s}$, which is much longer than the measuring time, so the potential difference of the PET layer will keep constant during the period of the measurement.

$U(t)$ is given by

$$\text{for } t < 20\mu\text{s}, \quad U(t) = \frac{Q}{C_p} + \frac{Qe^{-\frac{t}{\tau}}}{C_r} = U_p(0) + U_r(0)e^{-\frac{t}{\tau}} \quad (2.4)$$

$$\text{for } t > 20\mu\text{s}, \quad U(t) = U_p(0). \quad (2.5)$$

It takes several minutes to start measuring process from the occurrence of the surface discharge, so the potential on the PET surface decreases to the level given by equation (2.5).

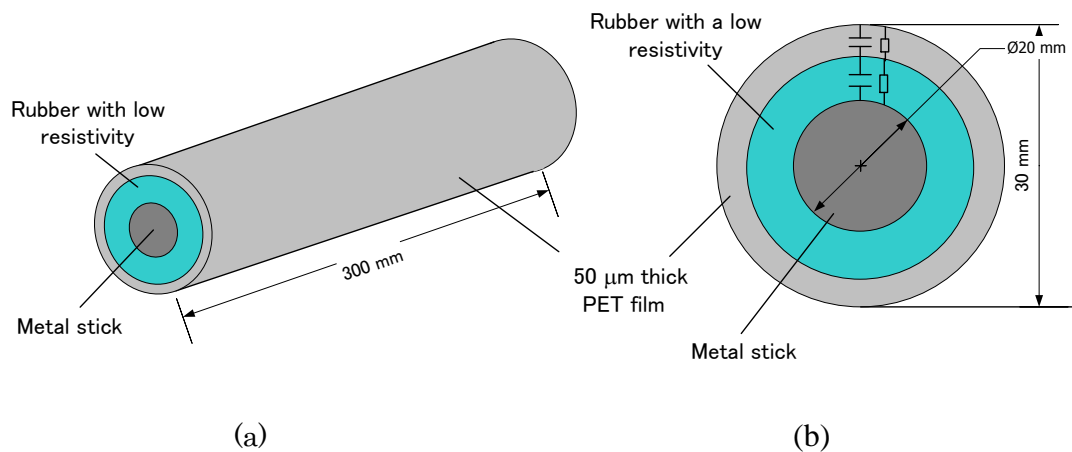


Fig. 2.19 Two-layers structure pipe, (a) overview, (b) equivalent circuit.

Table 2.8 Characteristic of the material

Material	ϵ_r [s]	ρ [Ωm]	τ [s]
PET	3.2	1×10^{18}	2.8×10^7
Rubber	50	1.87×10^4	8.2×10^{-6}

The data is got under 1 MHz

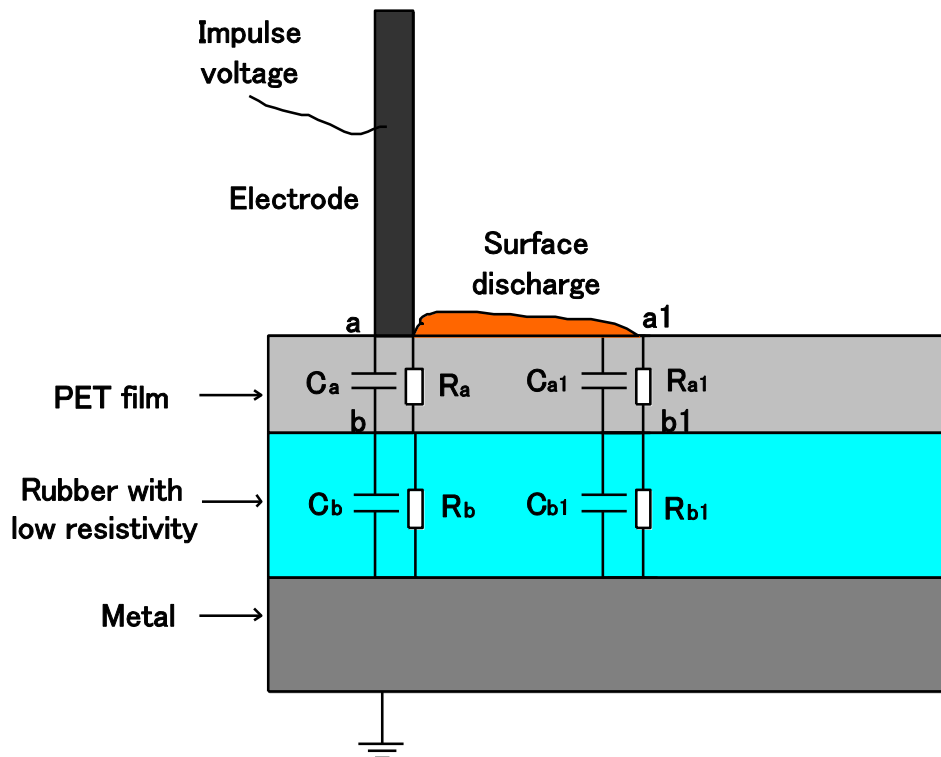


Fig.2.20 Equivalent circuit of two layer structure pipe

The time evolution of the potential on the PET surface is also simulated by using EMTP. Fig. 2.21 shows the circuit used for EMTP simulation, a is the point on the PET surface below the electrode and b is the point on the interface of PET and rubber which is between a and back-electrode. a1 is the point on the PET surface which is 2 cm away from a, and b1 is the point on the interface of PET and rubber which is between a1 and back-electrode. Fig. 2.22 shows the simulated result: V_a is the applied impulse voltage, V_{a1} and V_{b1} are respectively the potential at point a1 and b1. The potential at point b1 decreased to zero after about $50\mu\text{s}$, but the voltage between point a1 and b1 kept constant, so the potential at point a1 decreased to a constant which equal to the voltage between point a1 and b1 after about $50\mu\text{s}$.

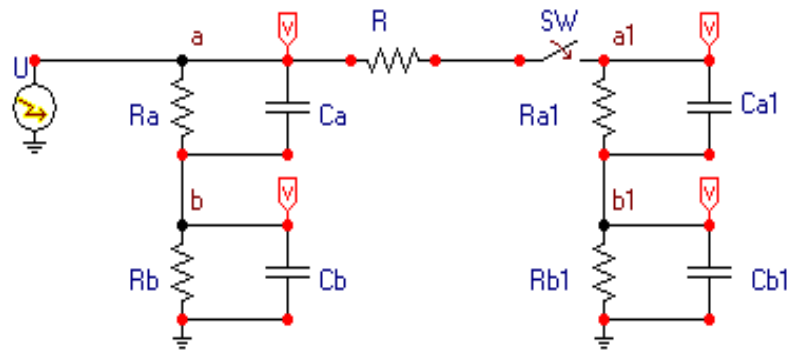


Fig. 2.21 Circuit used for EMTP simulation

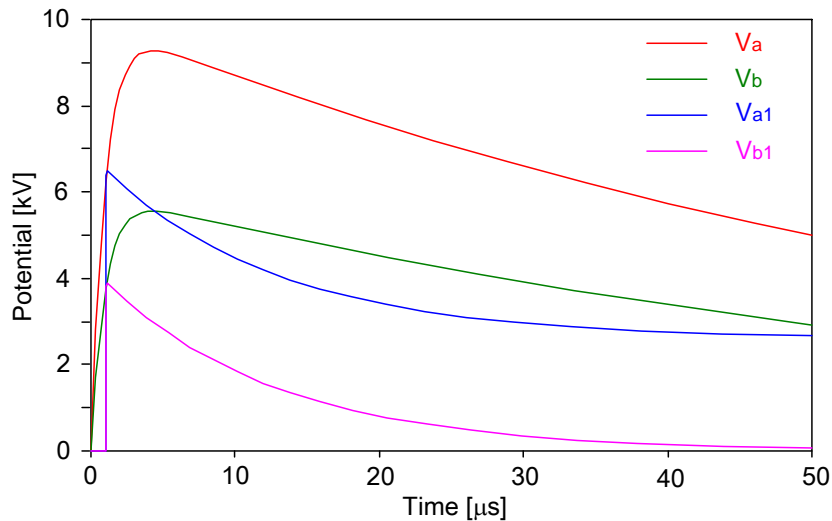


Fig. 2.22 EMTP simulated result

2.7 Surface charge decay

When a pipe is measured for 80 mm length with every 0.5 mm in z -direction and 2° in rotating axis, it will take 3 hours. In such a long time, some charge on the pipe surface may decay by the following three mechanisms; the leakage through volume and surface resistivity of the pipe, and the neutralization with ions supplied from air [10, 11].

To check how much the surface potential decays during the measuring process, the two-layer structure pipe with residual charge of surface discharge propagated under the application of 15.4 kV impulse voltage is scanned two times. The scanning time is 3 hours, which means the potential on the same point are scanned again after 3 hours. Table 2.9 and Fig. 2.23 (a) show the experimental conditions. Figures 2.23 (b) and (c) show the firstly scanned potential distribution and secondly scanned one, respectively. From these figures, potential profiles along z at $\xi = 12$ mm are extracted as shown in Fig. 2.24(a), and those along ξ at $z = 40$ mm are in Fig. 2.24(b).

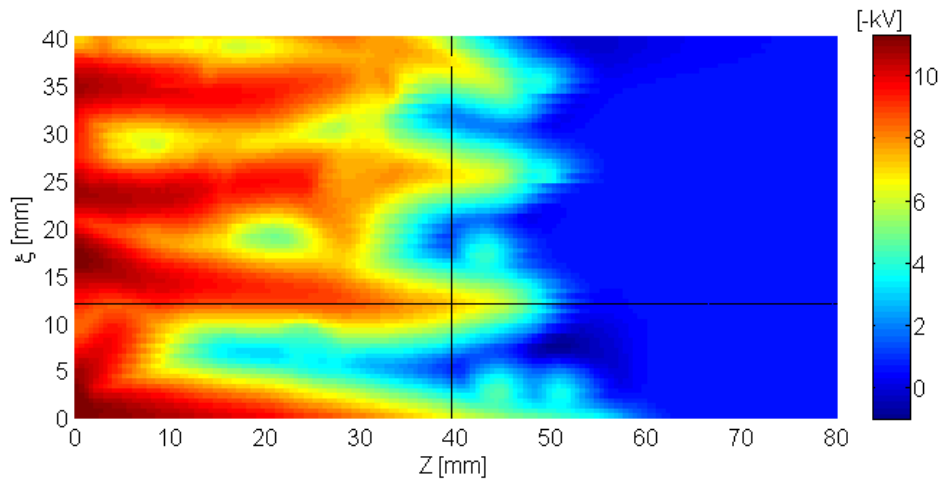
There is little difference between the two-dimensional potential distributions in Figs. 2.23(b) and 2.23(c). In the secondly scanned profile along ξ at $z = 40$ mm, the maximum value decreases to 90% of that in the firstly scanned profile. The potential gradient in the streamer section decreases to 75%, as shown in Fig. 2.24(a). It is possible to say that the charge decay during the measuring process has little influence on the measured potential on the insulator.

Table. 2.9 Experiment conditions

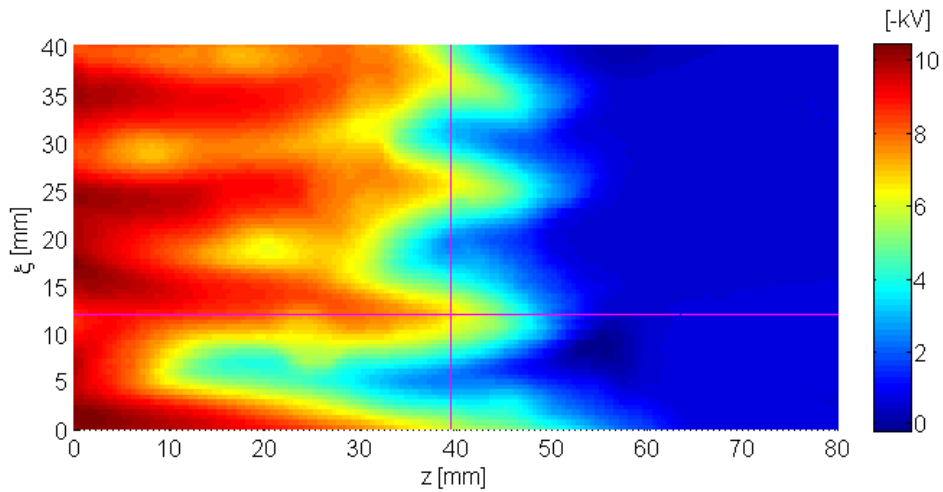
Insulator	200 μm -thick PET film
Back electrode	Grounded
Distance between ring electrodes	$d = 300\text{mm}$
Application Voltage	Impulse, 15.4 kV



(a)



(b)



(c)

Fig. 2.23 Two-dimensional potential distribution of surface streamer; (a) experimental condition, (b) firstly scanned result just after discharge, (c) secondly scanned result 3 hours later; the lines in the figures are respectively z at $\xi = 12$ mm and ξ at $z = 40$ mm.

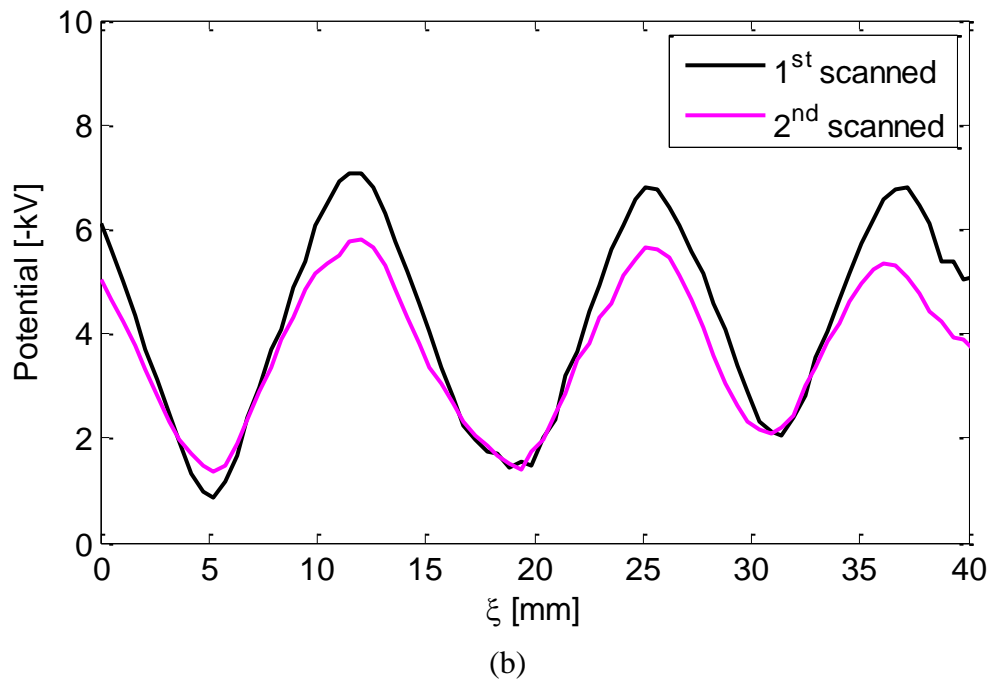
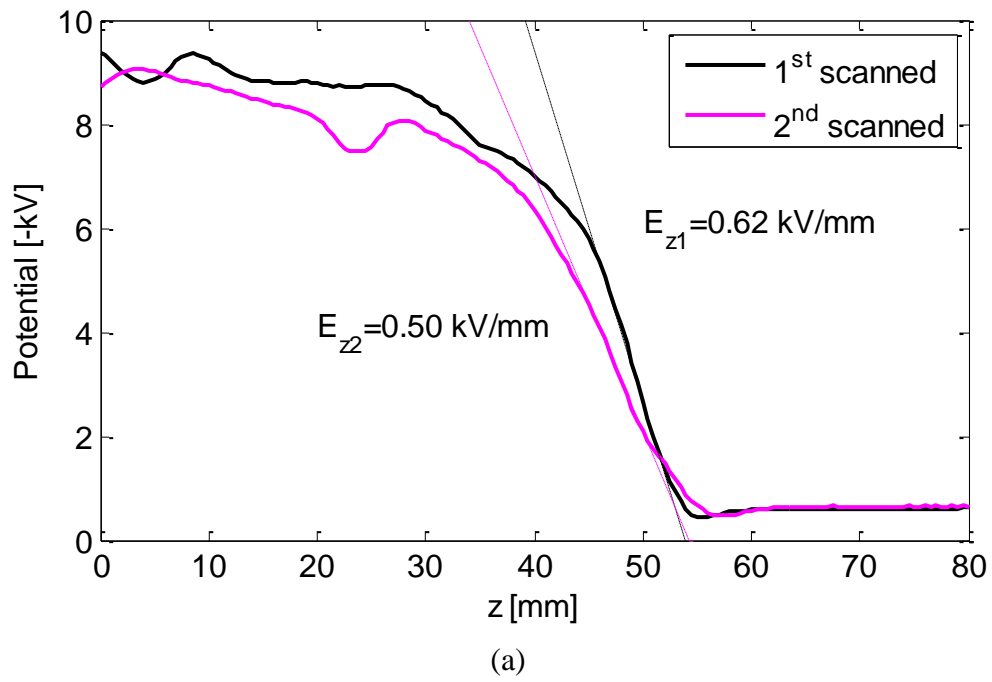


Fig.2.24 Change in potential profile along (a) z at $\xi = 12$ mm and (b) ξ at $z = 40$ mm

2.8 Summary

In this chapter, the experimental setup and measuring system are explained. A new impulse generator with a semiconductor thyristor switch is constructed, which shows a good performance.

To measure highly charged insulator, two-layer structure pipe is designed. The decay of the surface charge in 3 hours is about 10%, which shows the measuring results are acceptable.

References

- [1] IEEJ, “Handbook of Electrical Engineering” (in Japanese), 1988.
- [2] B. H. Blott and T. J. Lee. “A Two Frequency Vibrating Capacitor Method for Contact Potential Difference Measurement”. *J. Sci. Instrum.*, Vol.2, pp. 785-788, 1969.
- [3] R. J. D'Arcy and N. A. Surplice. “The effects of stray capacitance on the Kelvin method for measuring contact potential difference. *J.Phys. D: Appl. Phys.*, Vol. 3, pp. 482-488, 1970.
- [4] T. Takuma, M. Yashima, T. Kawamoto. “Measurement Principle of Charge Density Accumulated on the Surface of a Solid Insulator”, *Proceedings of the institute of electrostatics Japan*, Vol. 22, pp. 102-109, 1998.
- [5] Trek, Inc., “AC-feedback electrostatic voltmeter operation”, *Trek application note*, No. 3006, www.treking.com/pdf/3006_AC_Feedback_ESVM.pdf.
- [6] Trek Japan Inc., “The relation between the measured potential and distance”, www.treking.com/technology/data/data3.html.
- [7] A. Kumada, Y. Shimizu, M. Chiba, K. Hidaka, “Pockels Surface Potential Probe and Surface Charge Density Measurement”, *J. of Electrostatics*, Vol.58, 2003, pp.45-58.
- [8] A. Kumada, M. Chiba, K. Hidaka, “Potential Distribution Measurement of Back-discharge Phenomena by Using Electro-optic Effect”, *Trans. IEE of Japan*, Vol.121-A, Aug. 2001, pp. 797-798.
- [9] A. Kumada, M. Chiba, K. Hidaka, S. Hamada, T. Takuma, “The Direct Potential Distribution Measurement of Propagating Positive Surface Discharge by Using Pockels Effect”, *Trans. IEE of Japan*, Vol.120-A, Feb. 2000, pp. 2004-2010.

- [10] J. Kindersberger, C. Lederle, "Surface Charge Decay on Insulators in Air and Sulfurhexafluorid – Part I: Simulation", *IEEE Trans. on DEI*, Vol.15, Aug. 2008, pp. 941-948.
- [11] J. Kindersberger, C. Lederle, "Surface Charge Decay on Insulators in Air and Sulfurhexafluorid – Part II: Measurements", *IEEE Trans. on DEI*, Vol.15, Aug. 2008, pp. 949-957.

Chapter 3

Calculation Method of Surface Charge Density Distribution and Electrical Field Distribution

3.1 Introduction

With the potential measuring system, the potential distribution caused by the residual charge accumulated on the surface of the insulator pipe is measured. But the potential distribution is not the same as the charge distribution. When the electrostatic probe is used to measure the potential distribution, the calculation from the probe signal-output to the charge distribution is inevitable, because the probe signal-output is influenced by the surface charges on the measured object which are deposited not only in the front of the probe but also on the entire area of the object.

In recent years, with the development of the numerical computation techniques using computers, it is possible to treat more complicated objects with thousands of measuring points [1], [2], [3]. Prof. Hidaka, Prof. Kumada, and Dr. Okabe have introduced a digital image processing technique using the two-dimensional Fourier transformation in the spatial domain and the Tikhonov's regularization method for analyzing the details of charge distribution on an insulating plate, and have evaluated the spatial resolution of the measuring system [4], [5].

In this paper, an analysis method of surface charge density distribution and electrical field distribution is explained.

3.2 Multipoint measurement technique

A multi-point measuring technique with an electrostatic probe is used for measuring charge distribution as described in subsection 2.5. Figure 3.1 shows the principle of the multi-point measuring technique [7], [8], where the insulator surface is divided up into $M \times N$ elements. The probe's output potential $w(n_z, n_c)$, above each element is recorded. The probe output at position (n_z, n_c) is given by the summation of the induced voltage of the sensing electrode by accumulated charge on the insulator surface and the induced

voltage of the sensing electrode from the guard electrode:

$$w(n_z, n_\zeta) = \sum_{k_\zeta=1}^M \sum_{k_z=1}^N \{h(n_z - k_z, n_\zeta - k_\zeta)q(k_z, k_\zeta)\} + p \cdot w(n_z, n_\zeta), \quad (3.1)$$

where $h(n_z, n_\zeta)$ is a probe response sequence observed under such condition that the delta function $\delta(0, 0)$ is applied for q with the guard electrode being grounded. The response sequence “ h ” is called the point spread function (PSF). The second terms of Eq. (3.1), $pw(n_z, n_\zeta)$, represents the induced voltage of the sensing electrode from the guard electrode. The PSF and the coefficient “ p ” are numerically computed by using the surface charge method.

3.3 Surface charge distribution calculation and spatial resolution

For solving Eq. (3.1), the method reported in references [9, 10] is adopted as follows: By performing 2-dimensional Discrete Fourier Transformation (2D-DFT), Eq. (3.1) is written simply as

$$(1-p) \cdot W(f_z, f_\zeta) = H(f_z, f_\zeta) \cdot Q(f_z, f_\zeta), \quad (3.2)$$

where f_z and f_ζ are spatial frequencies and W, H, Q are 2D-DFT of w, h , and q , respectively.

Since the experimental noise is superimposed on the probe output distribution, w , the Tikhonov’s regularized technique based on the minimum least-squares error criterion is adopted in practice to solve Eq. (3.2) so as not to amplify excessively such noise.

The estimated solution $\hat{Q}(f_z, f_\zeta)$ is given by:

$$\hat{Q}(f_z, f_\zeta) = \frac{H^*(f_z, f_\zeta)}{|H(f_z, f_\zeta)|^2 + \frac{P_N}{P_S}} \cdot (1-p) \cdot W(f_z, f_\zeta) \quad (3.3)$$

where H^* is the complex conjugate of H and P_S and P_N are the power spectrum of the signal and noise, respectively. In this research, the experimental noise around 2% is superimposed on the measured value, small constant, whose amount is $\{0.02 |H(0, 0)|\}^2$, is substituted for P_N/P_S in Eq. (3.3).

Figure 3.2 shows the PSF for measuring 5 mm-thick PMMA pipe by the electrostatic probe with keeping 1-mm air gap. The 2D-DFT performed PSF, H , converges to 0 for high f_z and f_ζ as shown in Fig. 3.4.

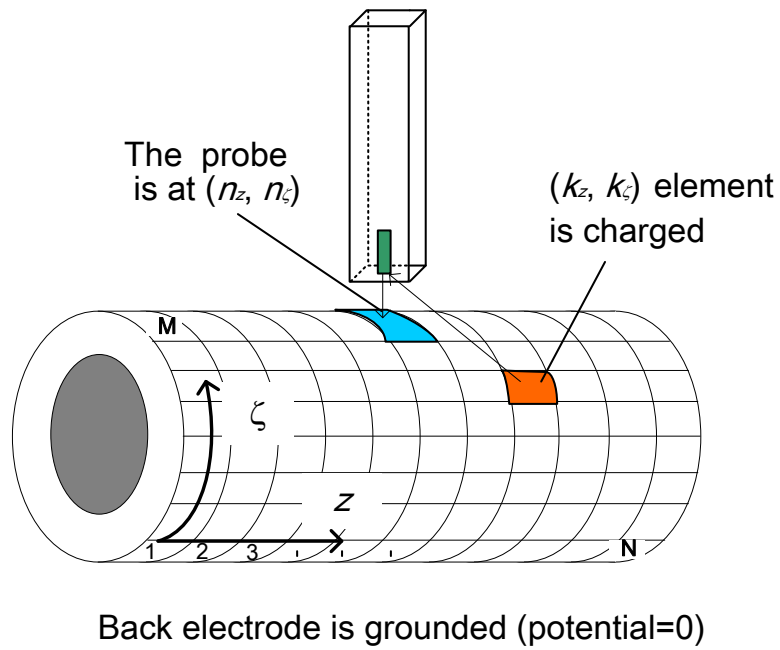


Fig. 3.1 Multipoint measurement.

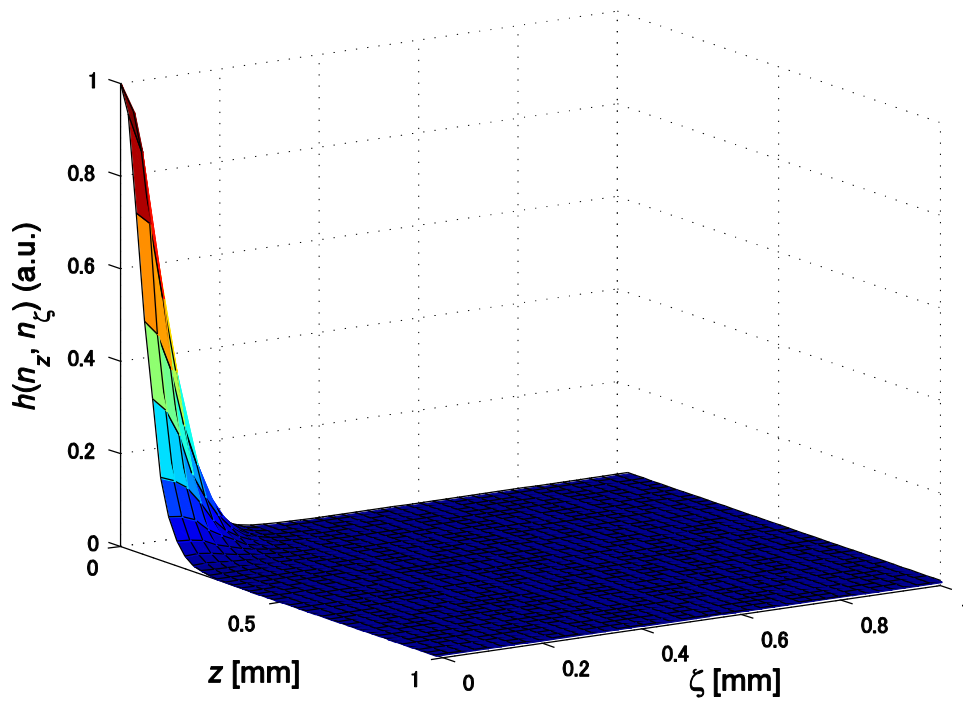


Fig. 3.2 PSF of the probe for charge measurement on 5 mm-thick PMMA.

By substituting Eq. (3.2) to Eq. (3.3), the relation between $\hat{Q}(f_z, f_\zeta)$ and $Q(f_z, f_\zeta)$ is expressed as

$$\hat{Q}(f_z, f_\zeta) = \frac{|H(f_z, f_\zeta)|^2}{|H(f_z, f_\zeta)|^2 + \frac{P_N}{P_S}} \cdot Q(f_z, f_\zeta). \quad (3.4)$$

The spatial resolution of the measuring system including the regularized inverse calculation can be defined as the reciprocal of the cutoff frequency where the intensity of transfer characteristics, $\frac{|H(f_z, f_\zeta)|^2}{|H(f_z, f_\zeta)|^2 + \frac{P_N}{P_S}}$, decreases to 0.5, in other words,

the reciprocal of the frequency where $|H(f_z, f_\zeta)|$ decreases to $0.02|H(0, 0)|$ [8,9]. The function $|H(f_z, 0)|$ and $|H(0, f_\zeta)|$ decreases to $0.02|H(0, 0)|$ at 0.58 cycle/mm and 0.55 cycle/mm, respectively as shown in Fig. 3.3. The spatial resolution for measuring along ζ -direction corresponds to $\lambda_\zeta = 1.7$ mm, and along z -direction to $\lambda_z = 1.8$ mm. As there is little difference between λ_ζ and λ_z , λ_z is tentatively adopted as representing value of the spatial resolution of the measuring system in this research.

The PSF expression in frequency domain of two-layer structure pipe and 200 μm -thick PET pipe are also calculated. Since the insulation layer is very thin, the difference between z -direction and ζ -direction is much smaller than that of 5 mm-thick PMMA pipe and does not influence the evaluation of spatial resolution, therefore, only PSF expression in z -direction is shown in Fig. 3.4.

The spatial resolution λ_z for measuring 5 mm-thick PMMA pipe, 200 mm-thick PET pipe, and two-layer structure pipe are calculated and listed in Table 3.1.

Table 3.1 Spatial resolution for different pipes.

	Spatial resolution λ_z [mm]
5 mm-thick PMMA pipe	1.8
Two-layer structure pipe	0.30
200 μm -thick PET pipe	0.28

For measuring thin insulator such as the two-layer structure cylindrical insulator described in 2.6, the 2D-DFT performed PSF, H , hardly decreases at higher spatial frequency as shown in Fig. 3.4. The estimated charge density σ at a measured point can be approximately given by the following simple scalar multiplication equation

$$\sigma = CV, \quad (3.6)$$

where C is the intrinsic capacitance to the grounded electrode for a unit area and V is the potential on that point. In this case, the transfer characteristics of measuring system forms the same shape with the normalized 2D-DFT performed PSF, which decreases 0.5 at the wavelength $\lambda_z = 0.8$ mm for two-layer structure pipe and $\lambda_z = 0.7$ mm for 200 μm -thick PET pipe.

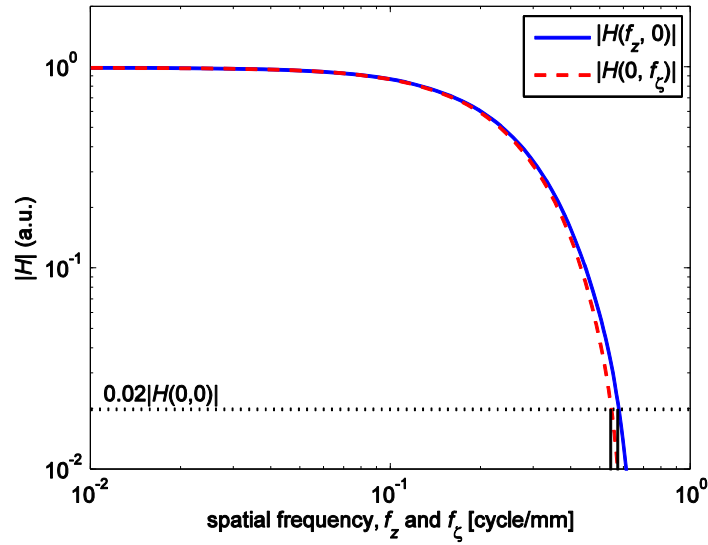


Fig. 3.3 PSF expression in frequency domain of 5 mm-thick PMMA pipe.

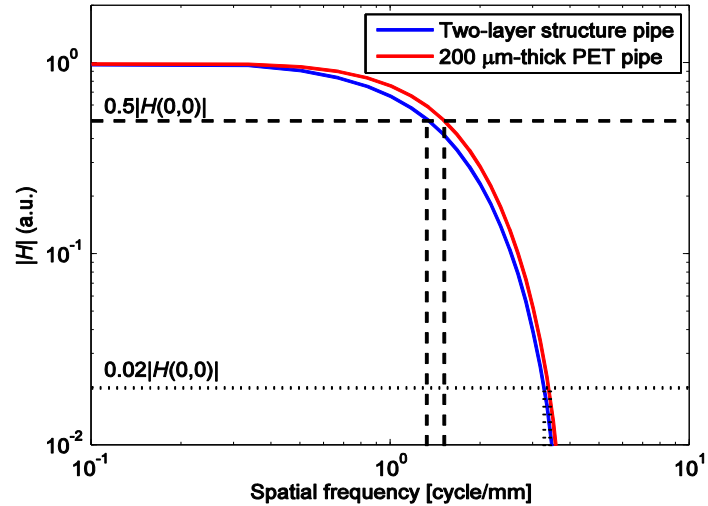


Fig. 3.4 PSF expression in frequency domain of two-layer structure pipe and 200 μm -thick PET pipe.

3.4 Electrical field distribution calculation

The calculation method of potential and electric field distributions on the insulator pipe just after the propagation of surface discharge are described in this subsection. For the two-layer structure pipe of the electrode configuration as shown in Fig. 3.5 and the 5 mm-thick PMMA pipe of the same electrode configuration, when 10 kV is applied to the HV electrode, the electrostatic potential at the point 20 mm away from the HV electrode is below 0.2 kV for two-layer structure pipe and below 0.8 kV for 5 mm-thick PMMA pipe, as shown in Fig. 3.6.

This suggests that the influence of the discharge electrode on the electric field at the point more than 20 mm away from the rod electrode is considerably low. The potential V and electrical field E (E_r , E_ζ , E_z) at the place of (n_ζ, n_z) on the insulator surface can be calculated by the following double convolution equations:

$$V(n_z, n_\zeta) = \sum_{k_\zeta=1}^M \sum_{k_z=1}^N \{h_v(n_z - k_z, n_\zeta - k_\zeta)q(k_z, k_\zeta)\} \quad (3.7)$$

$$E_r(n_z, n_\zeta) = \sum_{k_\zeta=1}^M \sum_{k_z=1}^N \{h_{er}(n_z - k_z, n_\zeta - k_\zeta)q(k_z, k_\zeta)\} \quad (3.8)$$

$$E_z(n_z, n_\zeta) = \sum_{k_\zeta=1}^M \sum_{k_z=1}^N \{h_{ez}(n_z - k_z, n_\zeta - k_\zeta)q(k_z, k_\zeta)\} \quad (3.9)$$

$$E_\zeta(n_z, n_\zeta) = \sum_{k_\zeta=1}^M \sum_{k_z=1}^N \{h_{e\zeta}(n_z - k_z, n_\zeta - k_\zeta)q(k_z, k_\zeta)\} \quad (3.10)$$

where $h_v(n_z, n_\zeta)$, $h_{er}(n_z, n_\zeta)$, $h_{ez}(n_z, n_\zeta)$, and $h_{e\zeta}(n_z, n_\zeta)$ are potential and electric field distributions under the condition that the delta function $\delta(0, 0)$ is applied for q , and are numerically computed using the charge simulation method. Fig. 3.7 shows schematic of two-layer structure pipe used for h functions calculation and the Fig. 3.8 shows the computed $h_v(n_z, n_\zeta)$, $h_{er}(n_z, n_\zeta)$, $h_{ez}(n_z, n_\zeta)$, and $h_{e\zeta}(n_z, n_\zeta)$ for the two-layer structure pipe.

To save the computational resource and time, the calculation is done in the frequency domain where Eqs (3.7) ~ (3.10) are expressed by simple scalar multiplications.

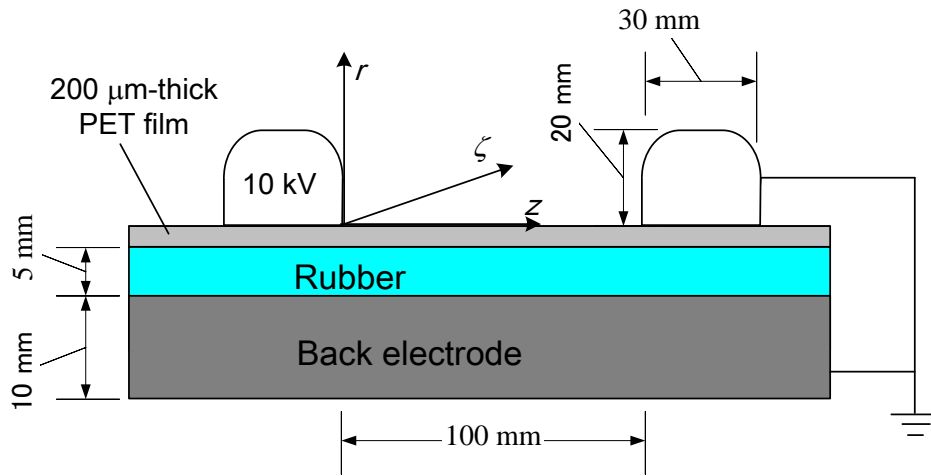


Fig. 3.5 Electrode configuration of two-layer structure pipe for potential distribution calculation.

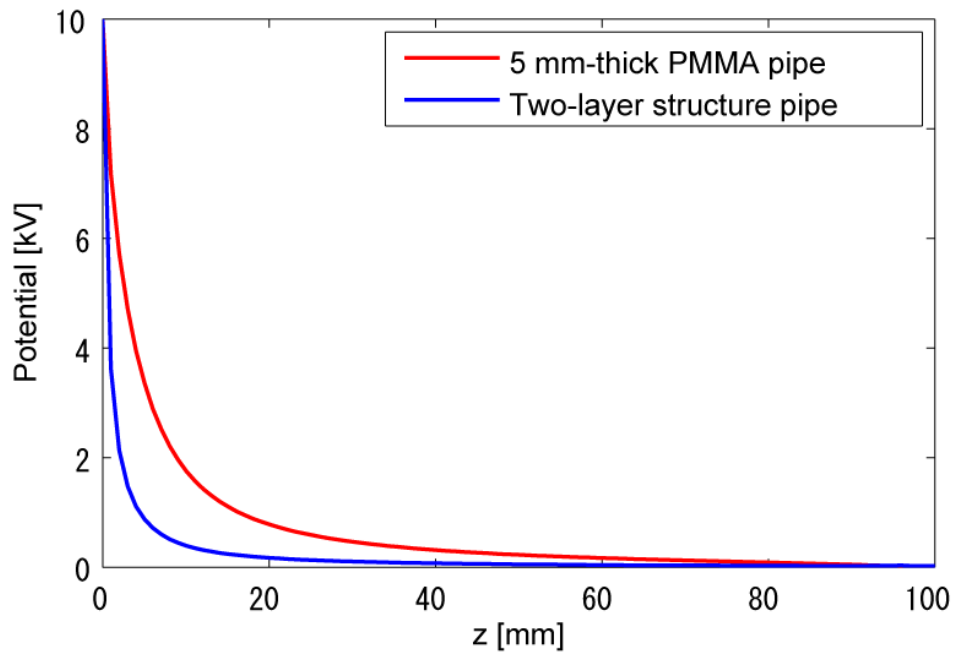


Fig. 3.6 Potential distribution induced by electrode under 10 kV application voltage.

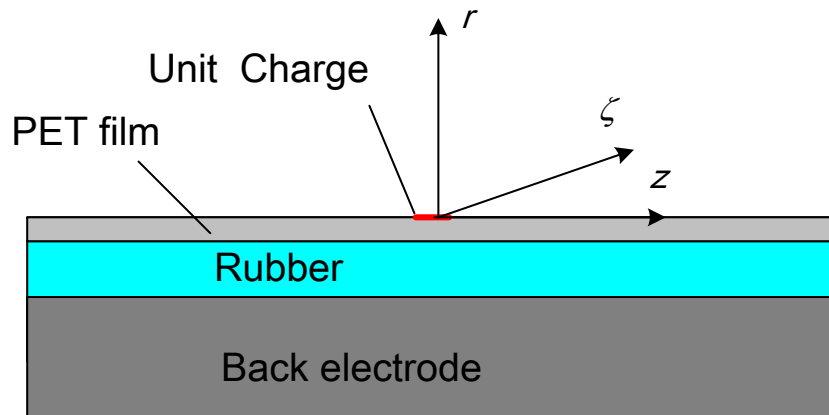


Fig. 3.7 Schematic of two-layer structure pipe used for h functions calculation.

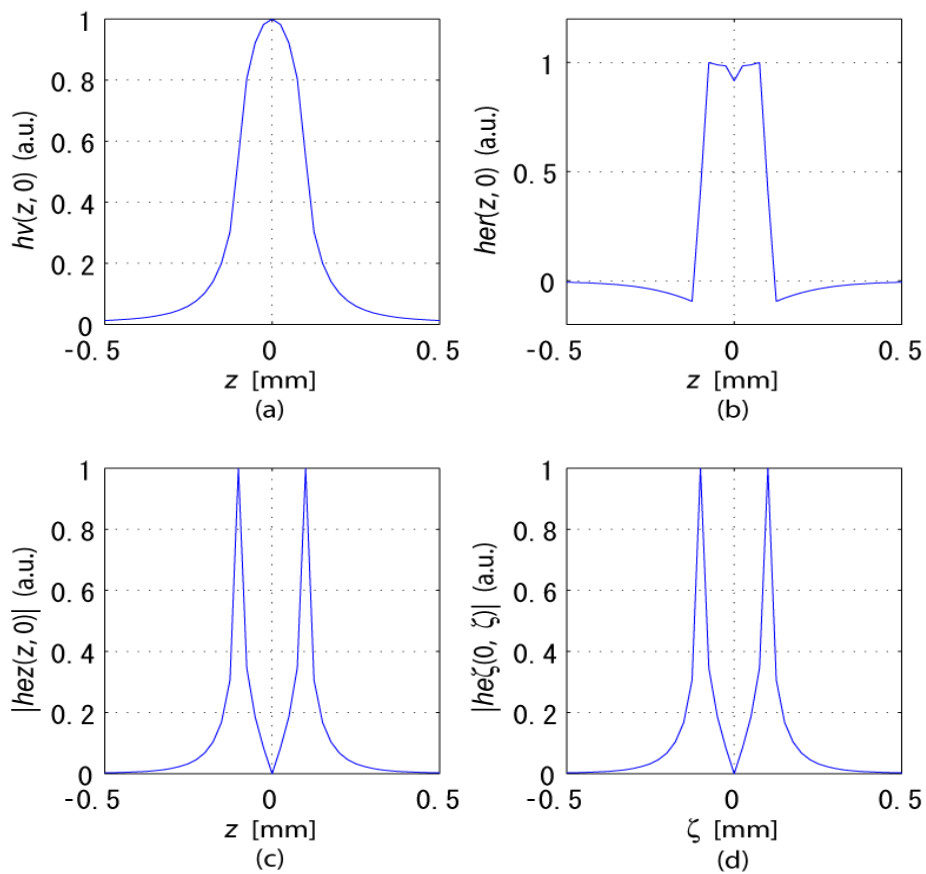


Fig. 3.8 The h functions of the two-layer structure pipe:

(a) $h_v(z, 0)$, (b) $h_{er}(z, 0)$, (c) $h_{ez}(z, 0)$, (d) $h_{e\zeta}(0, \zeta)$.

3.5 Summary

In this chapter, the calculation method of surface charge density distribution and electrical field distribution is described. In addition, the spatial resolution of the measuring system is calculated.

References

- [1] A. Kumada, Y. Shimizu, M. Chiba, K. Hidaka, "Pockels Surface Potential Probe and Surface Charge Density Measurement", *J. of Electrostatics*, Vol.58, 2003, pp.45-58.
- [2] A. Kumada, S. Okabe, "Charege Distribution Measurement on a Truncated Core Spacer under dc Voltage", *IEEE Trans. on DEI*, Vol.11, Dec. 2004, pp.929-938.
- [3] D.C. Faircloth, N.L. ALLen, "High Resolution Measurements of Surface Charge Densities on Insulator Surfaces", *IEEE Trans. on DEI*, Vol.10, April 2003, pp. 285-290.
- [4] A. Kumada, S. Okabe, K. Hidaka, "Residual charge distribution of positive surface streamer", *J. Phys. D: Appl. Phys*, Vol.42, 2009, 095209.
- [5] N.L. Allen, P.N. Mikropoulos, "Dynamics of streamer propagation in air", *J. Phys. D: Appl. Phys*, Vol.32, 1999, pp. 913-919.
- [6] T. Takuma, M. Yashima, T. Kawamoto, "Principle of Surface Charge Measurement for Thick Insulating Specimens", *IEEE Trans. on DEI*, Vol.5, Feb. 1998, pp.497-504.
- [7] A. Kumada, Y. Shimizu, M. Chiba, K. Hidaka, "Pockels Surface Potential Probe and Surface Charge Density Measurement", *J. of Electrostatics*, Vol.58, 2003, pp.45-58.
- [8] A. Kumada, S. Okabe, "Charege Distribution Measurement on a Truncated Core Spacer under dc Voltage", *IEEE Trans. on DEI*, Vol.11, Dec. 2004, pp.929-938.
- [9] I. Takahashi, "Surface Streamer propagation on Dielectric Barrier", Master Degree thesis of University of Tokyo, 2008.
- [10] N.L. ALLen, D.C. Faircloth, "Corona Propagation and Charge Deposition on a PTFE Surface", *IEEE Trans. on DEI*, Vol.10, April 2003, pp. 295-303.
- [11] D. Tanaka, S. Matsuoak, A. Kumada and K. Hidaka, "Two-dimensional potential and charge distributions of positive surface streamer", *J. Phys. D: Appl. Phys*, Vol.42, 2009, 075204.

Chapter 4

Propagation Characteristic of AC Surface Discharge

4.1 Introduction

The propagation characteristic of surface discharge under the application of power-frequency AC voltage is the most fundamental characteristics which should be studied. In this chapter, final propagation length of surface discharge, the relation between the discharge-occurrence phase and the propagation length, and the discharge pattern are measured by the high speed video camera with changing the insulator thickness.

4.2 Typical Discharge Images under AC and Impulse Application Voltage on PMMA Pipe Surface

In this section, the typical discharge images under AC and impulse application voltage on 5 mm-thick PMMA pipe surface, which are observed with the experimental setup shown in Fig. 2.1, are shown. Table 4.1 and Fig. 4.1(a) are the experimental conditions for AC experimental and Fig. 4.1 (b) are images of surface discharge under AC application voltage taken by high speed video camera whose exposure time is 22 μ s. Figure 4.1 (c) displays the image range taken by the high speed camera together with the structure schematic of surface discharge.

In this study, the length of the discharge is measured from the image from the electrode to the tip of streamer. In Fig. 4.1 (c), a leader discharge propagates in a stepwise way from the high voltage electrode to the grounded electrode. The leader discharge consists of a thin leader channel and filamentary streamers ahead of it.

Figure 4.2 shows the typical discharge images under impulse voltage application whose detailed experimental condition is described in Table 4.2. The image of positive impulse discharge shown in Fig. 4.2(c) is similar to those observed under AC voltage

application, while the negative impulse discharge shown in Fig. 4.2 (b) consists of leader channels and bunches of fine filamentary streamer.

Table 4.1 Experiment conditions

Insulator	5 mm-thick PMMA
Back electrode	Grounded
Distance between ring electrodes	$d = 100\text{mm}$
Exposure time	$22\ \mu\text{s}$
Application Voltage	60 kV AC voltage

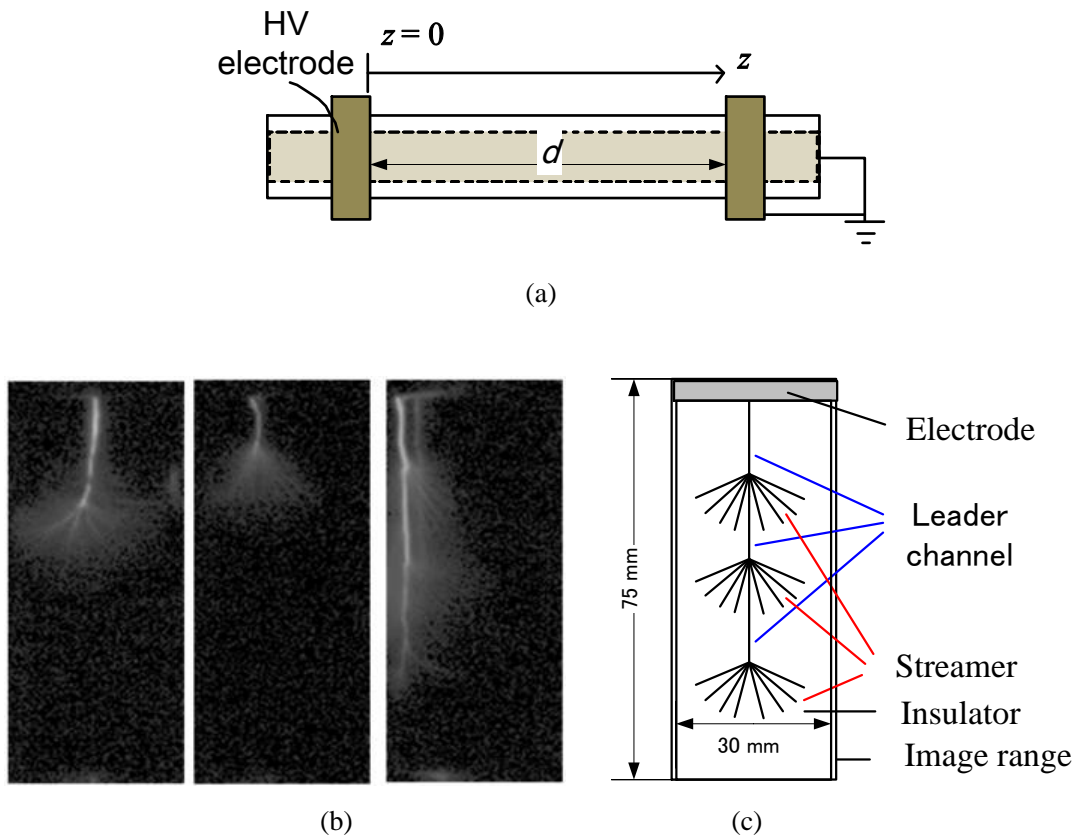


Fig. 4.1 Typical discharge images under AC application voltage: (a) experimental conditions, (b) typical images taken by high speed camera, (c) structure of leader discharge.

Table 4.2 Experiment conditions

Insulator	5 mm-thick PMMA
Back electrode	Grounded
Distance between ring electrodes	$d = 100\text{mm}$
Exposure time	$22\ \mu\text{s}$
Application Voltage	45 kV impulse voltage

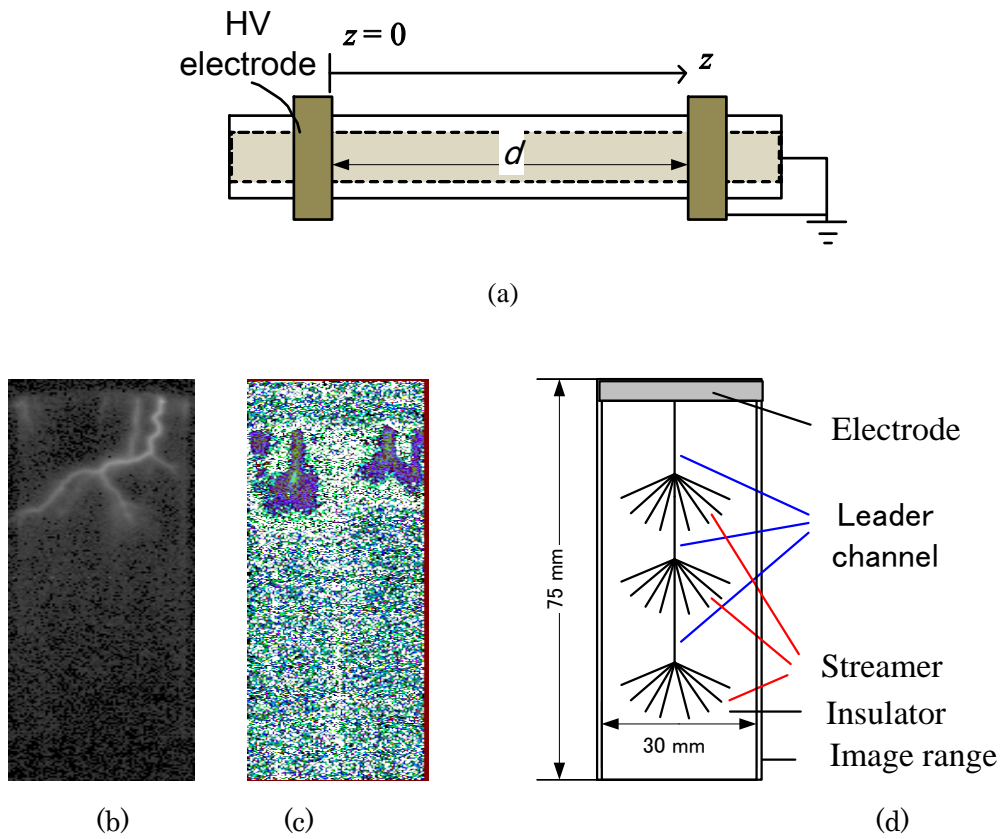


Fig. 4.2 Typical discharge images under impulse application voltage; (a) experimental conditions, (b) positive discharge image, (c) negative discharge image, (d) structure of leader discharge.

According to L. Niemeyer, the development of discharge in a non-uniform field gap can be schematically represented in Fig. 4.3 [1].

When the electrical field within a critical volume exceeds the critical value, primary electrons are produced by the negative ion detachment or by the field emission from the electrode, which is only under negative polarity, so that electron avalanches can grow. If the streamer transformation criterion is fulfilled, the ionization processes channel into filamentary streamers, and propagate beyond the limits of the critical volume, as shown in Fig. 4.3 (a).

The excitation and recombination processes within the first avalanches supply photo-ionizing quanta that trigger streamers at other locations to form the first corona with an envelope marked by a circle in Fig. 4.3 (b). The growth of the first corona eventually comes to a halt when the propagation conditions at the streamer tips ceased to be fulfilled. The electrons within the streamers then are rapidly attached and a pattern of positive and negative ion channels remains.

The former steamer channels, having received energy input from the current flow during the corona propagation phase, expand thermally, which became the origin of leader inception mechanism based on the channel expansion. If a sufficient number of streamers have fed their currents into a common stem then the latter receives an energy input that causes thermal expansion and a corresponding reduction of the gas density. This in turn reduced the critical field. Ionization then restarts and creates a conducting channel which becomes a leader section, as shown in Fig. 4.3 (c).

The leader is of good conductivity and can be served as an electrode from which new streamers can be launched and form a second corona with an envelope marked by a circle in Fig. 4.3 (d).

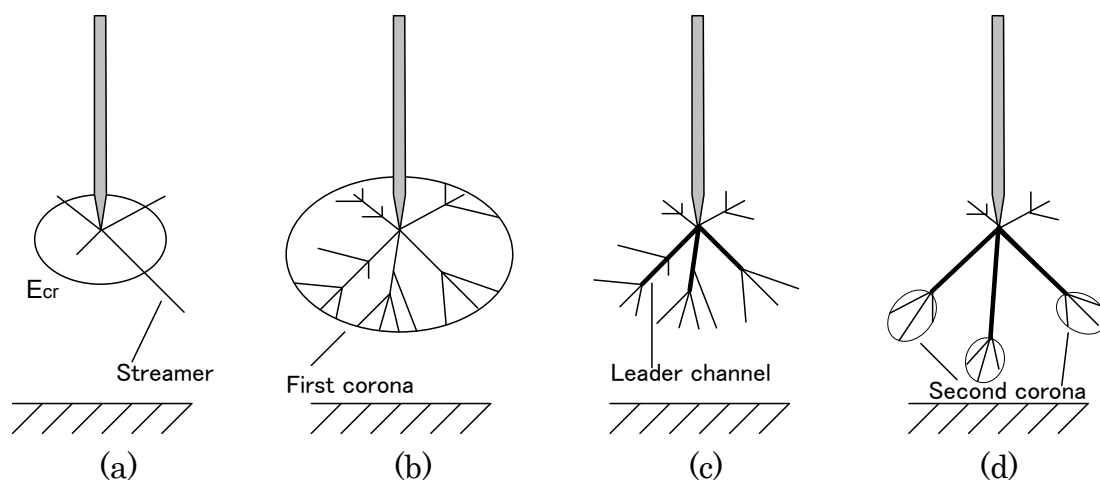


Fig. 4.3 Development of streamer and leader

4.3 The Influence of Grounding Conditions to Surface Discharge Propagation

The grounding condition of the back electrode will greatly influence the discharge propagation characteristics of surface discharge. Because the grounding condition of the back electrode will greatly influence the electrical field distribution and strength along the insulator surface. Table 4.3 and Fig. 4.4 (a) show the experimental conditions when the back electrode is grounded, the peak value of the applied AV voltage is 60 kV, and Table 4.4 and Fig. 4.5 (a) show the experimental conditions when the back electrode is ungrounded, the peak value of the applied AC voltage is 100 kV. The insulator is the same 5 mm-thick PMMA pipe and the distance between the two ring electrodes are both 100 mm.

Figure 4.4 (b) shows the relationship between the length of discharge and the phases of application voltage, and Fig 4.4 (c) shows the relationship between the length of discharges and the values of instantaneous voltage when the back electrode is grounded. The step number in the leader stem is also shown in here. All most all the discharges are found in the $-\pi \sim -0.5\pi$ range, that is, only when the instantaneous voltage is negative, and all the discharges start from the high voltage electrode. The short one step discharge occurs at the whole discharge range. With the increasing of absolute value of instantaneous voltage, the length and step number of the discharge increase.

Figure 4.5 (b) shows the relationship between the length of discharge and the phases of application voltage when the back electrode is ungrounded. The observed discharge number decreases greatly compared with that when the back electrode is grounded. The discharges occur at both the high voltage electrode side and grounded electrode side but only at the electrode whose voltage is at negative polarity.

Figure 4.6 shows the comparison of the leader length when the back electrode is grounded and ungrounded. When the back electrode is grounded, the discharge can occur at a much lower voltage and the leader can propagate much longer. This phenomenon can be explained as follows: When the back electrode is grounded, the electric field forms perpendicular to the surface of the pipe, and at the vicinity of the high voltage electrode, the field is very strong. On the other hand, with the ungrounded back electrode, the electric field distribution is almost parallel to the surface of the pipe. As reported in the reference [2], the discharge is easy to propagate when the field is perpendicular to the surface of the pipe.

The electrical field strength along the insulator surface is calculated using the electrical field calculation software UTEFC, which is developed by Hidaka-Kumda

Lab based on charge simulation method, and the results are shown in Fig. 4.7. When the back electrode is grounded, the electrical field nearby the high voltage is the strongest, and the electrical field nearby the grounded electrode is close to zero, as shown in Fig. 4.7 (a), that is why the discharges start only from the high voltage side. When the back electrode is ungrounded, the electrical field strength nearby the high voltage and the grounded electrode are almost the same, as shown in Fig. 4.7 (b), and is about half of the field strength nearby the high voltage electrode when the back electrode is grounded. If the influence of environmental factor is considered, the field nearby the high voltage electrode should be stronger than that nearby the grounded electrode. So the discharge occurs not only from the high voltage side, but also from the grounded electrode side.

Table 4.3 Experiment conditions

Insulator	5 mm-thick PMMA
Back electrode	Grounded
Distance between ring electrodes	$d = 200\text{mm}$
Application Voltage	60 kV AC voltage

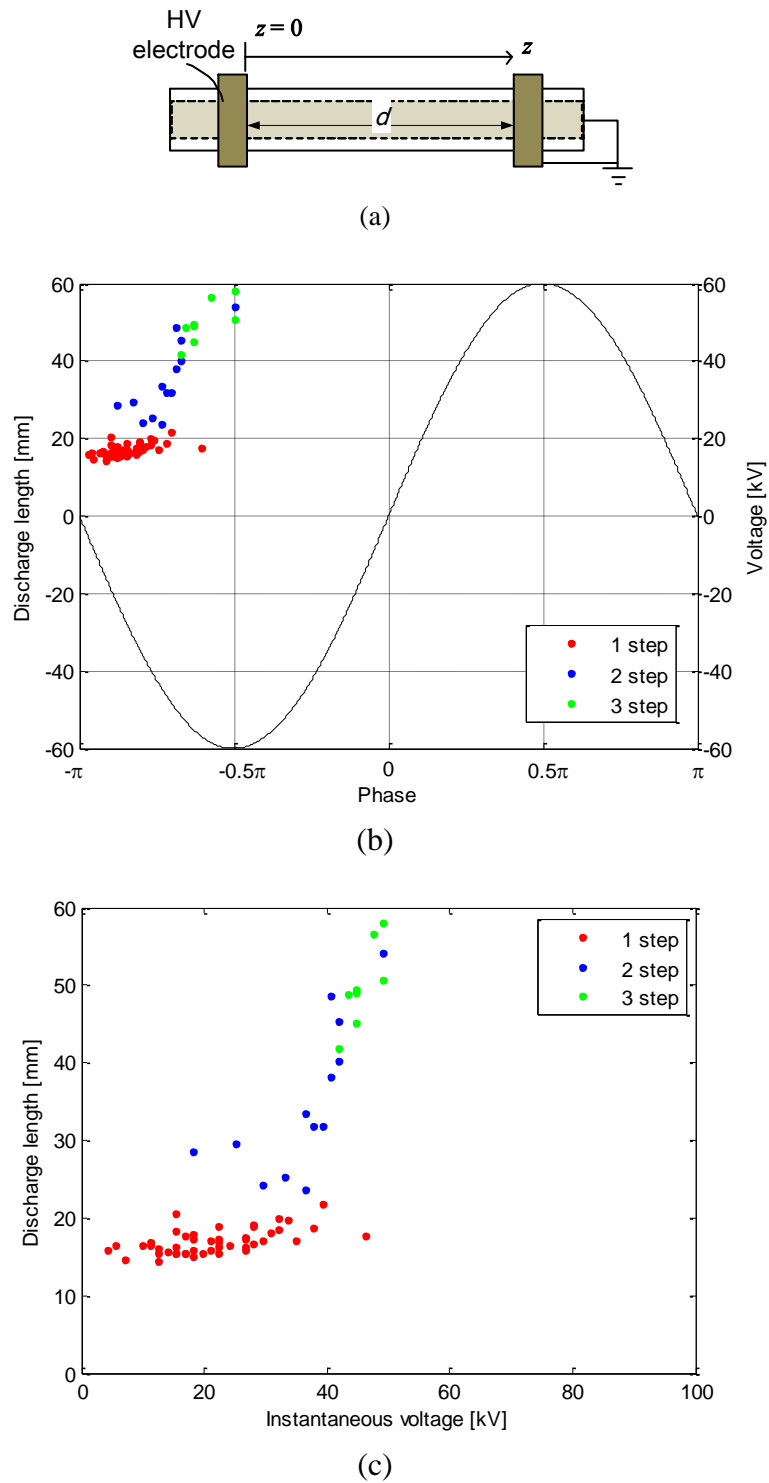
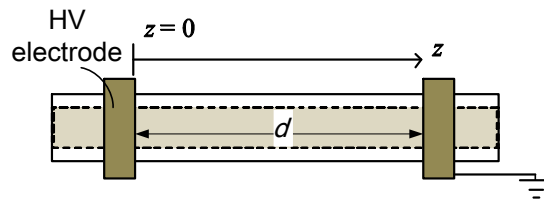


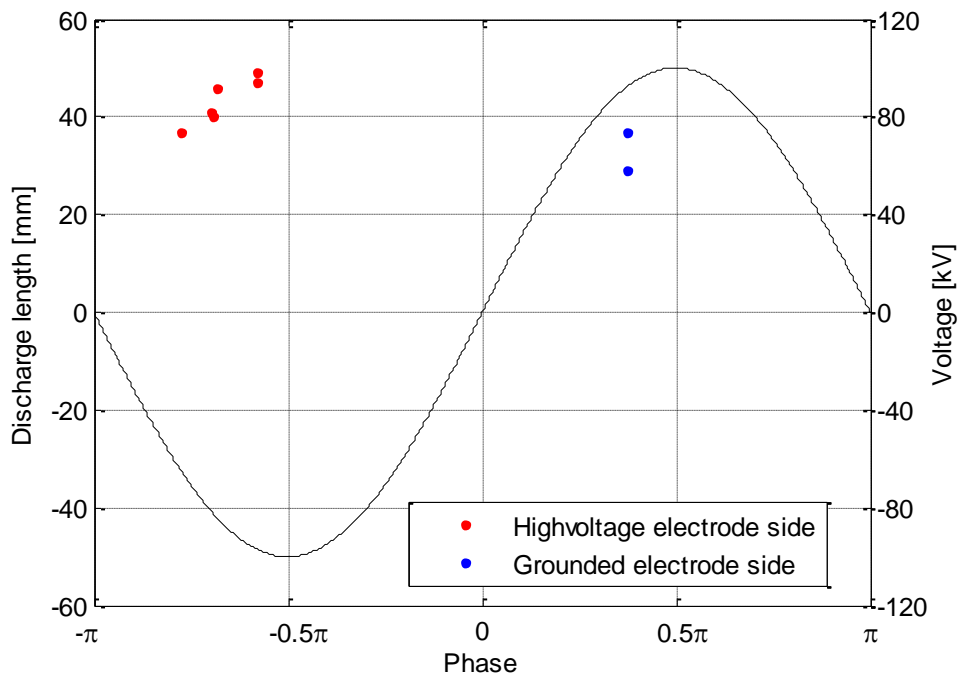
Fig. 4.4 Discharge propagation length when the back electrode is grounded; (a) experimental conditions, (b) relationship between the length of discharge and the phases of application voltage, (c) relationship between the length of discharges and the values of instantaneous voltage.

Table 4.3 Experiment conditions

Insulator	5 mm-thick PMMA
Back electrode	Ungrounded
Distance between ring electrodes	$d = 200\text{mm}$
Application Voltage	100 kV AC voltage



(a)



(b)

Fig. 4.5 Discharge propagation length when the back electrode is ungrounded; (a) experimental conditions, (b) relationship between the length of discharge and the phases of application voltage,

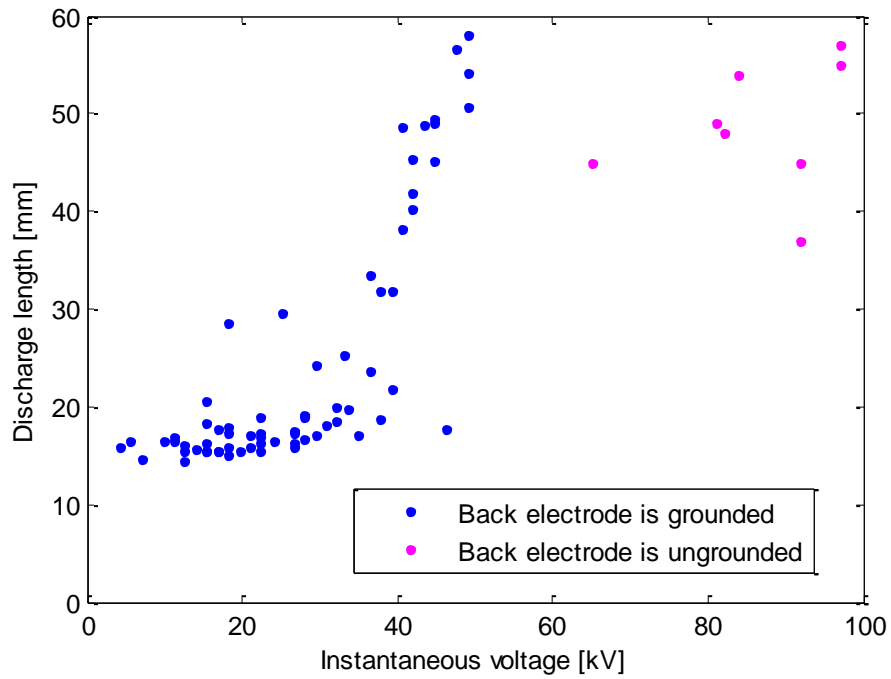


Fig. 4.6 Length of discharge when the back electrode is grounded and ungrounded

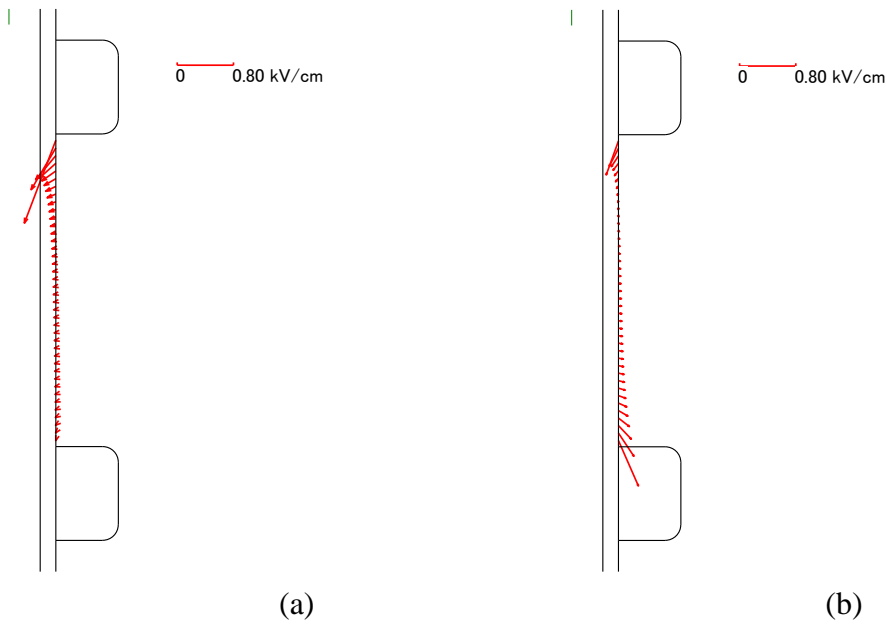


Fig. 4.7 Electrical field along insulator surface; (a) when the back electrode is grounded and (b) when the back electrode is ungrounded

4.4 Propagation Length and Occurrence Phase of AC Surface Discharge

4.4.1 Discharge propagation on 5 mm-thick PMMA pipe

AC voltage of 60 kV in its peak value is applied to the discharge electrode on the 5 mm-thick PMMA pipe, and the propagation of surface discharge is observed by the high speed video camera for 1 second, *i.e.*, 50 cycles. Table 4.4 and Fig. 4.8 show the experimental conditions. The exposure duration of each frame is set to 250 μ s.

As the discharge pattern hardly changes with the cycle number of the ac voltage application, the discharge photographs for a certain period are displayed in Fig. 4.10 as a typical case together with the voltage and current waveforms in Fig. 4.9. Fig. 4.10 (a) ~ (l) correspond respectively the discharge images taken at $t = 0$ ms, 1ms, ... , and 20 ms, in other words, at the phase $\phi = -\pi, -9\pi/10, \dots, 9\pi/10, \text{ and } \pi$.

In the region $\phi = -\pi$ to $-\pi/2$, the discharge length increases with the instantaneous voltage as shown in Fig. 4.10(a) to (e). Especially in $\phi = -\pi$ to $-\pi/4$, where the rising slope of voltage is fast, surface discharges can be seen in every frame; In $\phi = -3/4\pi$ to $-\pi/2$, the rising slope of the voltage becomes slower and surface discharges can not be seen in all frame. This phenomenon can be explained by the decrease of the electric field near the electrode due to the accumulated charge on the insulator surface. The electric field near the electrode is given by the superimposition of the applied field and the space charge field due to the residual charge of the surface discharges which have propagated on the insulator. The interval between the inceptions of a surface discharge and the previous surface discharge are determined by the increment of the applied field, and, therefore, it becomes longer when the rising slope of the application voltage is slow.

In the region $\phi = 0$ to $\pi/2$, short streamer discharges are observed as shown in Fig. 4.10(g) to (k). In this study, only the length of discharge in which leader occurs is considered, and the length of the short streamer discharge is not measured and not shown in the following figures. In the regions $\phi = -\pi/2$ to 0 and $\phi = \pi/2$ to π , no discharge is observed.

Changing the amplitude of the application voltage to 49 kV and 37 kV in its peak values, the propagations of surface discharge on 5 mm-thick PMMA pipe are observed and the results are shown in Figs. 4.11 to 4.14. Figures 4.11 and 4.12 show respectively the voltage and current waveforms and the discharge images taken under the application of 49 kV, and Figs. 4.13 and 4.14 show those under 37kV.

The information about the discharge length on 5 mm-thick PMMA pipe in 50 cycles is summarized in Fig. 4.15. Figure 4.15 (a) is the relationship between the length of discharge and its inception phases: Most discharges occur in the region of $\phi = -\pi$ to $-\pi/2$. With the increase of the application voltage. Figure 4.15 (b) is the relationship between the length of discharges and the instantaneous voltage. Under the same instantaneous voltage, the discharge length scatters widely, but the maximum discharge length increases almost linearly with the instantaneous voltage. Since the accumulated charge density on the insulator surface changes with time and place, the electrical field on the insulator surface also changes with time and place, and the propagation length of the discharge differs with each other even under the same instantaneous voltage. The maximum propagation length, as a stochastic result, increases almost linearly with the instantaneous voltage.

Figure 4.15 (c) shows the relationship between the maximum discharge length L_{\max} to the amplitude of AC voltage V_p . In this experiment, discharge images for 50 cycles are recorded and the maximum discharge length L_{\max} are obtained for each cycle.

In Fig. 4.15 (c), the longest 7 L_{\max} are plotted for each V_p , and L_{\max} can be fitted by the following equation:

$$L_{\max} = 0.17V_p^{1.5} \quad (4.1)$$

Table 4.4 Experiment conditions for the AC discharge on 5mm-thick PMMA sample.

Insulator	5 mm-thick PMMA
Back electrode	Grounded
Distance between ring electrodes	$d = 200\text{mm}$
Exposure time of each frame	$250\ \mu\text{s}$
Application Voltage	AC voltage
Amplitude of Voltage	$60\ \text{kV}_p, 49\ \text{kV}_p, 37\ \text{kV}_p$

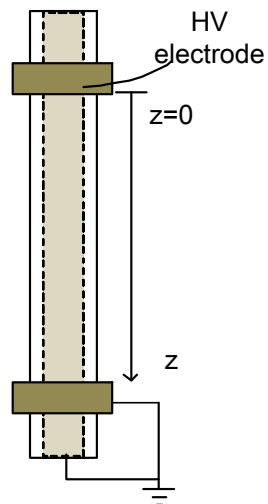


Fig. 4.8 Configuration of electrodes and insulator for AC discharge experiment.

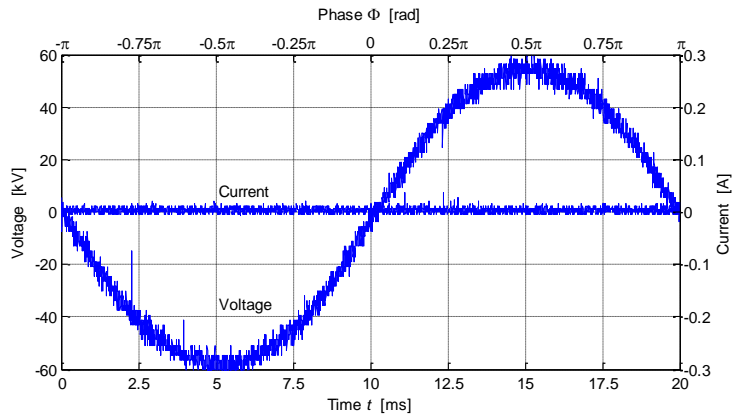


Fig. 4.9 Voltage and current waveforms for AC discharge on 5 mm-thick PMMA pipe.

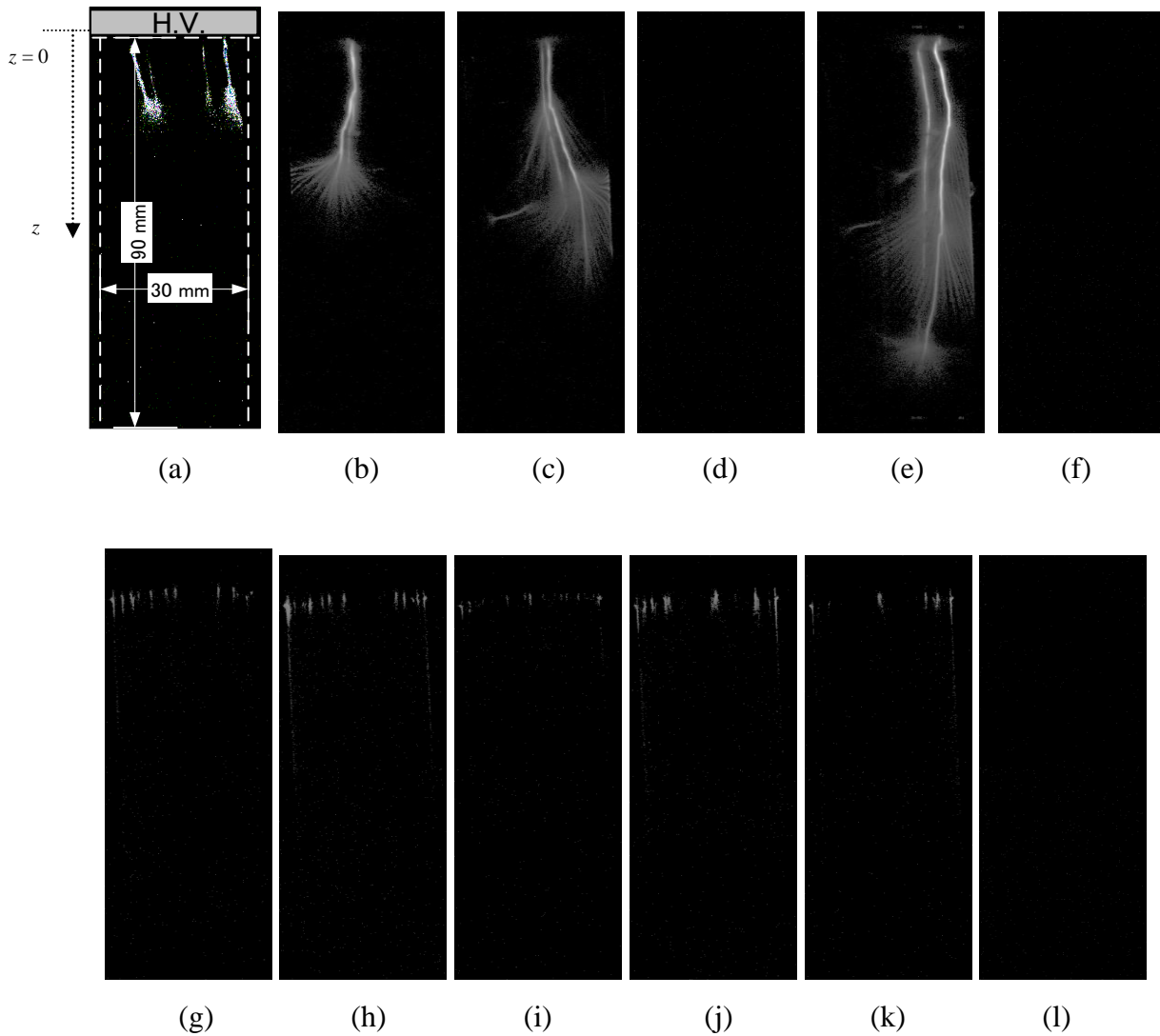


Fig. 4.10 Discharge images on 5 mm-thick PMMA pipe under 60 kV AC voltage taken at (a) $t = 0$ ms, (b) $t = 1$ ms, (c) $t = 2$ ms, (d) $t = 3$ ms, (e) $t = 4$ ms, (f) $t = 5 \sim 9$ ms, (g) $t = 10$ ms, (h) $t = 11$ ms, (i) $t = 12$ ms, (j) $t = 13$ ms, (k) $t = 14$ ms, (l) $t = 15 \sim 20$ ms.

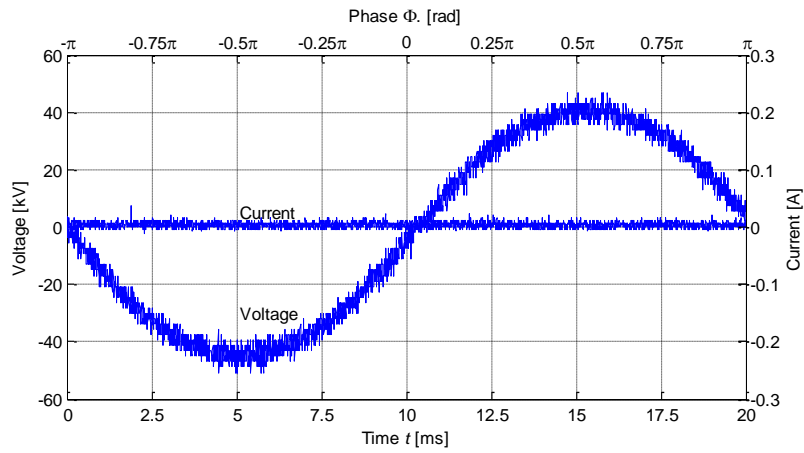


Fig. 4.11 Applied 49 kV AC voltage waveform and discharge current waveform on 5 mm-thick PMMA pipe.

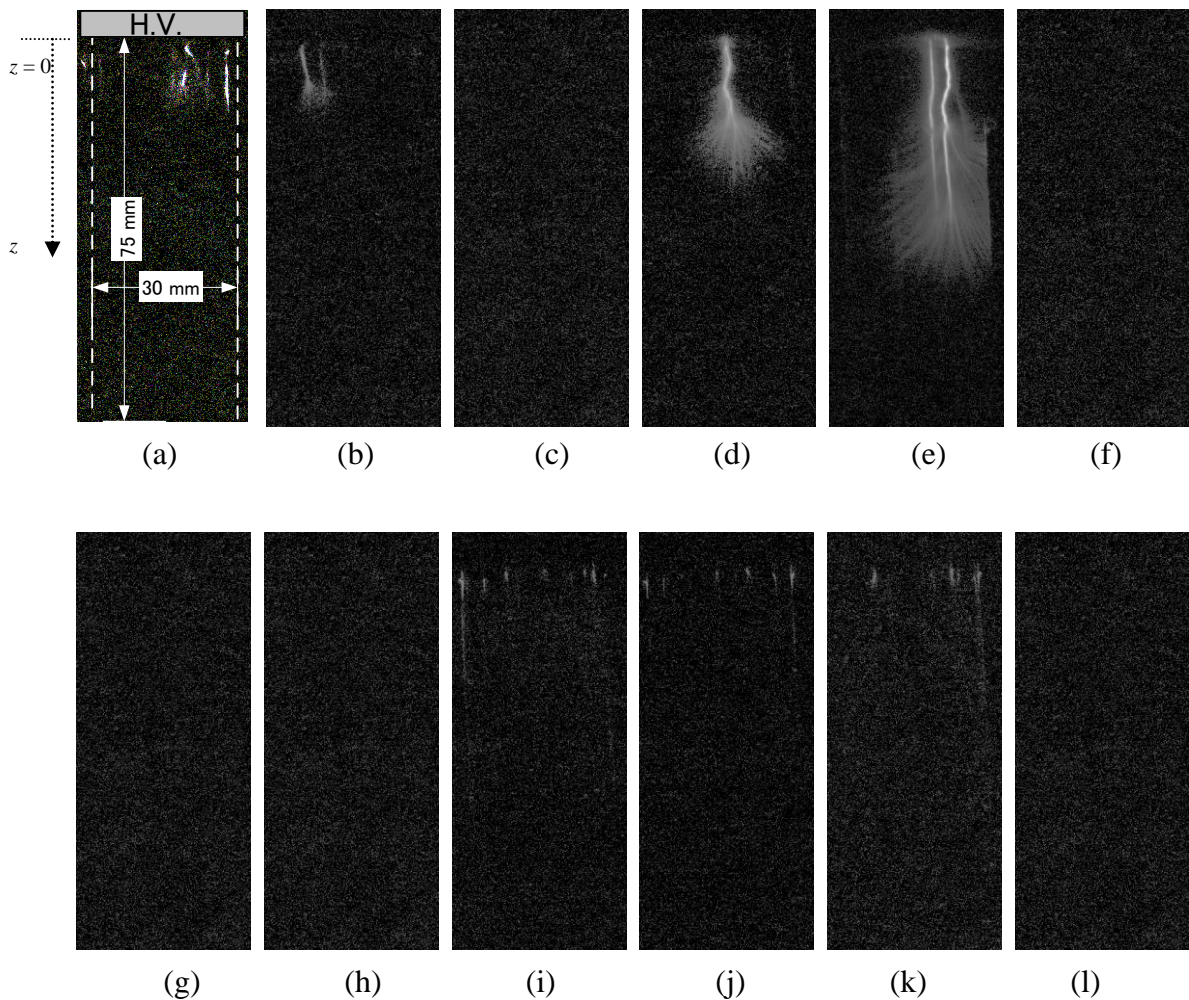


Fig. 4.12 Discharge images on 5 mm-thick PMMA pipe under 49 kV AC voltage taken at (a) $t = 0$ ms, (b) $t = 1$ ms, (c) $t = 2$ ms, (d) $t = 3$ ms, (e) $t = 4$ ms, (f) $t = 5 \sim 9$ ms, (g) $t = 10$ ms, (h) $t = 11$ ms, (i) $t = 12$ ms, (j) $t = 13$ ms, (k) $t = 14$ ms, (l) $t = 15 \sim 20$ ms.

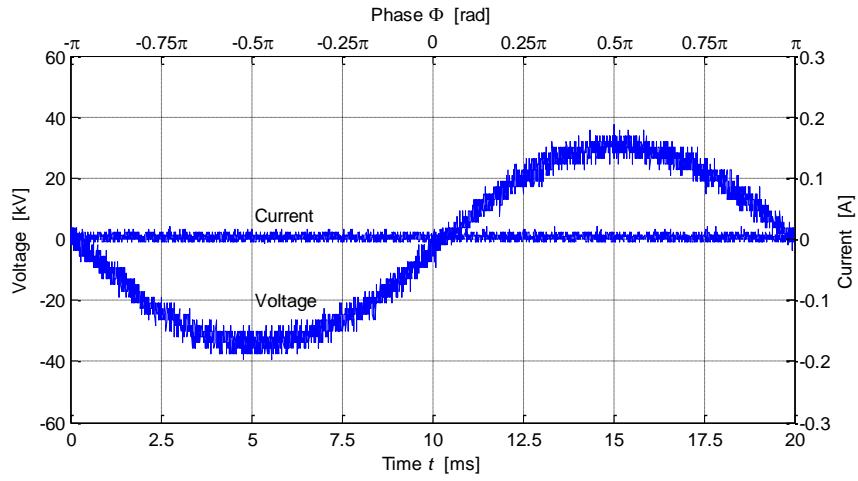


Fig. 4.13 37 kV application AC voltage waveform and discharge current waveform on 5 mm-thick PMMA pipe.

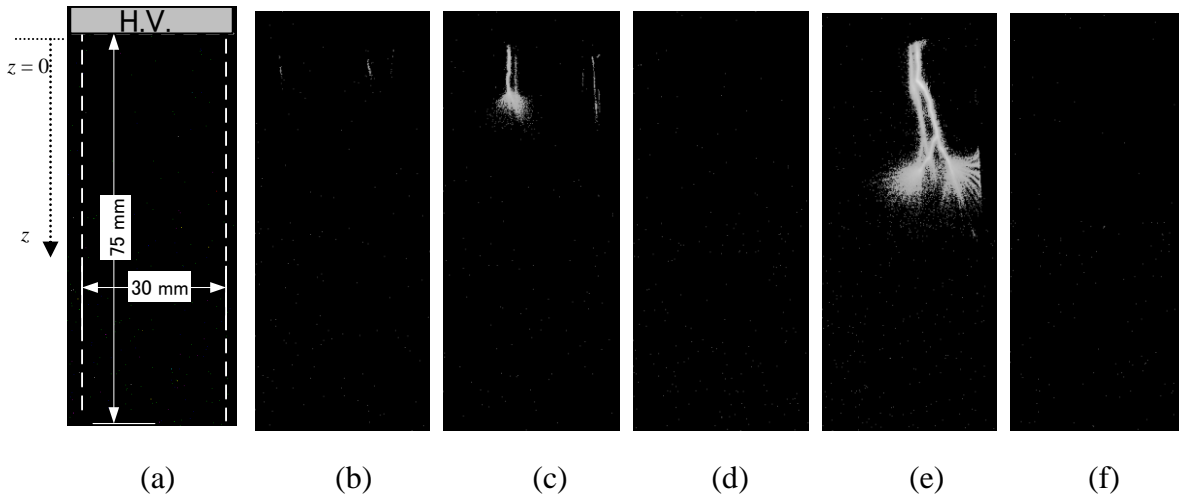
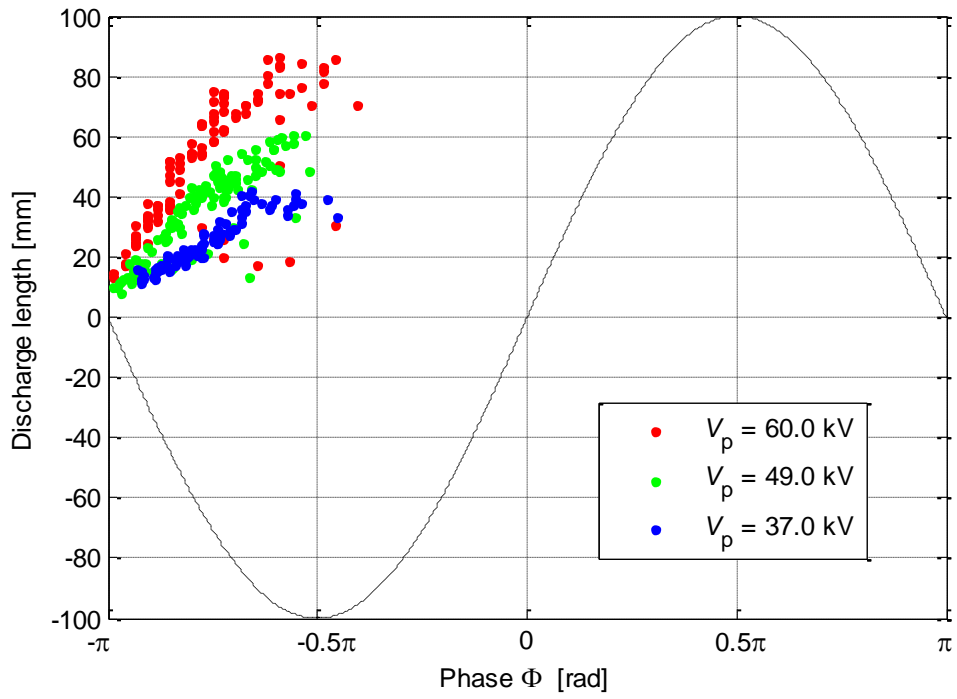
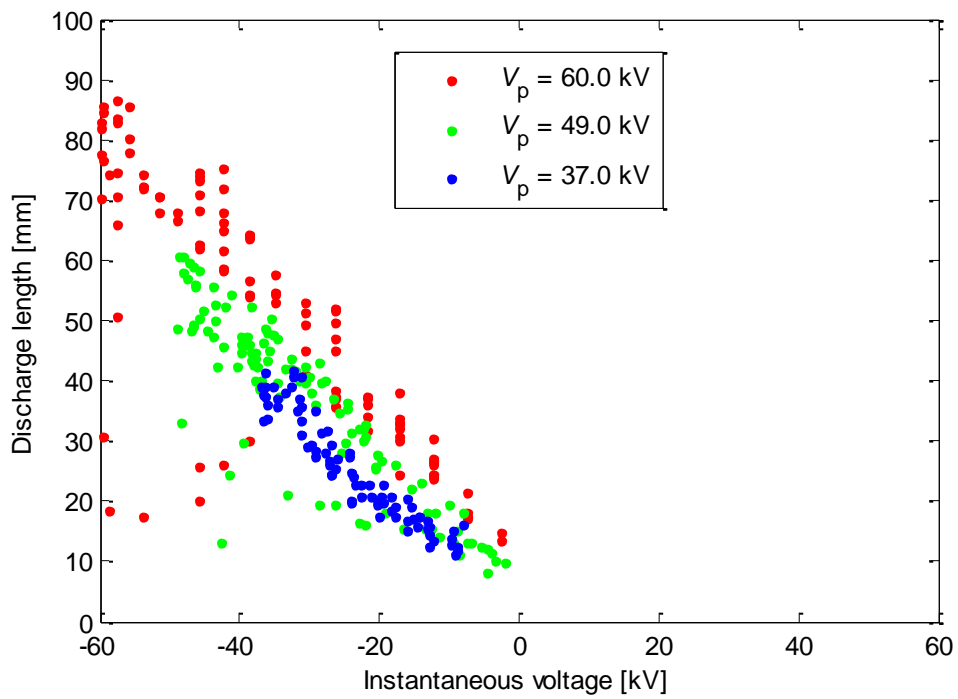


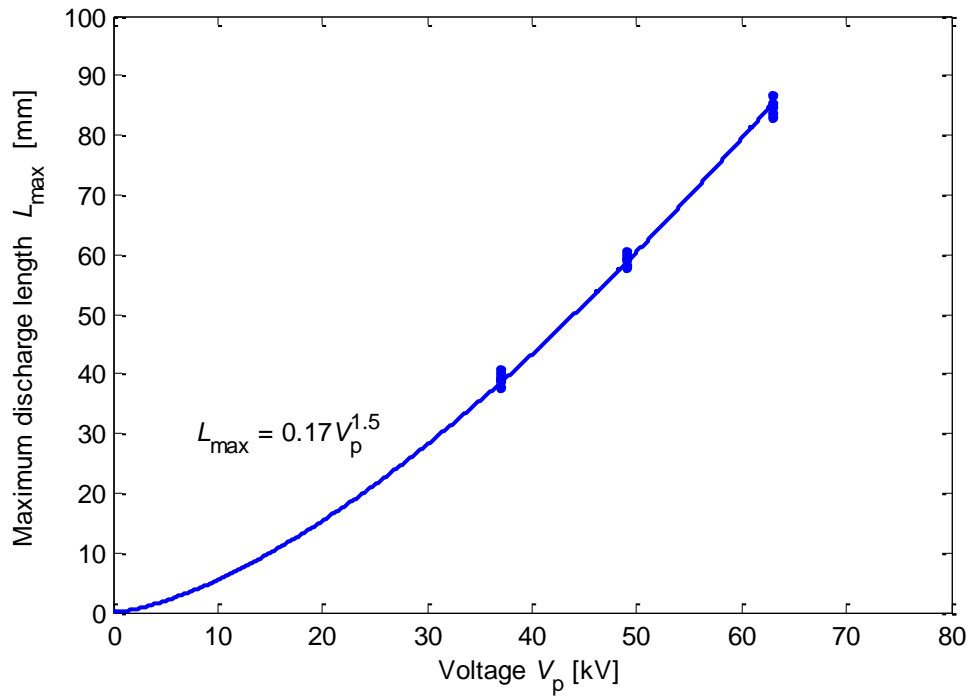
Fig. 4.14 Discharge images on 5 mm-thick PMMA pipe under 37 kV AC voltage taken at (a) $t = 0$ ms, (b) $t = 1$ ms, (c) $t = 2$ ms, (d) $t = 3$ ms, (e) $t = 4$ ms, (f) $t = 5 \sim 20$ ms.



(a)



(b)



(c)

Fig. 4.15 Propagation length of surface discharge on 5 mm-thick PMMA pipe; (a) relationship between the length of discharge and the inception phase, (b) relationship between the length of discharge and the instantaneous voltage, (c) maximum discharge length to the magnitude of AC voltage.

4.4.2 Discharge propagation on 3 mm - thick PMMA pipe

In the same manner, the propagation of surface discharge on 3 mm-thick PMMA pipe is observed by the high speed video camera for 50 cycles of AC voltage whose amplitude are set to 47.2 kV, 41.6 kV, 36 kV, and 30kV. Table 4.5 and Fig. 4.16 show the experimental conditions.

The discharge photographs for a certain period under the application 47.2 kV are displayed in Fig. 4.18 as a typical case together with the voltage and current waveforms in Fig. 4. 17. In the region $\phi = -\pi$ to $-\pi/2$, the discharge length increases with the instantaneous voltage as well as that on 5mm-thick PMMA shown in Figs 4.10 and 4.12 and 4.14. In the region $\phi = 0$ to $\pi/2$, where the positive voltage is applied to the high voltage electrode, streamer discharges and subsequent leader discharges are also observed and their length increases with the instantaneous voltage as shown in Fig. 4.18 (g) to (k). In the regions $\phi = -\pi/2$ to 0 and $\phi = \pi/2$ to π , no discharge is observed.

Figures 4.19 and 4.20 show the ac discharges on 3mm-thick PMMA pipe under the application of AC 41.6 kV. In this case, thin and short positive streamer discharges are observed in $\phi = 0$ to $\pi/2$ and positive leader discharge hardly observed as shown in Fig. 4.20(g) to (k).

The information about the discharge length on 3 mm-thick PMMA pipe in 50 cycles is summarized in Fig. 4.21. Figure 4.21 (a) shows the relationship between the length of discharge and its inception phase: the discharges occur not only in the region of $\phi = -\pi$ to $-\pi/2$, but also in the region of $\phi = 0$ to $\pi/2$. The occurrence number of discharge in $\phi = -\pi$ to $-\pi/2$, which hardly changes with the amplitude of ac voltage, is bigger than that in $\phi = 0$ to $\pi/2$, which increases with the amplitude of ac voltage.

Fig. 4.21 (b) shows the relationship between the length of discharges and the instantaneous voltage. As well as the discharge on 5 mm-thick PMMA pipe shown in Fig. 4. 15(b), the discharge length scatters widely for the same instantaneous voltage, whereas the maximum discharge length increases as a function of the instantaneous voltage.

In the same manner with Fig. 4. 15(c), the relationship between the longest L_{\max} and V_p is displayed in Fig. 4. 20(c). The L_{\max} can be fitted by the following equation:

$$L_{\max} = 0.022V_p^{2.1} \quad (4.2)$$

Table 4.5 Experiment conditions

Insulator	3 mm-thick PMMA
Back electrode	Grounded
Distance between ring electrodes	$d = 200\text{mm}$
Exposure time of each frame	$250\ \mu\text{s}$
Application Voltage	AC voltage,
Amplitude of Voltage	$47.2\ \text{kV}_p$, $41.6\ \text{kV}_p$, $36\ \text{kV}_p$, $30\ \text{kV}_p$

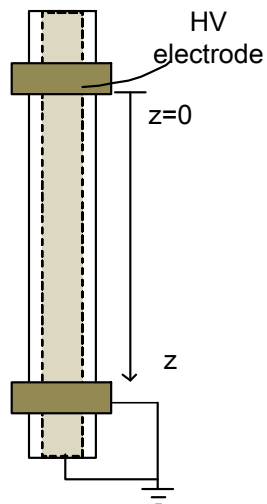


Fig. 4.16 Configuration of electrodes and insulator for AC discharge experiment.

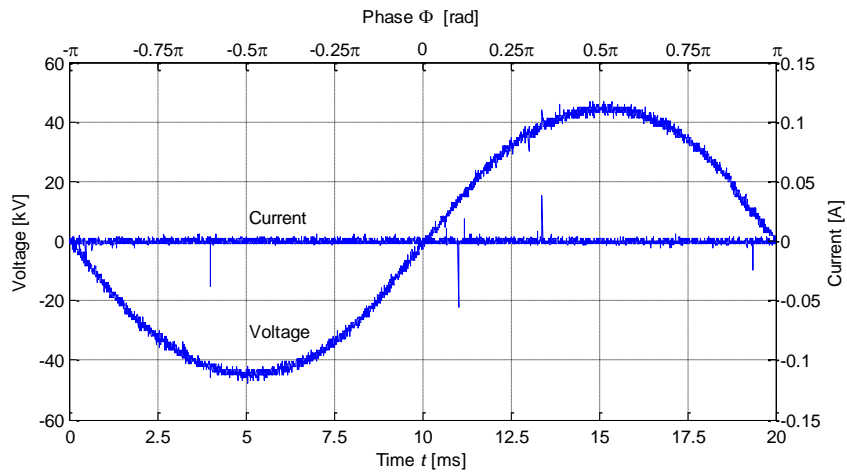


Fig. 4.17 47.2 kV application AC voltage waveform and discharge current waveform on 3 mm-thick PMMA pipe.

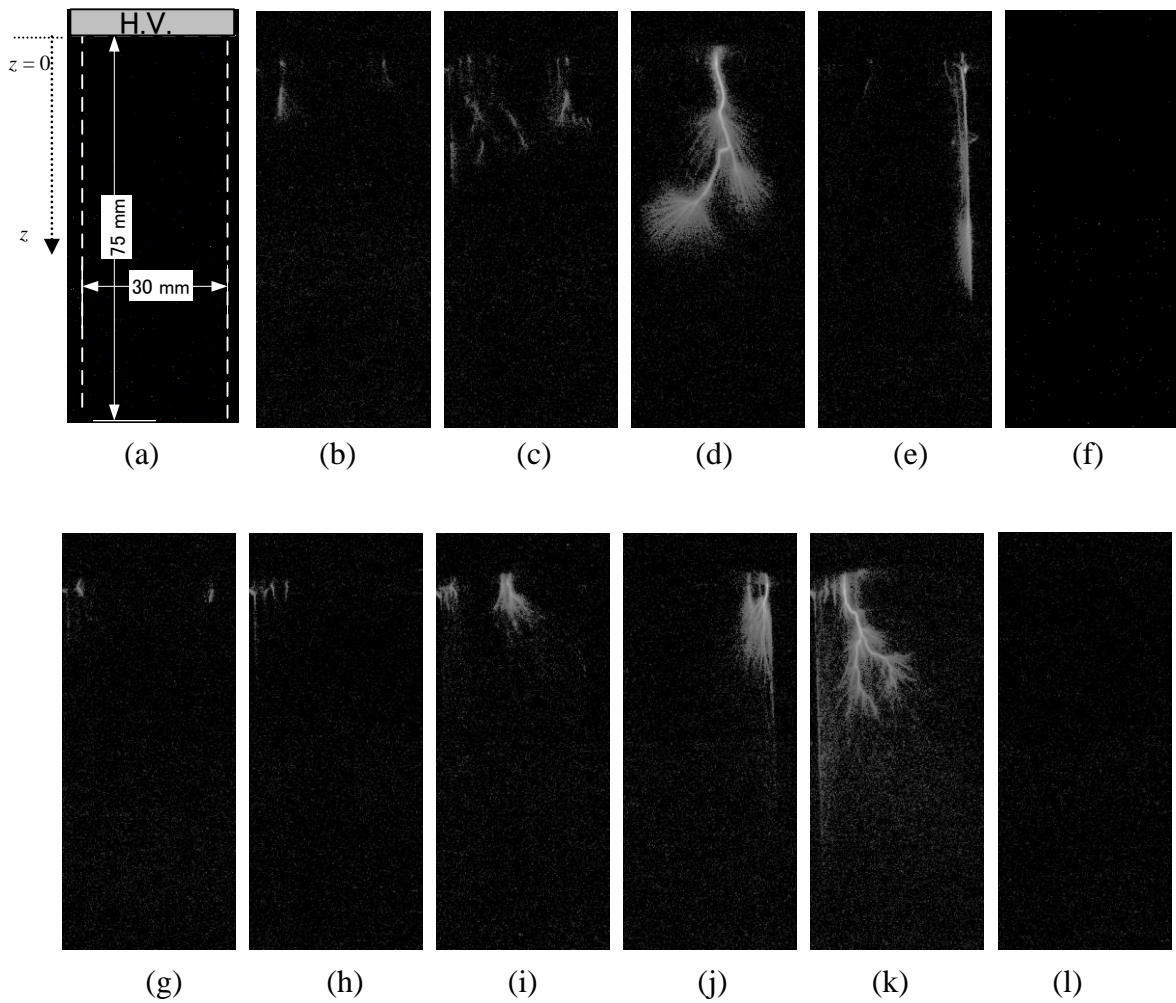


Fig. 4.18 Discharge images on 3 mm-thick PMMA pipe under 47.2 kV AC voltage taken at (a) $t = 0$ ms, (b) $t = 1$ ms, (c) $t = 2$ ms, (d) $t = 3$ ms, (e) $t = 4$ ms, (f) $t = 5 \sim 9$ ms, (g) $t = 10$ ms, (h) $t = 11$ ms, (i) $t = 12$ ms, (j) $t = 13$ ms, (k) $t = 14$ ms, (l) $t = 15 \sim 20$ ms.

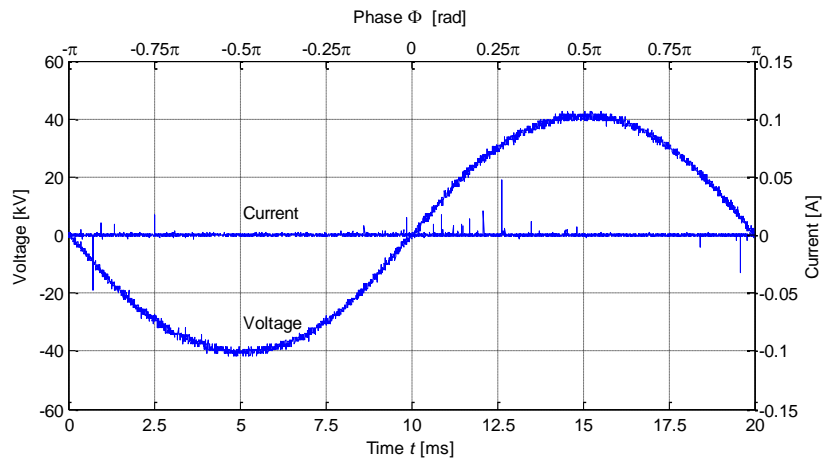


Fig. 4.19 41.6 kV application AC voltage waveform and discharge current waveform on 3 mm-thick PMMA pipe.

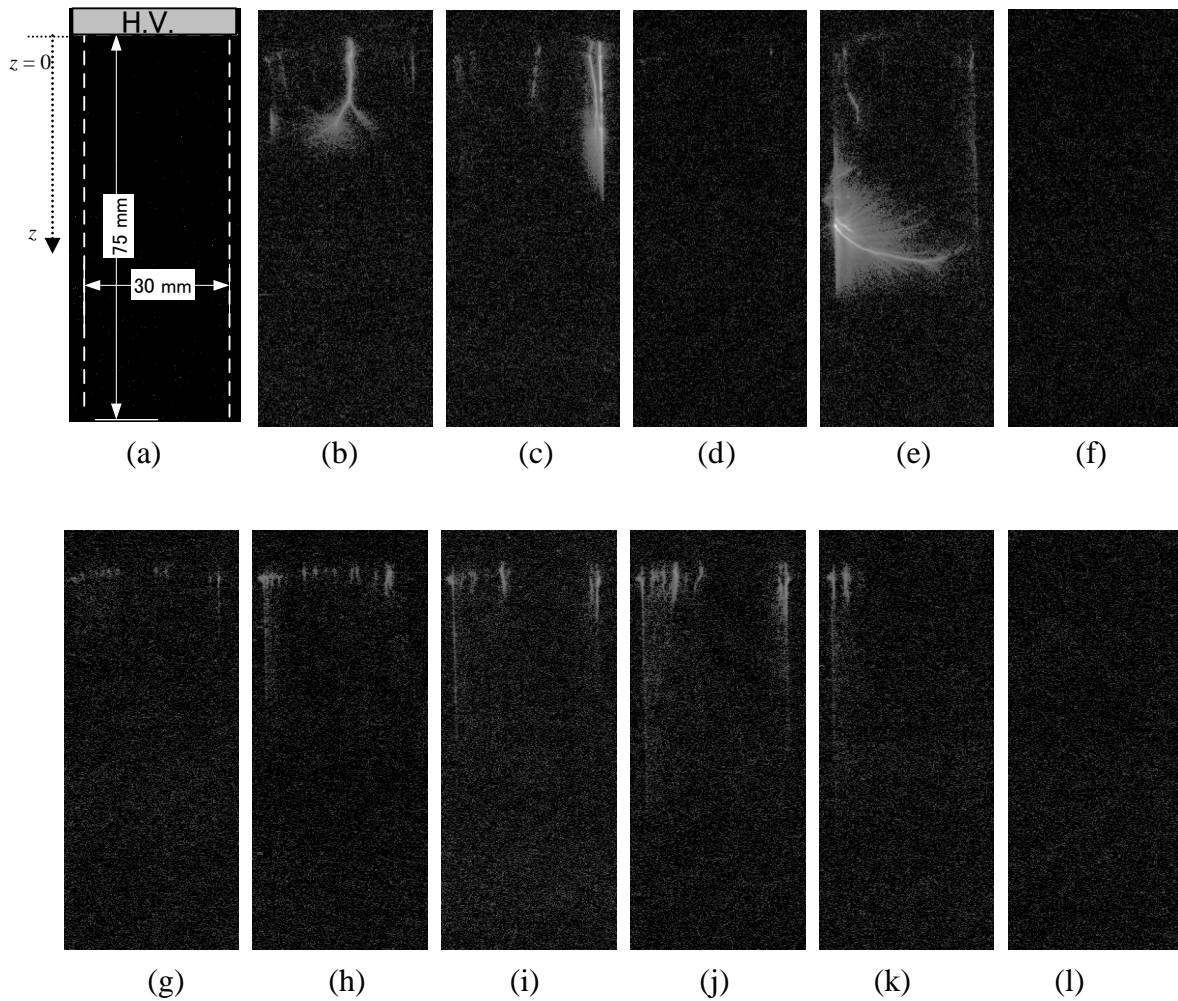
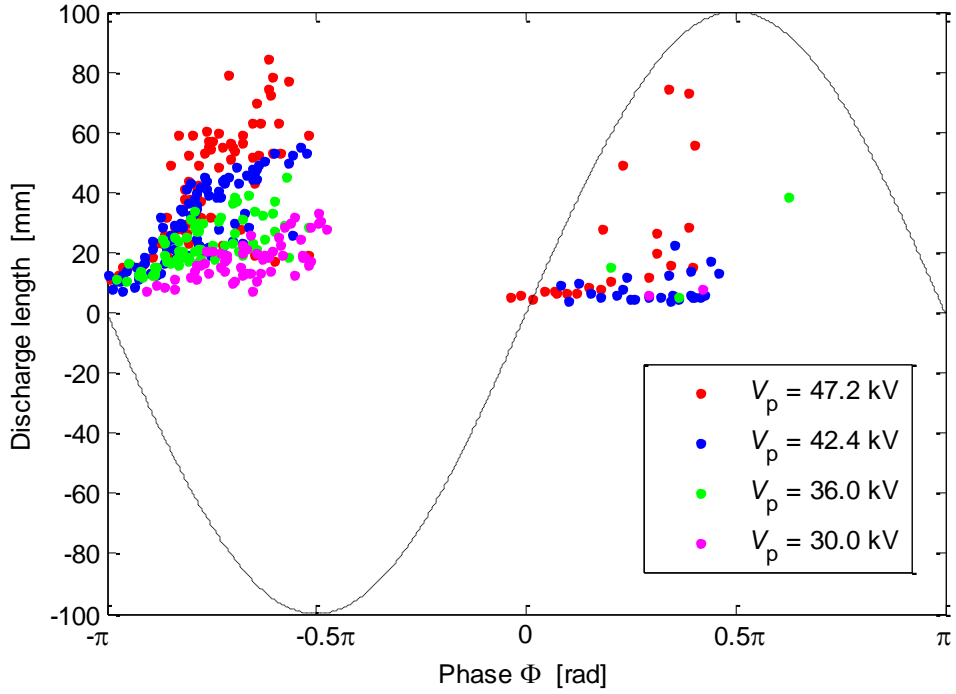
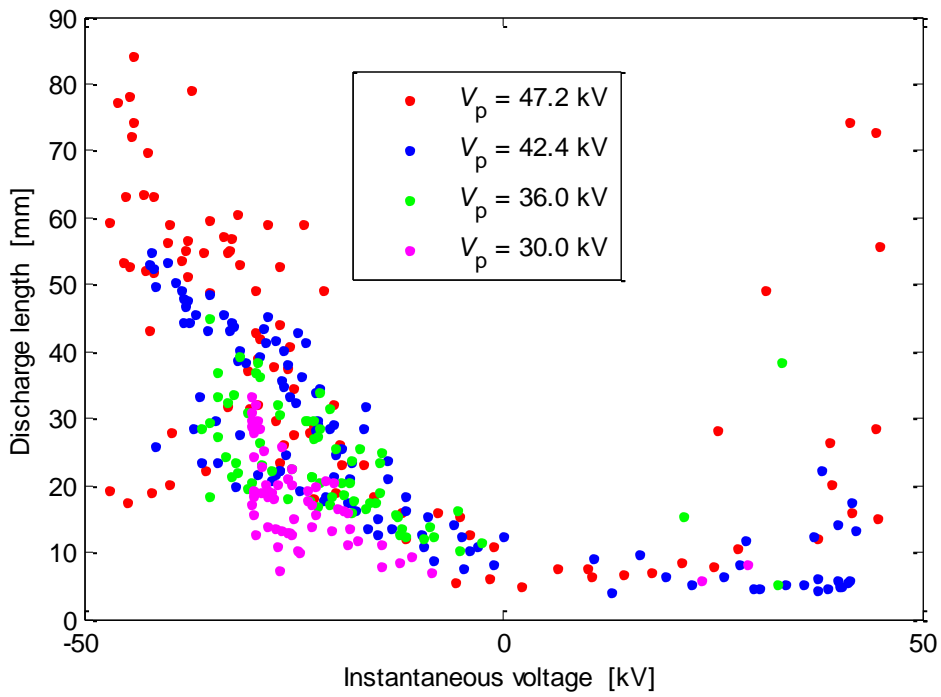


Fig. 4.20 Discharge images on 3 mm-thick PMMA pipe under 41.6 kV voltage taken at (a) $t = 0$ ms, (b) $t = 1$ ms, (c) $t = 2$ ms, (d) $t = 3$ ms, (e) $t = 4$ ms, (f) $t = 5 \sim 9$ ms, (g) $t =$

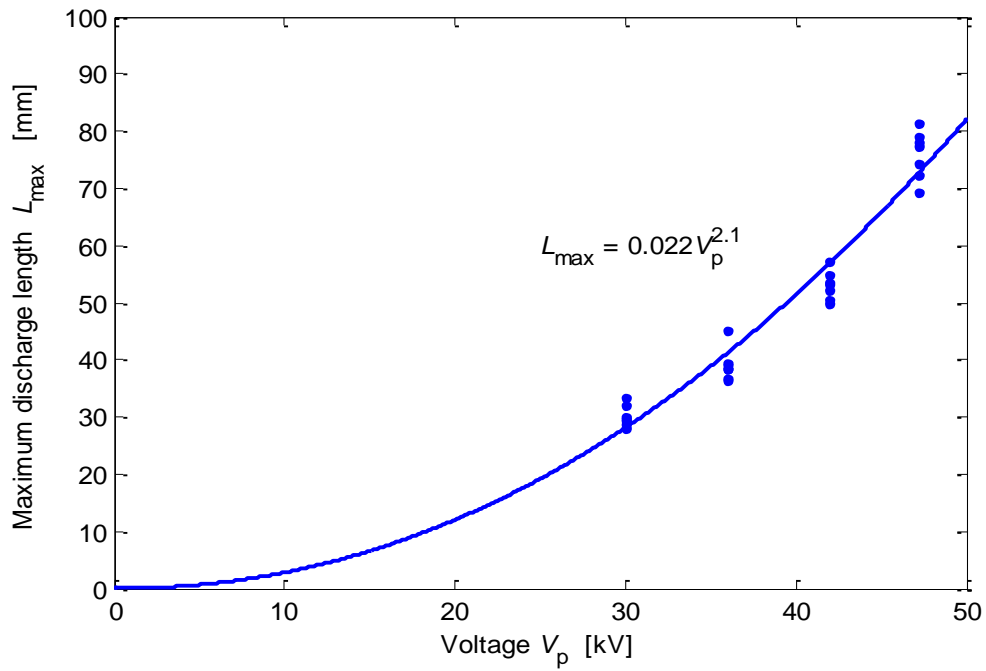
10 ms, (h) $t = 11$ ms, (i) $t = 12$ ms, (j) $t = 13$ ms, (k) $t = 14$ ms, (l) $t = 15 \sim 20$ ms.



(a)



(b)



(c)

Fig. 4.21 Discharge propagation length on 3 mm-thick PMMA pipe; (a) relationship between the length of discharge and the phases of application voltage, (b) relationship between the length of discharges and the values of instantaneous voltage, (c) maximum discharge length to the magnitude of AC voltage.

4.4.3 Discharge propagation on 200 μm - thick PET pipe

The propagation of surface discharge on 200 μm -thick PET pipe is observed by the high speed video camera for 50 cycles of AC voltage whose amplitude are set to 17.5 kV, 16.8 kV, 13.0 kV, and 11.5 kV. Table 4.6 and Fig. 4.22 show the experimental conditions.

The discharge photographs for a certain period under the application 17.5 kV are displayed in Fig. 4.24 as a typical case together with the voltage and current waveforms in Fig. 4. 23. In the region $\phi = -\pi$ to $-\pi/2$, the discharge length increases with the instantaneous voltage as well as those on 5mm-thick and 3 mm-thick PMMA pipes described in the previous two subsections. In the region $\phi = 0$ to $\pi/2$, where the positive voltage is applied to the high voltage electrode, streamer discharges and subsequent leader discharges are also observed and their length increases with the instantaneous voltage.

Some of discharges are regarded as back-discharge: when the magnitude of the instantaneous voltage decreases, the inverse electrical field is formed because of the residual charge accumulated on the insulator surface and, back-discharge may occur[3]

Figure 4.25 and 4.26 show voltage and current waveforms and discharge images on 200 μm -thick PET which are taken at $V_p = 16.8$ kV. With the decrease of V_p , very few leader discharge is observed in the regions of $\phi = -\pi$ to $-\pi/2$ and $\phi = 0$ to $\pi/2$, and no back-discharge is observed in the regions of $\phi = -\pi/2$ to 0 and $\phi = \pi/2$ to π .

The information about the discharge length on 200 μm -thick PET pipe in 50 cycles is summarized in Fig. 27. Figure 27 (a) shows the relationship between the length of discharge and its inception phase: the discharges occur not only in the region of $\phi = -\pi$ to $-\pi/2$, but also in the region of $\phi = 0$ to $\pi/2$. The occurrence number of discharge in $\phi = -\pi$ to $-\pi/2$, which hardly changes with the amplitude of ac voltage, is bigger than that in $\phi = 0$ to $\pi/2$, which increases with the amplitude of ac voltage. In the regions of $\phi = -\pi/2$ to 0 and $\phi = \pi/2$ to π , a few back-discharges are observed.

Figures 4.27 (b) and (c) show the relationship between the length of discharges and the instantaneous voltage and the relationship between the longest 7 L_{max} and V_p , respectively.

The L_{max} can be fitted by the following equation:

$$L_{\text{max}} = 0.0033V_p^{3.3} \quad (4.3)$$

Table 4.6 Experiment conditions

Insulator	200 μm -thick PET
Back electrode	Grounded
Distance between ring electrodes	$d = 200\text{mm}$
Exposure time	250 μs
Application Voltage	AC voltage
Amplitude of Voltage	17.5 kV _p , 16.8 kV _p , 13.0kV _p , 11.5kV

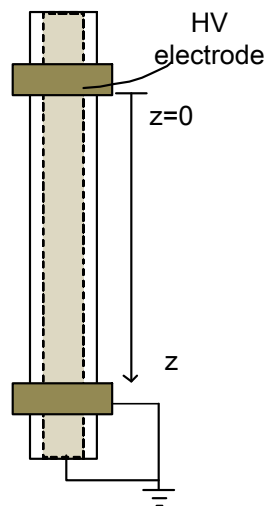


Table 4.22 Configuration of electrodes and insulator for AC discharge experiment.

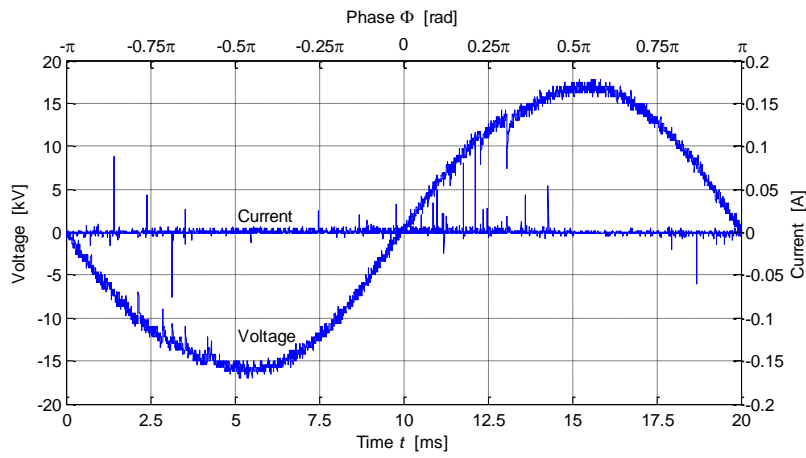


Fig. 4.23 17.5 kV application AC voltage waveform and discharge current waveform on 200 μm -thick PET pipe.

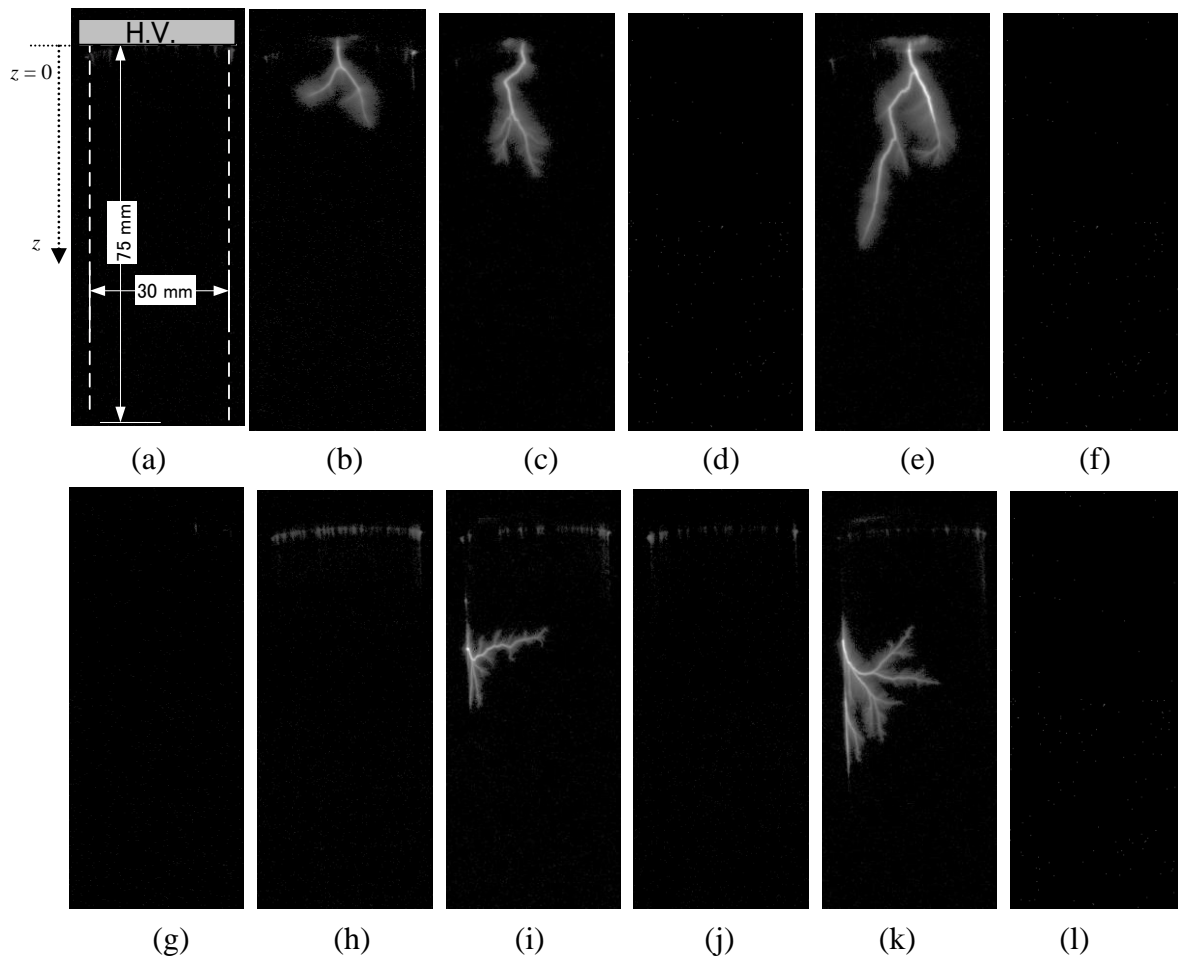


Fig. 4.24 Discharge images on 200 μm -thick PET pipe under 17.5 kV voltage taken at (a) $t = 0$ ms, (b) $t = 2$ ms, (c) $t = 4$ ms, (d) $t = 5 \sim 6$ ms, (e) $t = 7$ ms, (f) $t = 8 \sim 9$ ms, (g) $t = 10$ ms, (h) $t = 11 \sim 12$ ms, (i) $t = 13$ ms, (j) $t = 14$ ms, (k) $t = 15$ ms, (l) $t = 16 \sim 20$ ms.

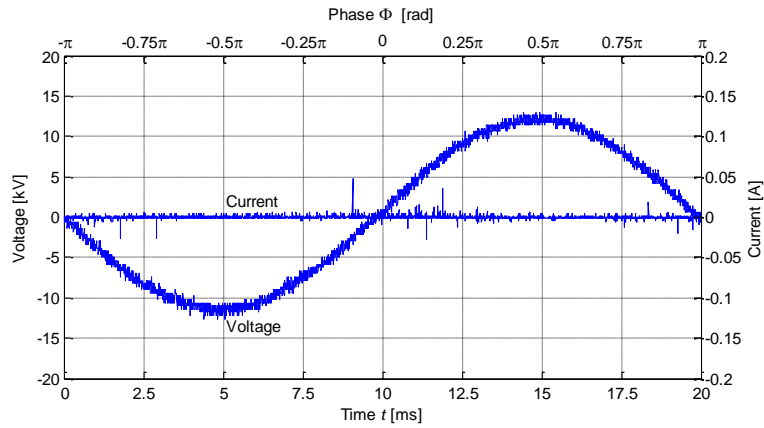


Fig. 4.25 13.0 kV application AC voltage waveform and discharge current waveform on 200 μm -thick PET pipe.

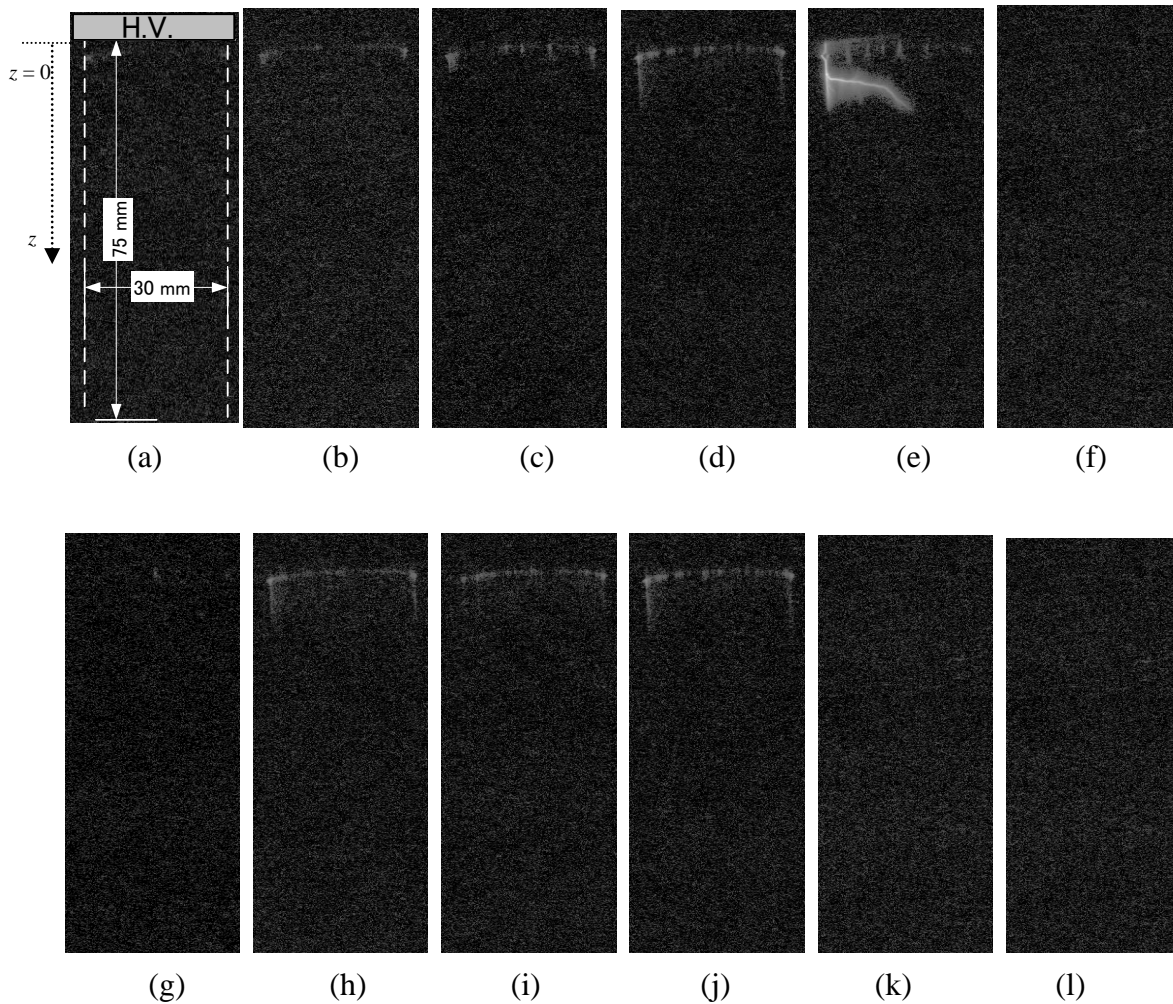
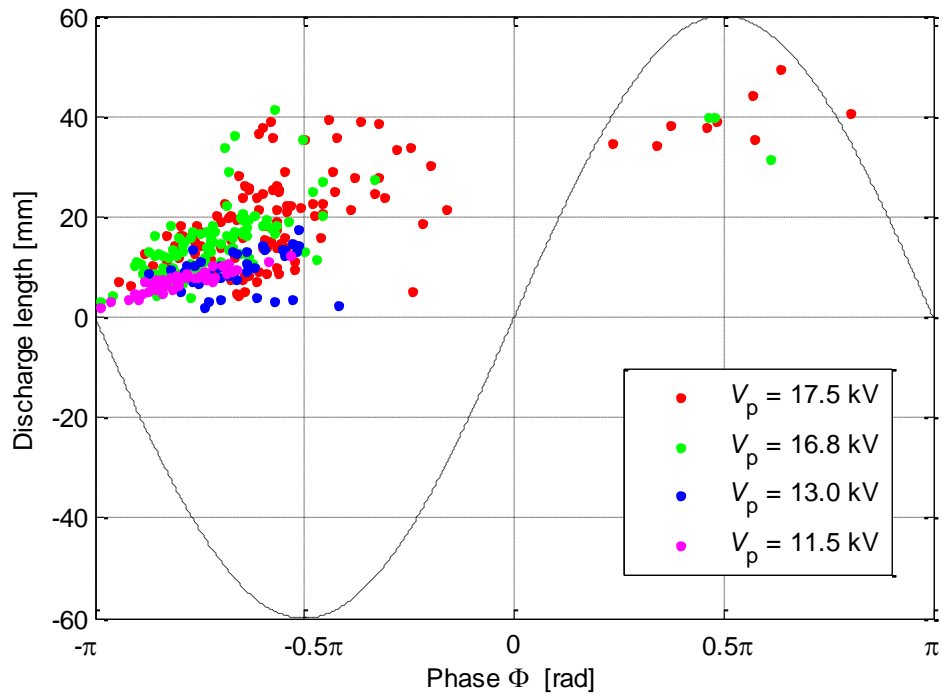
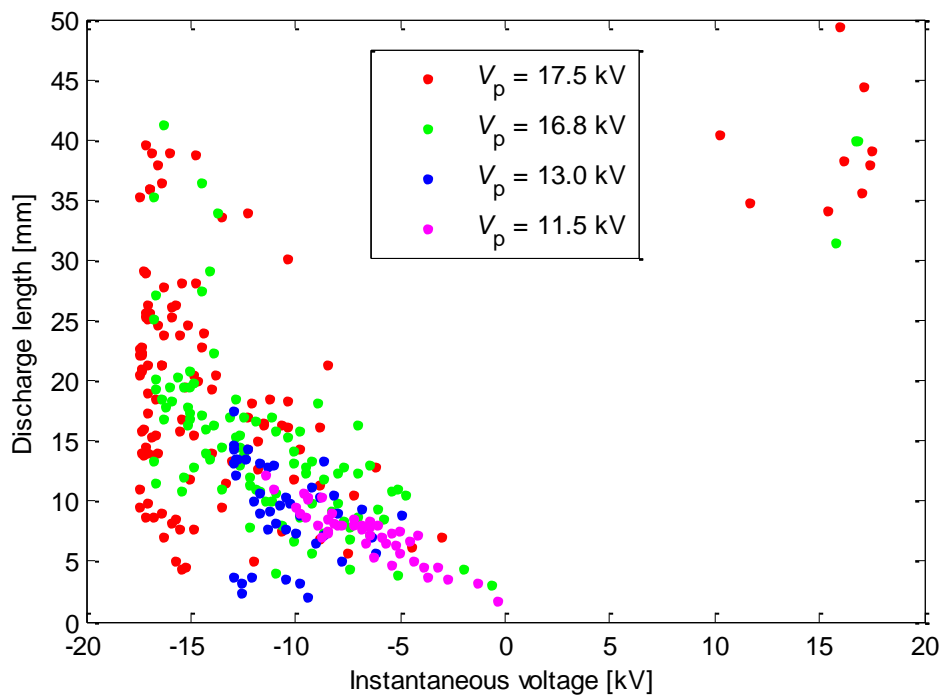


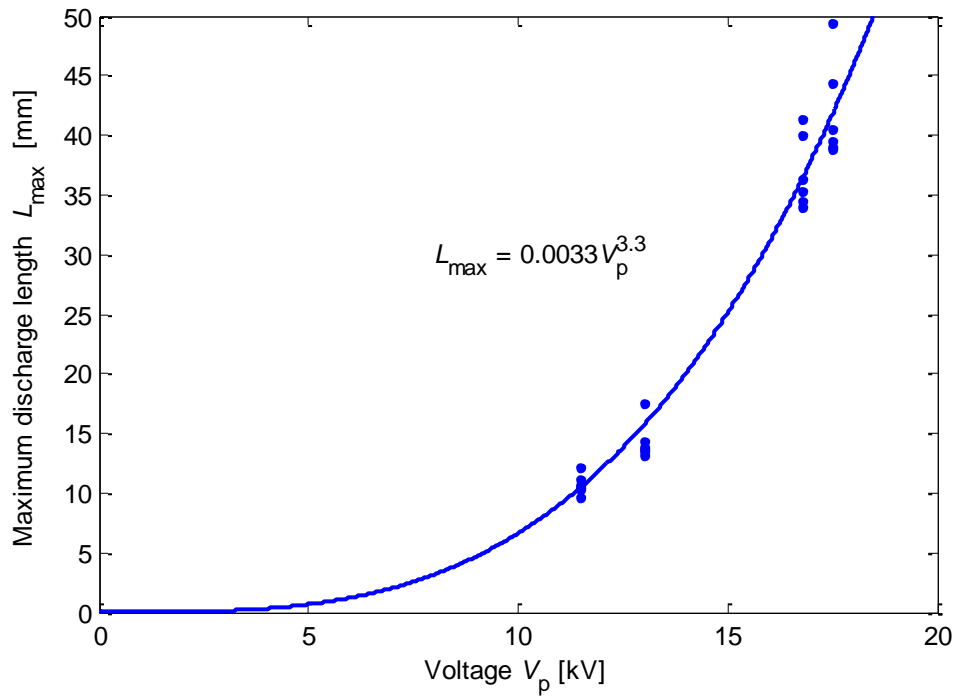
Fig. 4.26 Discharge images on 200 μm -thick PET pipe under 13 kV voltage taken at (a) $t = 0$ ms, (b) $t = 1$ ms, (c) $t = 2$ ms, (d) $t = 3$ ms, (e) $t = 4$ ms, (f) $t = 5 \sim 9$ ms, (g) $t = 10$ ms, (h) $t = 11$ ms, (i) $t = 12$ ms, (j) $t = 13$ ms, (k) $t = 14$ ms, (l) $t = 15 \sim 20$ ms.



(a)



(b)



(c)

Fig. 4.27 Discharge propagation length on 200 μm -thick PET pipe; (a) relationship between the length of discharge and the phases of application voltage, (b) relationship between the length of discharges and the values of instantaneous voltage, (c) maximum discharge length to the magnitude of AC voltage.

4.4.4 Maximum discharge propagation length

The relational curves between the maximum propagation length of surface discharge L_{\max} and the amplitude of AC voltage V_p for 3 kinds of insulation pipe are re-plotted in Fig. 4.30. From this figure, it is possible to say that the discharge on thin insulator pipe easily propagates for a long length. The maximum length of discharge L_{\max} can be expressed as the following equation:

$$L_{\max} \propto V_p^n, \quad (4.4)$$

where V_p is the amplitude of AC voltage, and n is 1.5-3.3.

In Fig. 4.28, the maximum propagation length of surface discharge under the application of impulse voltages on 2 mm-thick PMMA pipe, which have been reported by *M. Chiba*[4], are also plotted by dotted line for comparison. *M. Chiba* has made a lot of researches about the discharge under impulse voltage [4, 5, 6]. In his study, three types of high voltage electrode were utilized: A cylindrical electrode made of aluminum, and the cylindrical electrode with a point electrode of 0.1mm thickness and of 3mm length, and the cylindrical electrode with a 0.1mm-thick foil electrode of 20mm width. The insulator is a PMMA pipe with a diameter of 14mm, and a thickness of 2mm. A rod electrode with a diameter of 10mm is inserted in the insulator as a back electrode. With these three kinds of electrode, he studied the effect of many factors, including the ultraviolet (UV) radiation, the magnitude of applied voltage, and the waveform of applied voltage on the length of the surface discharge. He concluded that that the length of discharge L hardly depends on the shape of electrode and can be expressed as the following equation:

$$L \propto V^n, \quad (4.5)$$

where V is the magnitude of the applied impulse voltage, and n is 3~5.

Compared to the propagation length of impulse surface discharge, those of ac surface discharge is almost one third for the same peak voltage. It is natural to say that this phenomenon is caused by the influence of the residual charge and the difference of voltage-waveform. The detail will be discussed experimentally in section 6. 3.

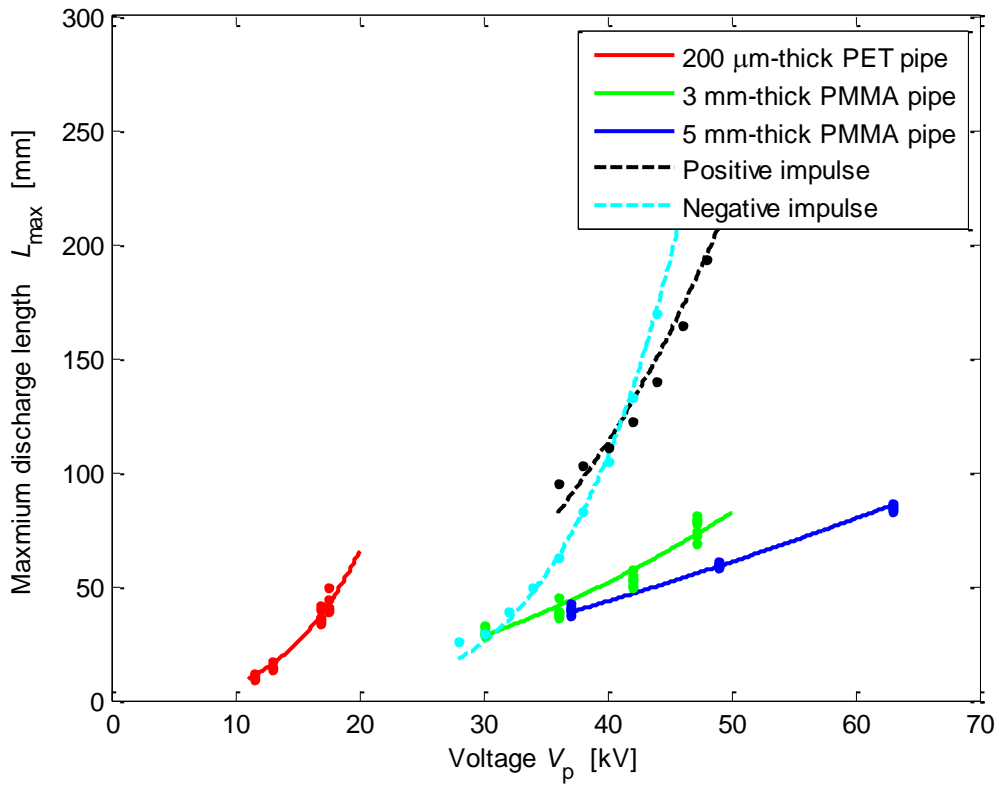


Fig. 4.28 Relationship between maximum discharge length and the peak voltage.

4.5 Summary

In this section, discharge propagation characteristics on the surface of a PMMA and PET pipe under AC voltage are investigated with a high speed video camera. The relation among the propagation length, the inception voltage and the phase angle was studied, and the following conclusions were obtained.

- 1) The discharge is easy to occur under the negative polarity of AC voltage.
- 2) The discharge is easy to propagate when the field distribution is perpendicular to the surface of the pipe.
- 3) For the discharge on the thin insulator pipe surface, the discharge is easy to propagate to a long distance.
- 4) The maximum length of discharge L_{\max} under AC voltage can be expressed as the following equation:

$$L_{\max} \propto V_p^n \quad (4.6)$$

where V_p is the amplitude of AC voltage, and n is 1.5 ~ 3.3.

References

- [1] L. Niemeyer, L. Ullrich, "The Mechanism of Leader Breakdown in Electronegative Gases", IEEE Trans. On EI, vol.24, Apr. 1989, pp. 309-324.
- [2] Discharge handbook, IEE Japan, 1998.
- [3] A. Kumada, M. Chiba, and K. Hidaka, "Potential Distribution Measurement of Back-discharge Phenomena by Using Electro-optic Effect," Trans. IEE Japan, Vol. 121-A, No. 8, pp. 797-798 (2001) (in Japanese).
- [4] M. Chiba, "Study about the developing mechanism of surface discharge on the solid dielectrics" Ph.D. dissertation, Dept. Elect. Eng., Tokyo Univ., Tokyo, Japan, 2002.
- [5] M.Chiba, A.Kumada and K.Hidaka, "Inception Voltage of Positive Streamer and its Length on PMMA in Air", IEEE Trans. on DEI, Vol.9, Jan. 2002, pp.118-123.
- [6] M. Chiba, A. Kumada, K. Hidaka and T. Kouno, "Fundamental Characteristics of Surface Streamer Development in Air", Trans. IEE of Japan, Vol. 116-A, Nov. 1996, pp. 999-1004.